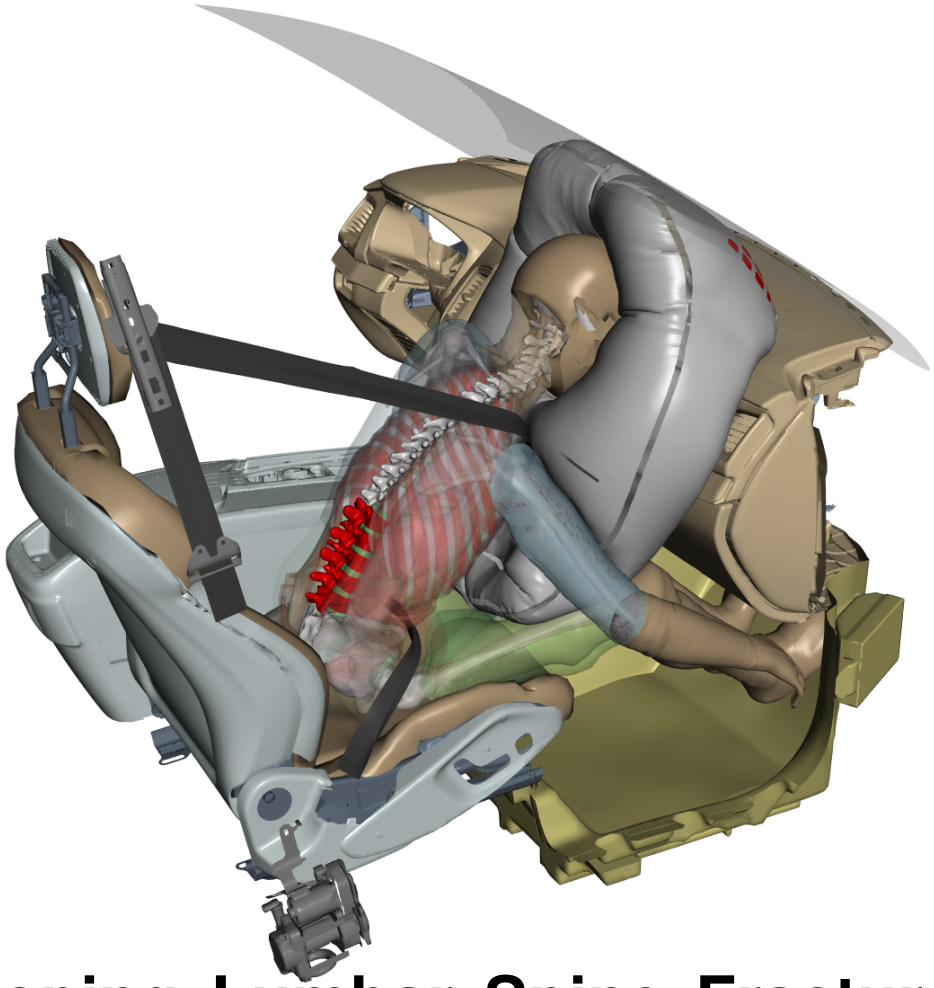

Developing Lumbar Spine Fracture Injury Risk Functions for Frontal Impact Anthropomorphic Test Devices using Paired Human Body Model Simulations

Master's thesis in Applied Mechanics

Simon Svensson Qvistberg
Gustav Zetterlund

DEPARTMENT OF MECHANICS AND MARITIME SCIENCES

CHALMERS UNIVERSITY OF TECHNOLOGY

Gothenburg, Sweden 2024

www.chalmers.se

MASTER'S THESIS IN APPLIED MECHANICS 2024

Developing Lumbar Spine Fracture Injury Risk Functions for Frontal Impact Anthropomorphic Test Devices using Paired Human Body Model Simulations

Simon Svensson Qvistberg
Gustav Zetterlund

CHALMERS
UNIVERSITY OF TECHNOLOGY

Department of Mechanics and Maritime Sciences
Division of Vehicle Safety
CHALMERS UNIVERSITY OF TECHNOLOGY
Gothenburg, Sweden 2024

Developing Lumbar Spine Fracture Injury Risk Functions for Frontal Impact Anthropomorphic Test Devices using Paired Human Body Model Simulations
Simon Svensson Qvistberg
Gustav Zetterlund

Master's Thesis, 2024
Department of Mechanics and Maritime Sciences
Division of Vehicle Safety
Chalmers University of Technology
SE-412 96 Gothenburg
Telephone +46 31 772 1000

Cover: Full frontal crash simulation using SAFER HBM with highlighted lumbar spine.

Typeset in LaTeX
Printed by Chalmers Reproservice
Gothenburg, Sweden 2024

Developing Lumbar Spine Fracture Injury Risk Functions for Frontal Impact Anthropomorphic Test Devices using Paired Human Body Model Simulations
Simon Svensson Qvistberg
Gustav Zetterlund
Department of Mechanics and Maritime Sciences
Chalmers University of Technology

Abstract

Thoracolumbar fractures from car crashes have gained importance over the past half-century. While fatal injuries have declined due to vehicle structural- and infrastructural improvements, the rate of moderate and more severe thoracolumbar fractures has remained steady or slightly increased. Recent research has introduced a new Finite Element (FE) lumbar spine model and a corresponding Injury Risk Function (IRF), integrated into the SAFER Human Body Model (SHBM) to enhance fracture risk prediction capabilities in car crash simulations. This thesis aimed to develop new lumbar spine injury prediction functions for current 50^{th} percentile male frontal impact Anthropomorphic Test Devices (ATD), Hybrid III and the Test device for Human Occupant Restraint (THOR) using paired simulations with SHBM to find potential Injury Criteria (IC) in the ATDs. This to enable evaluations of lumbar spine fracture risks in simulated crashes at an early stage in the development of car restraints using models of ATDs and in real crash tests.

Occupant models were positioned on the passenger side in a FE model of a medium-sized SUV front occupant compartment with seat back angles of 20°, 25°, and 30° using primer and ANSA. Paired simulations were run for all models using LS-DYNA. Data sampling employed a full factorial method, varying simulations with factors like impact pulse severity, belt forces, and seat pan stiffness. The study focused on common accident scenarios for moderate spine injuries: full frontal and run-off road impacts. Data analysis using linear regression identified correlations between ATD measures and SHBM peak lumbar strain. After data post-processing, Peak Pelvis Z-Acceleration (Peak Pelvis A_Z) for both ATD's and Peak T12 A_Z for THOR showed the highest correlation. To improve the correlation between peak lumbar strain and ATD IC, the Dynamic Response Index (DRI) was assessed. The DRI measures maximum dynamic spinal compression using a simplified mass-spring-damper model. By using pelvis A_Z as input, an optimized DRI was achieved, establishing it as a viable IC. IRFs for the ATDs were generated by substituting SHBM's peak lumbar strain with linearly regressed strains from ATD ICs for specific loading scenarios. Bootstrapping established a 95% confidence interval to account for simulation and SHBM IRF variations. Verification in a medium-sized SUV's rear seat mid-position showed predicted risks for Hybrid III within 30% of SHBM risk, while THOR's differed by up to 40%. Generally, ATD IRFs underestimated fracture risk, except for the Hybrid III in the most severe crash pulse. In summary, Peak Pelvis A_Z is recommended as IC for both Hybrid III and THOR. DRI can also be used for improved correlation but needs additional processing. The new IRFs provide a basis for fracture risk prediction using Hybrid III and THOR in frontal and run-off road crashes.

Keywords: FE, SAFER HBM, THOR, Hybrid III, Injury Risk Function, Lumbar fractures, DRI, Biomechanics, Injury Criteria

Preface

This master thesis project was carried out at the Volvo Cars Safety Centre in Torslanda, Gothenburg, Sweden during the spring semester of 2024.

Acknowledgements

We would like to express our appreciation to all those who have provided assistance and support throughout the completion of our master's thesis.

We would like to express our appreciation to Volvo Car Corporation for the opportunity to work on our master's thesis. We are extremely grateful to our supervisor, **Jonas Östh**, for his invaluable guidance, assistance, and moral support throughout the project.

We also acknowledge **Johan Davidsson** for his guidance in the project, as well as for being the examiner for our thesis.

We would like to extend our appreciation to **Johan Iraeus**, among others, who laid the foundations for the project by developing the new lumbar spine model and contributing valuable insights into risk function generation.

Our appreciation extends to **Anders Bernhardsson** from DYNAmore for holding the LS-DYNA course, which provided us with essential knowledge. We are also thankful for the continued support we received for LS-DYNA even after the course concluded.

Additional thanks to **Alexandros Leledakis**, **Ulrich Sander**, and **András Bálint** for their assistance with data sampling and statistical analysis of the thesis.

We extend our gratitude to **Max Nylund** and **Nils Olofsson** for their assistance throughout this thesis.

Our heartfelt thanks go to the entire **Crashworthiness Targets & Concepts** team at Volvo Cars Safety Centre in Torslanda.

Simon Svensson Qvistberg, Gustav Zetterlund, Gothenburg, June 2024

List of Acronyms

Below is the list of acronyms that have been used throughout this thesis listed in alphabetical order:

AIS2+	Abbreviated Injury Scale 2+
ATD	Anthropomorphic Test Devices
CFC	Channel Frequency Class
CDF	Cumulative Distribution Function
CIREN	Crash Injury Research and Engineering Network
DRI	Dynamic Response Index
EuroNCAP	European New Car Assessment Programme
EPP	Expanded Polypropylen
FE	Finite Element
FMVSS	Federal Motor Vehicle Safety Standards
GHBMC	Global Human Body Model Consortium
HBM	Human Body Model
IC	Injury criteria
IRF	Injury Risk Function
kph	Kilometers Per Hour
LHS	Latin Hypercube Sampling
MAIS2+	Maximum Abbreviated Injury Scale 2+
MLRM	Multiple Linear Regression Model
NHTSA	National Highway Traffic Safety Administration
PMHS	Post Mortem Human Subject
SHBM	SAFER Human Body Model
SRS	Supplemental Restraint System
SUV	Sports Utility Vehicle
THOR	Test device for Human Occupant Restraint
THUMS	Total Human Model for Safety
US-DOT	United States Department of Transportation

Contents

List of Figures

List of Tables

1
Introduction

Over the last half century, vehicle safety research has led to better understanding on how the human body is affected in car crash impacts and fatal injuries has been the prior focus. Compression-related thoracolumbar fractures in car crashes on the other hand is an injury type where the safety systems can be improved to prevent the mechanism causing the fractures. Collected data with incidence rates in frontal impact crashes between 1986 to 2008 has shown that the rate of thoracic and lumbar spine fractures to a car occupant has remained relatively constant or evenly slightly increased [Pintar et al., 2012]. Overall injury rates in car crashes measured according to Maximum Abbreviated Injury Scale 2+ (MAIS 2+), has decreased by two-thirds, comparing data with Volvo car models involved in crashes between 1975 and 2004 in Sweden [Isaksson Hellman and Norin, 2005]. Injuries related to the thoracic and lumbar spine have not shown the same decreasing trend as overall injury reduction when comparing crashes in Sweden from 2001-2005 to those from 1991-1995 [Jakobsson et al., 2016]. Thoracolumbar fractures due to car crashes can cause considerable harm to an occupant or even be fatal [Wang et al., 2009]. In particular, majority of the fractures has found to be in the transition area between the lumbar and thoracic spine [Pintar et al., 2012]. The most common Abbreviated Injury Scale 2+ (AIS2+) thoracolumbar spine fracture type is due to compression, followed by anterior wedge fracture which occurs in the presence of a combined flexion moment on the upper body. These injuries typically occur in frontal crashes and run-off road situations where the resultant impact forces on the car come towards the front respectively undercarriage [Jakobsson et al., 2016].

In safety development of a new car model, Finite Element (FE) models of the Human Body (HBM) can be used to evaluate occupant impact responses in car crash simulations. One such HBM is the SAFER HBM (SHBM). In the SHBM v11.0.1, a newly developed lumbar spine model has been implemented. The lumbar spine model has a corresponding strain-based Injury Risk Function (IRF) for accurate estimation of fracture probability on vertebrae levels [Iraeus et al., 2023]. One benefit with strain as Injury Criteria (IC) is that it scales with spine dimensions which also works for morphed HBMs, in contrast to earlier lumbar spine IRFs that has been estimated based on cross-sectional forces and moments [Tushak et al., 2022]. Towards the end of the development cycle for a car physical car crash tests with Anthropomorphic Test Devices (ATDs) are commonly performed to verify the occupant protection systems. Two types of ATDs are the Test device for Human Occupant Safety (THOR) and the Hybrid III. They are designed for frontal impact tests. The Hybrid III family consist of ATDs sized as a small adult female (5^{th} percentile), mid-sized adult male (50^{th} percentile), large male (95^{th} percentile) and children in age 3, 6 and 10 years old. The Hybrid III 50^{th} percentile adult male is the most

widely used frontal crash ATD [Schmitt et al., 2019]. THOR is an ATD representing a 50^{th} percentile male. Compared with Hybrid III all components have been improved except the arms which is the same as for Hybrid III. For the moment THOR is the most advanced ATD for frontal impact evaluations up to date. FE models of these ATDs exist and ICs with respectively IRFs has been developed to relate a measurable parameter with the risk of a specific injury [Schmitt et al., 2019]. There is interest in developing ATD lumbar spine IRFs to stay ahead of future vehicle development. Although there is currently no European New Car Assessment Programme (EuroNCAP) rating for this, the likelihood of its implementation is high if lumbar fractures remain constant while other injuries decrease. Vehicle manufacturers have internal requirements for all possible injuries, and having this IRF could help fine-tune lumbar spine requirements. By enabling IRFs for ATDs, physical crash tests can be verified and evaluated with an additional method.

Due to expectations of automated vehicles in the future, it has been anticipated that the occupants have a more reclined seat position since no driver is needed. This mean that the seat position would need to be considered in a wider range of postures. Hence the loading conditions at impact onto the lumbar and thoracic spine will differ from before [Östling and Larsson, 2019]. With the new lumbar spine IRF and seat position there is a need for continued development of tools to assess occupant risk in crash test simulations that relates to increased loading on the lumbar spine when using ATDs.

1.1 Aim

The aim of this thesis was to develop new lumbar spine injury risk functions for current 50th percentile male frontal impact ATDs using paired simulations with a state-of-the-art HBM with strain-based fracture prediction. More specifically the aims were:

1. To perform paired simulations of the ATDs and the SHBM and use regression models in order to find suitable measures as potential IC in the ATDs.
2. To determine as representative injury risk functions as possible based on the selected lumbar spine IC to be used with the ATDs.
3. To verify the developed ATD IRFs using different vehicle enviroment.

1.2 Limitations

In this project, SHBM version 11.0.1 was used which was the latest version available. The SHBM is a 50^{th} percentile male occupant, and for the present work it was paired with FE models of the Hybrid III and THOR 50th male percentile ATDs. If the method developed to pair results from the HBM and the ATD is successful, it can be applied also for other ATD sizes such as the 5^{th} female and 95^{th} male, but this was outside the scope of the present thesis due to the available time for the project.

2
Background

In the subsequent sections, a concise overview of human anatomy, spine injury mechanisms, finite element modeling, and associated analysis tools are provided, complemented by illustrative figures.

2.1 Anatomy of the Spine

The main function of the spinal column is to provide support for the body. It has an essential role in almost every movement performed in an upright standing posture. The column is built up by 24 individual movable vertebrae stacked on top of each other with intervertebral discs in between the vertebrae in order to allow for flexion and extension, and flexible tendons and ligaments that surround the vertebrae for stabilization and protection of the discs. The spinal column is divided into three regions with vertebrae numbered according to Figure 2.1. The regions are cervical, thoracic, lumbar, sacrum, and coccyx. It is only the cervical, thoracic, and lumbar vertebrae that allow for some flexion [Hines, 2018]. The sacrum and coccyx are fused. The spine is divided into the different regions since they have unique features. The cervical spine supports the weight of the head and allows for a large range of motion in the connection to the skull. The thoracic spine supports the ribcage and the additional load/weight of the upper body and arms. The vertebrae dimensions are therefore larger and the range of motion is limited. The lumbar spine is dimensioned to carry the load from the whole upper body and therefore includes vertebrae with the greatest dimensions in order to absorb larger load magnitudes. The main function of the fused sacrum is to connect the spine with the hip bones, and the coccyx or tailbone provides attachment for ligaments and muscles [Hines, 2018].

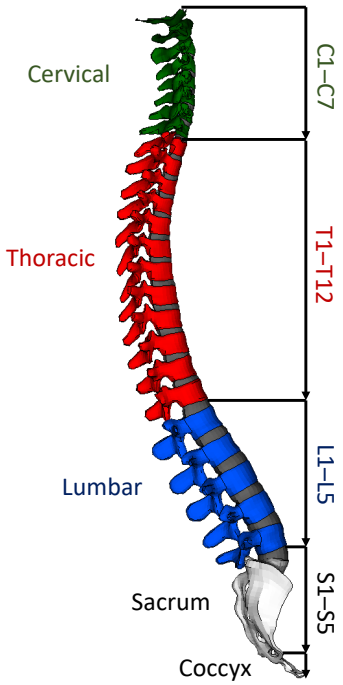

Figure 2.1: Spine anatomy model with sections in colors representing the vertebrae levels with corresponding labels.

2.2 Thoracolumbar spine injuries in car crashes

The injury risk in car crashes for MAIS2+ and AIS2+ thoracolumbar injuries was studied by Jakobsson *et al.*,(2006). In their study, accidents occuring between 1991 to 2005 with occupants 15+ years were collected from Volvo's statistical accident database [Jakobsson et al., 2006]. Among the 21,034 occupants in accidents, 1,293 experienced AIS2+ injuries and 189 of these sustained AIS2+ thoracic or lumbar spine injuries. Another study was made by Isaksson-Hellman and Norin (2005) that shows similar results, implying the trend that only a small reduction of thoracic and lumbar spine injuries can be seen comparing accidents occuring between 1991-1995 and 2001-2005. This in contrast to the reduction of MAIS2+ injuries that decreased more than half [Isaksson Hellman and Norin, 2005]. Jakobsson *et al.*,(2006) also presented the distribution of injury types in different crash scenarios. The different injury types were AIS2+ spine injured occupant, MAIS2+ injured occupant and all occupant injuries. The result showed that the most frequent accident scenario was frontal impact with 39% of the AIS2+ spinal injuried occupants. Other accident scenarios where a larger portion of AIS2+ spinal injuries could be identified were run-off road, multiple impacts and roll or turnover events.

The type of fractures in the spine due to frontal impact has been investigated by Pintar *et al* .,(2012). In the study, thoracic and lumbar vertebral body fracture AIS codes for spine

level T10 or below where searched for using the United States Department of Transportation (US-DOT) National Highway Traffic Safety Administration (NHTSA) Crash Injury Research and Engineering Network (CIREN). The CIREN database has radiographic information from each fracture accident such that the fracture could be categorized into burst or minor compression of the vertebral body in the case of uniform compression from anterior to posterior, wedge-type if the anterior was more compressed than the posterior, and other types of fractures outside those categories. The result showed that the most common burst fractures occured predominantly at vertebra T12, L1 or L5 and wedge fractures at L1 [Pintar et al., 2012].

2.3 Finite Element Modeling

Nonlinear FE analysis plays a vital role in modern computer-aided design processes. Traditional methods of prototype testing are gradually being supplanted by simulation techniques employing nonlinear finite element methods. This transition offers a swifter and more cost-effective means of assessing design concepts and intricacies. For instance, within the automotive sector, crash simulations are now used more than full-scale tests for vehicle development. These simulations serve not only to evaluate early design concepts but also to fine-tune details of the final design, such as the optimal placement of accelerometers for airbag deployment, interior padding configurations, and the selection of materials and component cross-sections to meet stringent crashworthiness standards [Belytschko et al., 2014].

In FE Analysis , implicit and explicit solvers are two different types of approaches to solve problems. Implicit solvers solve equations through matrix inversion, suitable for stable solutions in larger models with non-linearities, complex contact conditions, and highly nonlinear material behaviour. They are ideal for static or quasi-static analyses, allowing for larger time increments. Explicit solvers solve for acceleration, requiring smaller time steps due to stability concerns, making them better suited for dynamic events with rapid changes, such as impact, crash or explosion scenarios [Hurlston, 2021].

2.4 FE Human Body Model

A FE HBM is a computational representation of the human body. Compared with an ATD the HBM has a more accurate representation of the human anatomy, such that all ribs and vertebrae are modelled. The HBMs are used with FE methods that splits the domain of the HBM into discrete finite element with different shapes such as tetrahedrons, hexahedrons with different number of nodes. These elements create the visual and nonvisual anatomical structure of the HBM [Schmitt et al., 2019]. This detailed representation allows for omnidirectional kinematics and kinetics that can be used to evaluate injury risk at tissue level. FE HBMs is used in biomechanical, crashworthiness analyses and for injury prediction purposes. By applying a specific loading conditions together with boundary conditions, FE simulation can be performed and prediction of the tension, deformation and stresses in the model. The use of HBMs in biomechanical applications play a crucial role in the study of crash responses, injury risk prediction and

by the development of safer vehicles [Iraeus et al., 2023].

The purpose of impact biomechanics HBMs is to model the human anatomy at a fine enough level to simulate injury mechanisms of interest, for instance in automotive impacts, while still being computationally efficient which together with identification of material properties and anatomical is complex. In order to validate the HBM to the human experimental data, Post Mortem Human Subject (PMHS), and actual crash data is used. This creates an approximation of the accuracy and the reliability of the model [Schmitt et al., 2019]. There are several HBMs and versions on the market today and some of these are the Total Human Model for Safety (THUMS) version 7, Global Human Body Model Consortium (GHBMC) version 6 and SAFER HBM. During this project the SAFER HBM was used.

2.4.1 SAFER HBM v11

The aim for the SAFER HBM was to develop an omnidirectional, tunable, and scalable model that was capable of injury risk and biofidelic kinematics for both low and high g-forces [Pipkorn et al., 2023]. The baseline of the model corresponds to a 50^{th} percentile male, with the weight of 77 kg and height of 175 cm. The model has been iterated through the years and this project was using the latest available version v11.0.1. The latest version consists of a new finite element lumbar and thoracic spine with corresponding tissue-based injury risk function for compressive fractures, validated for the lumbar spine. The injury criteria for the injury risk function are maximum axis superior inferior strain on the trabecular bone and can be adjusted to fit diverse ages of population [Pipkorn et al., 2023].

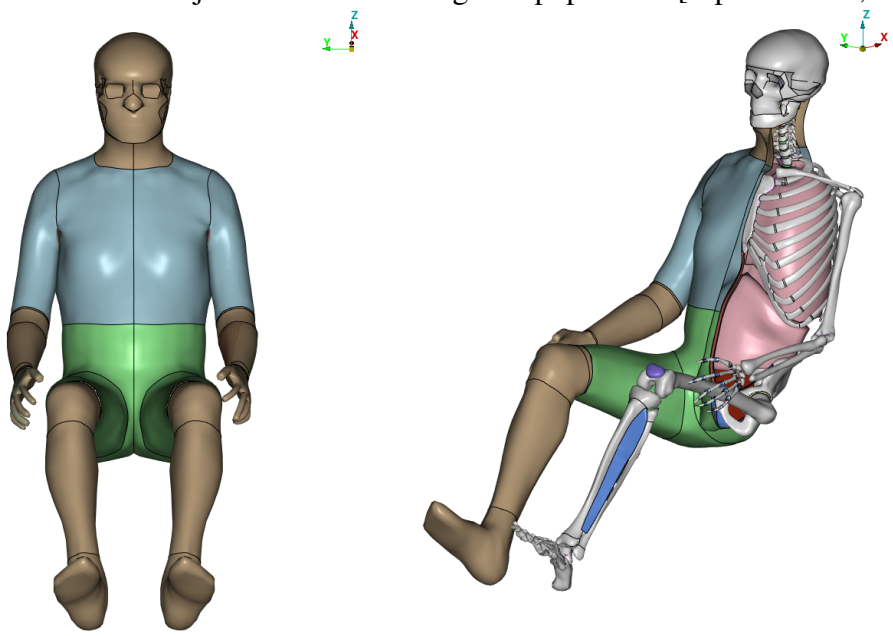

Figure 2.2: Visualisation of The SAFER HBM in seating position showing the level of details in anatomy.

2.5 Anthropomorphic Test Devices

An ATD is a mechanical model of the human body used to represent the human impact response during a car crash scenario. The ATDs are robust and simplified representations of the human body designed to be used repeatedly in car crash tests maintaining precise sensing accuracy. They are made of steel or aluminium for skeleton parts, poylmers for joint surfaces or skin and foam material as flesh. They are also equipped with several accelerometers and load cells to record acceleration, force and deformation, [Schmitt et al., 2019]. Several different types of ATDs are available with different mechanical constructions in order to capture a specific type of impact as accurately as possible. For the present work FE-models of the 50^{th} percentile frontal impact ATDs THOR and Hybrid III were used.

2.5.1 THOR

The ATD Test device for Human Occupant Restraint THOR is the most advanced frontal impact ATD up to date. The ATD is based on the anthropometry of a 50^{th} percentile male. THOR has a advanced biofidelity and geometry of the rib cage equiped with four sensors in order to capture deformations due to seat belt and airbag impact [Schmitt et al., 2019]. Also the upper abdomen has two sensors for intrusion measurements. More specific for this project the thoracolumbar spine was of interest. The THOR spine is not designed to record sensor data representative to each vertebra in a human body. Relevant available output sensors that could be used was the T12- and pelvis accelerometer and the thoracic spine load cell which can capture forces and moments [Humanetics, 2020].

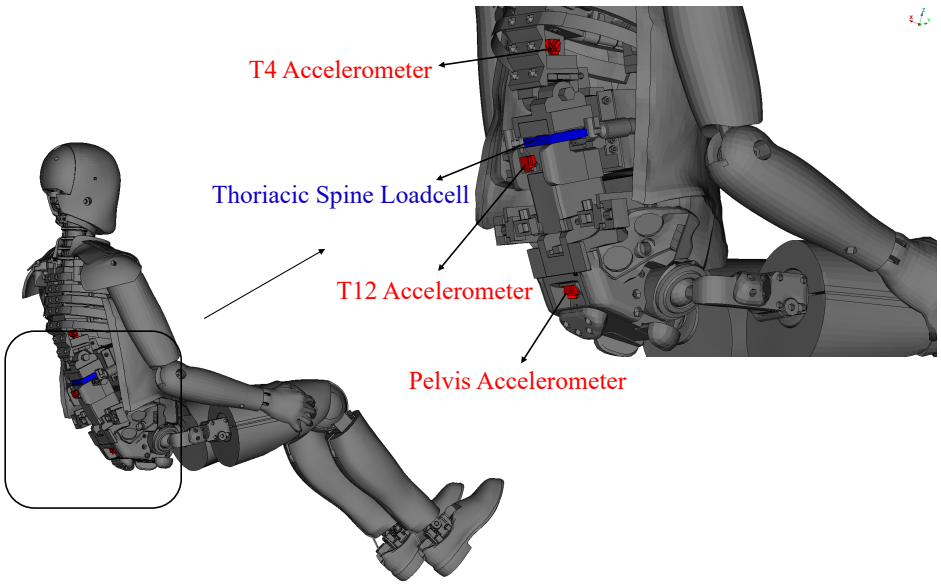

Figure 2.3: Placement of THOR sensors with corresponding labels.

2.5.2 Hybrid III

The Hybrid III family is the most widely used ATD and is defined in the Federal Motor Vehicle Safety Standards (FMVSS). The family consist of children three-, six- and ten-year-old, an adult female (5^{th} percentile), an adult male (50^{th} percentile) and an adult male (95^{th} percentile). The Hybrid III family does not have individual segments of the spine causing a lack of sensoring on vertebrae level. Available sensors to capture relevant measurments related to loads and motions on the lumbar spine are the pelvis accelerometer and the lower- and upper lumbar load cell for measurments of forces and moments. In the physical ATD only the pelvis accelerometer and the lower lumbar load cell is available for measurements. The upper lumbar load cell is an additional sensor available in the FE model version which is included for a more extended lumbar load analysis. The lumbar load cells are mounted in connection with a curved cylindrical rubber mount in order to make the spine less stiff in the connection between the lumbar spine and the pelvis [Schmitt et al., 2019].

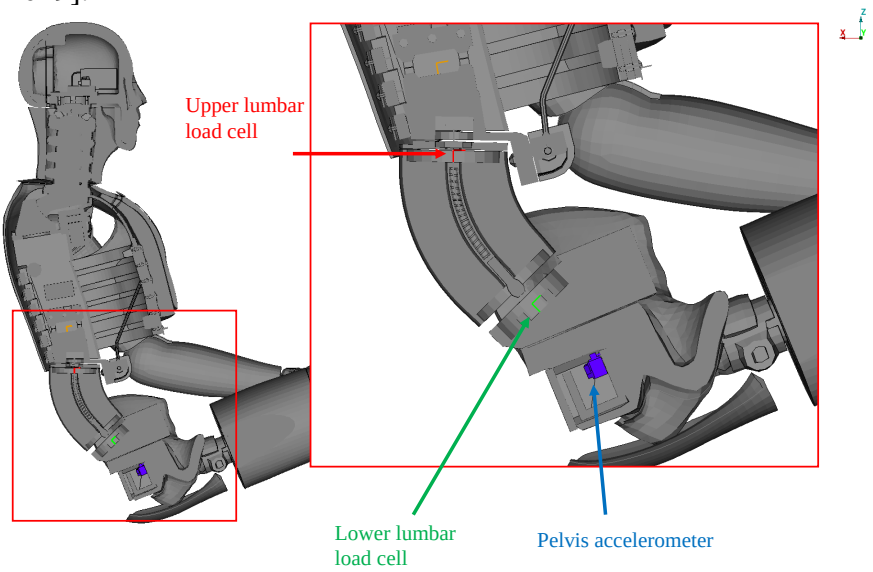

Figure 2.4: Placement of Hybrid III sensors with corresponding labels.

2.6 Signal filtering

When performing explicit FE crash simulations using sensors such as accelerometers and load cells, output data tend to become erratic. This can pose a problem during data analysis because the output lacks a clear trend. By employing filters for the output, high-frequency signals are attenuated, allowing the trends in sensor output to become discernible. It is crucial to use a suitable filter for each signal to correctly capture the peaks of the signal. There are several types of filters for different applications, and in this project, filtering using Channel Frequency Class (CFC) in accordance with SAE J211-1 was employed [Society of Automotive Engineers, 2007]. In table 2.1 is the filtering for each sensor and corresponding model listed.

Table 2.1: The IC and their CFC filtering class for both ATD models and the SHBM.

Measure	Filter
Hybrid III	CFC
Pelvis A	1000
Lower Lumbar F	600
Lower Lumbar M	600
Upper Lumbar F	600
Upper Lumbar M	600
THOR	CFC
Pelvis A	1000
T-Spine F	600
T-Spine M	600
T4 A	180
T12 A	180
SHBM	CFC
Sacrum A	060
Lumbar F	-
Lumbar M	-
Lumbar ϵ	-

2.7 Statistical Analysis

In this section, statistical analysis containing the necessary information about regression models using one and multiple variables is explained.

2.7.1 Linear Regression Model

Linear regression is a statistical method used to create a prediction of a variable based on a value of another variable. This is done by using dependent and independent variables, the dependent value is the one to be predicted while the independent value is the one used to predict the dependent one. This analysis method estimates the coefficients of the linear equation using one or more independent variables that best predicts the value of the dependent variable. The linear regression uses the data to fit a straight line or surface that minimizes the discrepancies between predicted and the actual output value. The figure 2.5 below shows a visualization of the model.

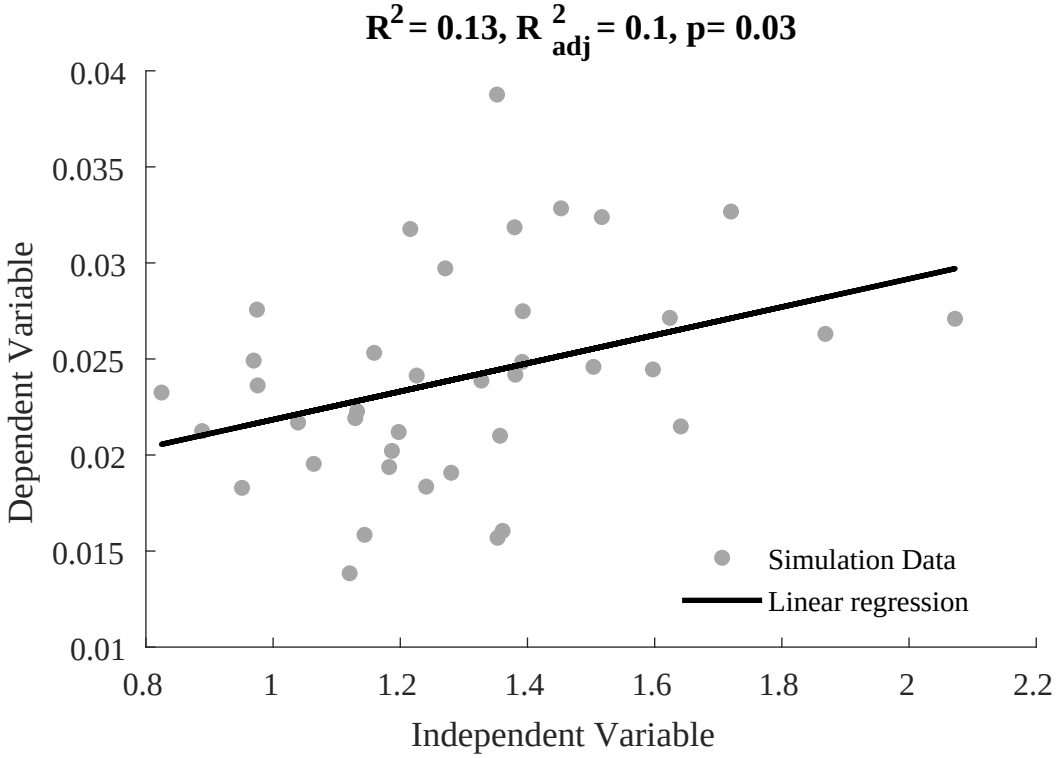

Figure 2.5: Visualization of the Linear Regression Model with 95% confidence interval.

Linear regressions are widely used, mainly due to simplicity and does provide a mathematical formula that generates predictions. The model can be used in various applications such as biological, behavioral, and social sciences among others. The regression model has become a scientific way of predicting the future. During this project, linear regression is used to analyze injury criteria candidates for the ATDs [Vijay, 2023].

To evaluate the linear regression model, different kind of measures can be used to analyze its accuracy. Relevant measure for this project are the R^2 and P-Value. Goodness of fit or R-Squared method is a correlation analysis that measures how well the data points fits

into the linear model. This measure can take any value between 0-1 and values close to 1 is considered a perfect correlation. P-Value is a measurement that calculated the probability of obtaining an extreme value. It can be used as a validation of hypothesis against observed data and the range at which the measure can take is between 0 and 1. A value below 0.05 considers to be statistically significant [Schneider et al., 2010].

2.7.2 Multiple Linear Regression Model (MLRM)

As a complement to linear regression, there is Multiple Linear Regression (MLR), which is a statistical technique used to predict the outcome of a variable based on two or more independent variables. It extends the concept of linear regression by incorporating multiple predictors. The dependent variable, or the one to be predicted, is influenced by independent variables, also known as explanatory variables. The regression formula involves coefficients representing the impact of each independent variable on the dependent variable. Assumptions include linearity between variables, independence of observations, constant variance of residuals, absence of multicollinearity, and multivariate normality of residuals. The technique is valuable for analyzing relationships between multiple factors and predicting outcomes in various fields, such as biomechanical data [Taylor, 2024].

MLRM is a suitable technique for analyzing the influence of the independent variables. In the results of the model, there is a p-value corresponding to each independent variable, and if it is below 0.05, it is considered to be statistically significant. This means that the variable has statistical evidence that it influences the dependent variable. The model also outputs an estimated effect and the standardized error for each variable [Taylor, 2024].

2.8 Injury Risk Function and Injury Criteria

Injury criteria, or fracture criteria, are measures of physical parameters like acceleration, forces and moments used to establish a correlation to the likelihood of specific types of injuries occurring in particular body regions. Typically, ICs are developed through a combination of experimental studies on PMHS and empirical data [Schmitt et al., 2019]. The likelihood of injury can be assessed using an injury risk function which is generated and dependent on relevant injury criteria for the specific body regions studied. In the present study the body region of particular interest was the lumbar spine. The new lumbar spine IRF to be used with the SHBM is presented in Equation 2.1 and distribution and recommended parameters for the lumbar spine model is presented in Table 2.2. In addition to the IC, it can be noted that an extra covaraite accounting for age is included, which has shown to be a significant factor for the lumbar spine fracture risk [Iraeus et al., 2023]. The effect of age diversity can be seen in Figure 2.6.

$$Risk = \frac{1}{2} + \frac{1}{2} erf\left(\frac{ln(injury\ criteria) - (\beta_1 + age * coef_{age})}{\sqrt{2 * (\beta_2)^2}}\right) \tag{2.1}$$

Table 2.2: Distribution and parameters for the injury risk function recommended for the new lumbar spine IRF, Equation 2.1

Injury risk	Injury criteria	Distribution	β_1	β_2	$coef_{age}$	$\beta_{1,SE}$	$\beta_{2,SE}$	$coef_{age,SE}$
Fracture	Strain	Log-normal	-2.833	0.41254	-0.0149	0.10983	0.02924	0.00218

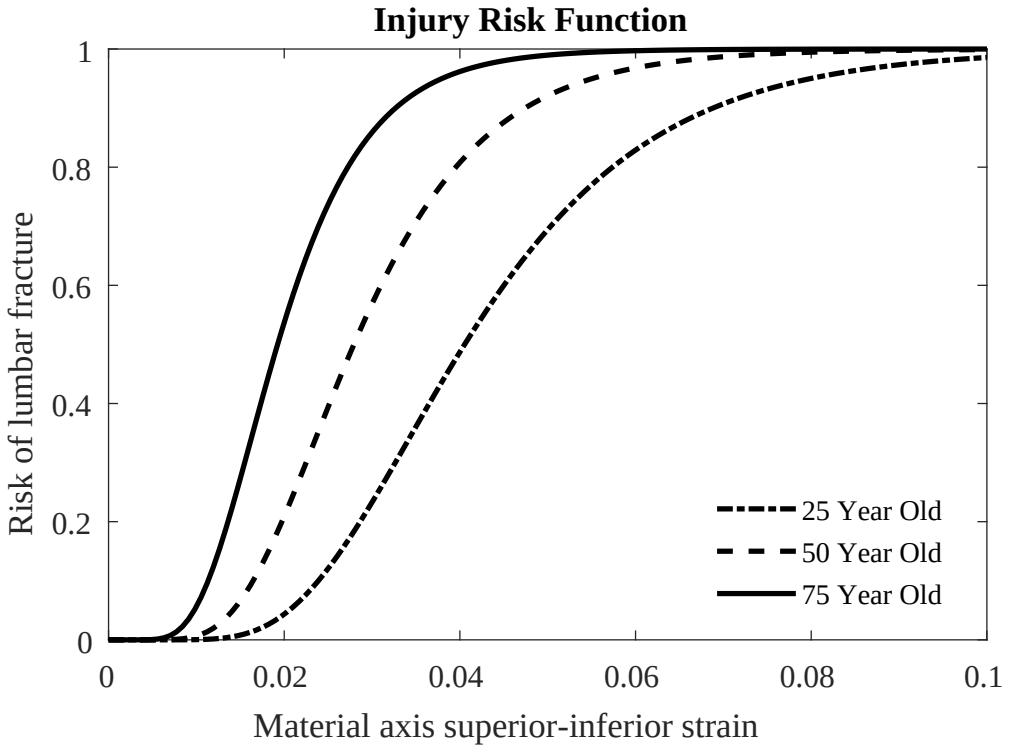

Figure 2.6: Risk of lumbar fracture according to Iraeus*et al.*,(2023) for the newly implemented lumbar spine model.

2.8.1 Bootstrapping for confidence bounds

Bootstrapping is a statistical procedure that involves resampling a single dataset to create numerous simulated samples. This technique enables the calculation of standard errors, the construction of confidence intervals, and the performance of hypothesis testing for various sample statistics. As an alternative to traditional hypothesis testing, bootstrap methods are not only easier to understand but also applicable under a wider range of conditions. In this project, bootstrapping is used to create confidence bounds where the coefficients and their standard errors are known. This involves performing a arbritary number of bootstrap iterations for each coefficient along the normal distribution. For each iteration, the IRF is calculated, as well as the area under the curve. To extract the 95% confidence interval, the IRFs are sorted from high to low with respect to the area. Then, the 2.5^{th} percentile ($0.025 \times$ Num Iterations) and the 97.5^{th} percentile ($0.975 \times$ Num Iterations) of the sorted IRFs are selected [Tibshirani, 2024]. These two IRF creates the boundaries of the 95% confidence interval.

3
Methods

The overarching method that enables this thesis work was the use for explicit FE simulations and FE models of both the HBM and ATDs.

3.1 Simulation setup

In this project paired simulations of the SAFER HBM and the two ATDs THOR and Hybrid III were performed using LS-DYNA MPP R9.3.1 Single Precision (LSTC, Livermore, CA) as explicit solver. The models were positioned on the passenger side in a front occupant compartment model of a medium-sized Sports Utility Vehicle (SUV), see Figure 3.1. The vehicle body structure of the occupant compartment was modelled as rigid, and hence no intrusions were considered in any of the simulations. The position of the seat was possible to move within the ”seat travel box”, see Figure 3.1, where the H-point, according to the SAE H-point manikin [Humanetics, 2023], needs to be inside the bounds. For all performed simulations in this project the seat was positioned with the H-point in the lowest vertical position and middle position in horizontal direction. The front passenger seat in the setup was positioned with seat back angles $20°$, $25°$ and $30°$ in order to simulate the impact on the lumbar spine in different postures.

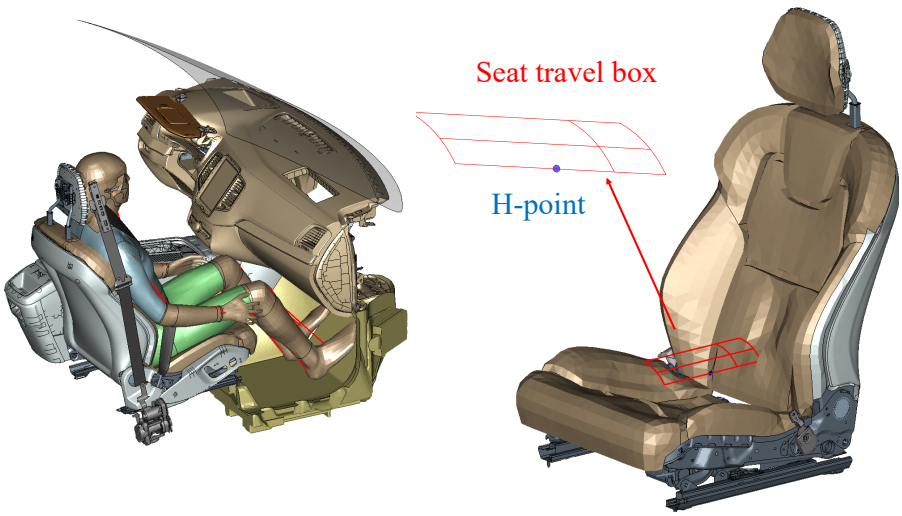

Figure 3.1: Illustration of the front interior simulation setup on the passenger side (Left), and the possibility to adjust the seat position within the seat travel box (Right).

3.1.1 Positioning of the SAFER HBM

The SHBM was positioned 10 mm above and 10 mm forward of the seat H-point location. For the 25° seat back angle position, the default HBM spinal curvature with a pelvis angle of 45° (measured from the top of the pubic symphysis to a mid point between the anterior superior iliac spines [Izumiyama et al., 2018]) was used. For the 20° and 30° seat back angles, the pelvis was rotated 2.5° anterior or posterior and 1° flexion or extension was applied at the sacrum-L5 joint, 1° at L2-L3 and 0.5° at L1-T12. For the 20° position 2° additional neck flexion was applied to avoid intersection of the back of the head with the head restraint cushion. Visualization of the spinal curvatures in the three seat back angles can be seen in Figure 3.2. For all postures the feet were positioned above the carpet and the arms along the side of the thighs.

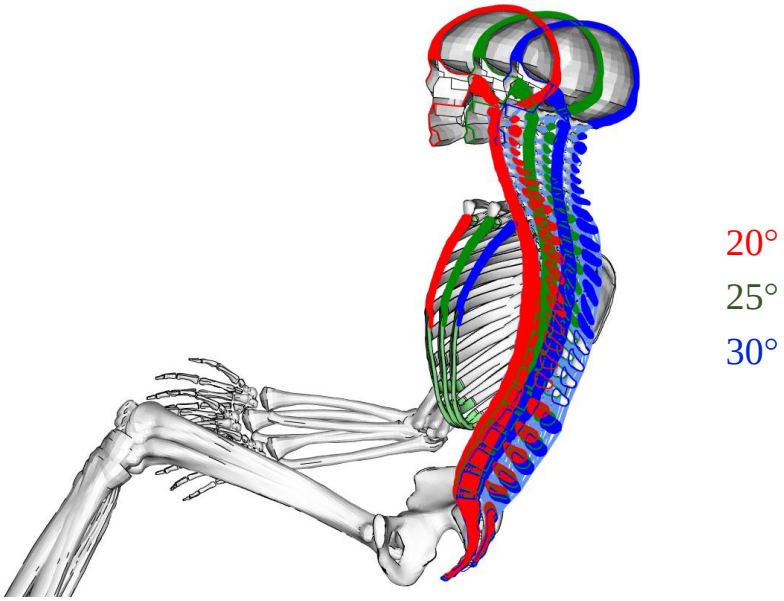

Figure 3.2: Visualization of spinal curvature of the SHBM in the three seat back angles 20°, 25° and 30°.

3.1.2 Positioning of Hybrid III

The positioning of Hybrid III was performed with similar strategy as for SHBM and THOR. The ATD was positioned with and offset of 6 mm upwards related to the H-point. The default pelvis angle was 22.5° which was used in the positioning in the seat with seat back angle of 25°. For the 20° and 30° seat the pelvis and torso was rotated in a similar way as for THOR for which the pelvis was rotated ±2.5° and the remaining reclination by the upper and lower torso according to Table 3.1. As for the other two models the feet were positioned slightly above the carpet and the arms and hands along the side of the thighs. Visualization of Hybrid III in the three seat back angles can be shown in Figure 3.3.

Table 3.1: Adjusted angles in Hybrid III for the various seat back angles.

Seat back angle	Pelvis Angle	Torso/lower lumbar	Torso/upper thorax
20.0°	20.0°	−1.0°	−1.5°
25.0°	22.5°	0.0°	0.0°
30.0°	25.0°	1.0°	1.5°

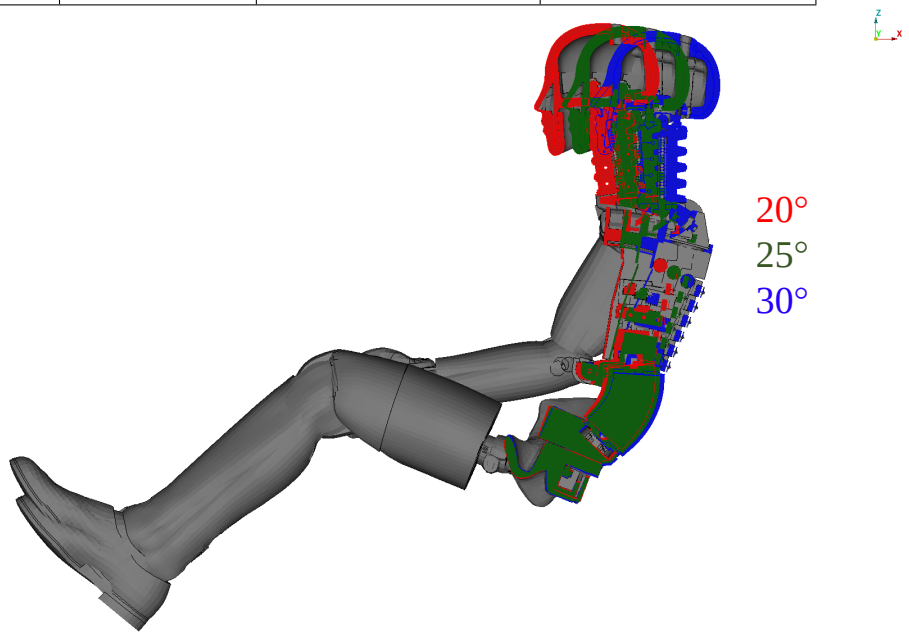

Figure 3.3: Hybrid III ATD postures for three different seat back angles.

3.1.3 Positioning of THOR

The THOR ATD was positioned with an offset of 30 mm upwards and 20 mm forward relative the H-point manikin location to be accurately seated. The THOR ATD was positioned for three seat back angles, 20°, 25° and 30°, the same as for the SHBM. In all postures the legs was positioned symetric with 225 mm width from the middle of the knee joint clevises. The feet was placed at 90° with respect to the lower leg and heels on the floorboard. The arms was positioned with hands placed beside the thighs and elbows slightly touching the backrest of the seat. The mainly adjusted measurements for the variety of seating positions are listed in Table 3.2.

Table 3.2: Adjusted angles in THOR for the various seat back angles.

Seat back angle	Pelvis Angle	Lower Spine bottom	Upper Spine bottom
20.0°	30.5°	−2.5°	−2.5°
25.0°	33.0°	−3.5°	−3.5°
30.0°	35.5°	−1.5°	−1.5°

In Figure 3.4 below there is a schematic overview of the different postures of THOR from 20° to 30°. By changing the pelvis angle half of the total seat back angle, it's neccesary to

change the upper and lower spine bottom to match the other $2.5°$. This could be observed by the spine of THOR in the red and blue color.

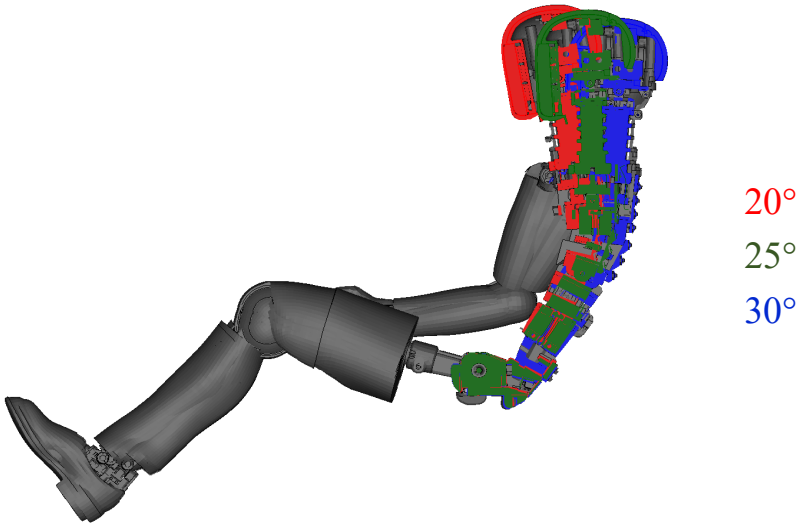

Figure 3.4: THOR ATD postures for three different seat back angles.

3.2 Impact pulses

The impact pulses considered in the simulations was full frontal-, run-off road and droptower scenarios since studies have shown that it is in these loading conditions lumbar spine fractures are of most relative importance, see Section 2.2. Visualization of principal pulse impact angles can be shown in Figure 3.5. Frontal impact pulses were taken from simulations of standardized crashes consisting of full frontal rigid barrier impacts. Three different pulses of the full frontal scenario was considered with initial velocities of 50, 56 and 64 Kilometers Per Hour (kph). Two possible run-off road accident scenarios were considered. One of them called “ditch” captures the characteristics when drifting into a ditch with rather narrow angle and finally hitting an embankment which could represent a crossing road [Jakobsson et al., 2014]. The embankment forces the vehicle into an upward motion giving rise to a large impact pulse into the occupant through the seat. The other run-off road scenario called “airborne” captures when leaving the road with an offset in z-direction introducing a phase of free flight before landing. The hard impact on wheels give rise to vertical forces into the occupant through the seat [Jakobsson et al., 2014]. The final droptower pulse was added in order to get a loading scenario with a pure z-component. The pulse give rise to a force by letting the sled fall down in a z-directional motion impacting ground.

During the impact some Supplemental Restraint System (SRS) functions was activated. For the full frontal scenarios, the airbag and pretension of the seat belt was triggered according to the impact pulse with longer trig times for the slower speeds. For the 56

kph pulse the load level of the seat belt force was also lowered at the time of interaction with the airbag in order to lower the pressure on the chest. In none of the run-off road scenarios the pyrotechnical restraints were activated.

To expand the dataset, several variations were implemented in the simulation setup. Specifically, the pulse impact angle for the full frontal crashes was varied by ±10°. Furthermore, the seat stiffness was enhanced by doubling the thickness of the seat pan and increasing the size of the springs below the cushion. Additionally, the seat belt force was varied by ±1kN.

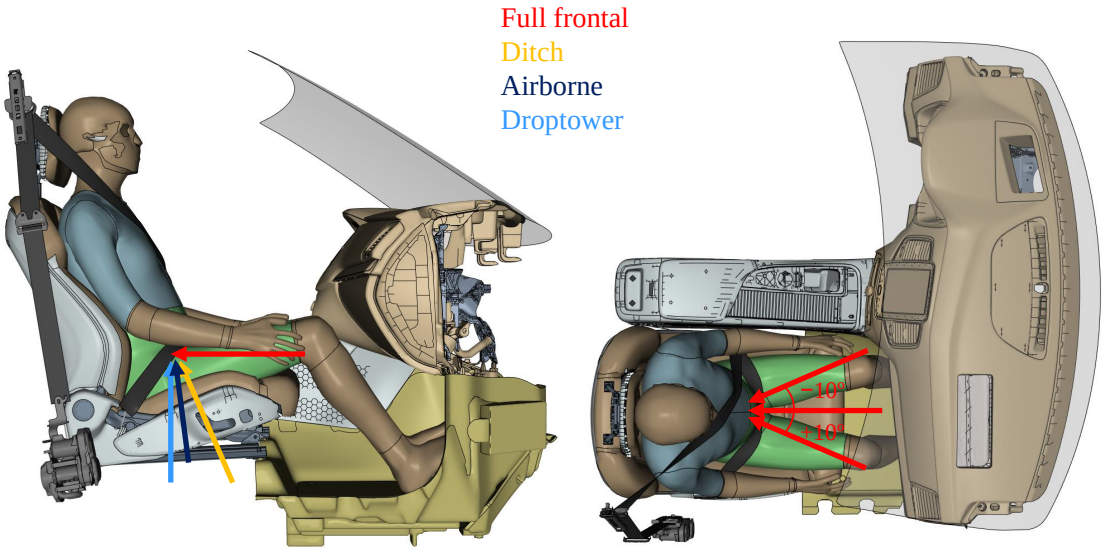

Figure 3.5: (Left) Principal visualization of XZ-components of impact pulses. (Right) Oblique variation of full frontal pulses.

3.3 Design of experiment

In the study, it was of interest to observe the effect of several independent variables on the fracture risk in the lumbar spine as predicted by the SHBM. More specifically, the effect of seat back angle, oblique pulse, seat pan stiffness, and belt force was of interest. In order to fully capture the behavior of different parameters, a full factorial study was conducted, meaning that all possible combinations of variations were simulated. In Figure 3.6, a schematic illustration can be shown to visualize how the variations were combined. It can be noted that for the run-off-road and droptower pulses, only the seat back angle and the seat stiffness were varied due to irrelevant oblique variations and no seat belt pretensioning applied as described in Section 3.2. This setup gave for the run-off-road and droptower scenarios 3 loading conditions with 3 seat back angles and 2 different seat pan stiffnesses, resulting in 18 simulations for each occupant model. The full-frontal scenario included 3 pulses, 3 belt forces, 3 oblique angles, and 2 seat stiffnesses, resulting in 162 combinations. In total, the sum of simulations performed for each occupant model was 180.

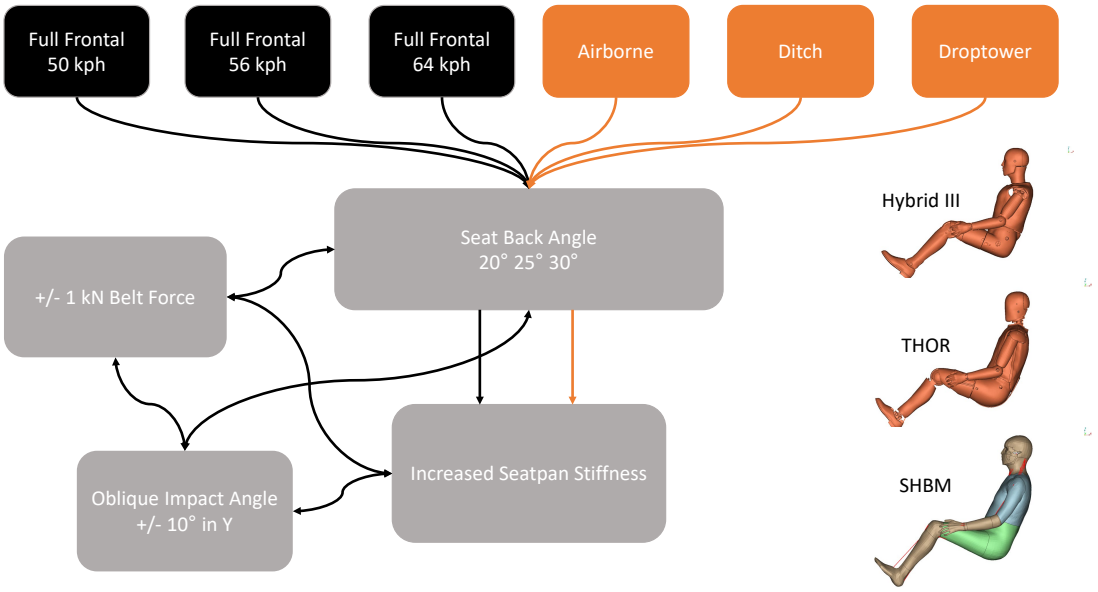

Figure 3.6: Simulation setup for the various loading conditions and variations.

From the simulations, sensor data from lumbar and pelvis sensors described in Section 2.5 was extracted, as well as superior-inferior compressive strain from lumbar vertebrae L1-L5 in the SHBM. The risk for lumbar spine fracture was calculated based on the inferior-superior strain from the SHBM, giving a probability of fracture from 0 to 1 for the ages 25, 45 and 65 years, according to Equation 2.1. Additionally, the kinematics of the ATDs and SHBM were analyzed in the simulations to ensure that the models did not slide under the seat belt, a phenomenon also called submarining, which could cause unexpected loads onto the lumbar spine that are not relevant in this study. It was also ensured that the occupant models did not penetrate any seat- or front panel surfaces in order to avoid getting stuck as the simulation proceeds.

3.4 Analysis

In the following subsections, the methods used during the analysis of the performed simulations are presented. This includes the analysis of how well recorded measures correlate with respect to the SHBM peak lumbar strain, how different simulation variations affect the peak lumbar strain, and a possible approach to optimize the correlation using DRI.

3.4.1 Correlation analysis between ATD measures and SHBM strains

In order to evaluate whether the extracted ATD measures could work as IC for the creation of new ATD IRFs, a correlation analysis was performed. This was done by evaluating a linear correlation between the measured responses extracted from the ATDs and the strain response in the SHBM. The evaluation of the linear relationship was conducted using the MATLAB function `fitlm`, which performs a linear regression as described in Section

2.7.1, and returns R^2, R^2_{adj}, and p-values for evaluating the linearity. The results were listed, and the regressions with the highest R^2 values were evaluated further.

3.4.2 SHBM internal correlation of measures against lumbar compression strain

As previous studies developing lumbar spine fracture criteria [Tushak et al., 2022] [Ortiz-Paparoni et al., 2021], used lumbar spine forces and moments as IC, the lumbar spine strains of the SHBM was compared with similar measures in the model to evaluate their potential as ICs. This was done by extracting several measures from the model and then compare it to lumbar strain. The measures chosen is the sacrum acceleration, peak force of the lumbar vertebrae and the forward bending moment. Outputs were evaluated using CFC in accordance with SAE J211-1 according to Table 2.1. These measures are located around the area of the lumbar spine and the combination of acceleration, force and moment would be good enough to capture the driving forces of the compressive strain in the lumbar. Linear regression are performed for the exported peak of the measures and the same regression analyze tools is used to evaluate the results.

3.4.3 Multiple Linear Regression

To examine the impact of each variation on the risk of lumbar spine fractures, multiple linear regression were performed. The variations were assumed to have a linear relationship with the risk response, and linear regressions were performed with multiple independent variables as input. Apart from the selected IC, the independent variables included the variation of seat back angle, oblique pulse angle, seat stiffness and seat belt force. Since the variation of seat belt force and oblique pulse angle was not applied in the run-off road scenarios and droptower crashes explained in section 3.3, they were included in a separate multiple regression, which only encompassed the full frontal crashes. The multiple regression analysis was carried out using the MATLAB function `fitlm` with multiple input variables, which returns coefficients β_i to be utilized in the formulation of a multiple regression as described in Eq. 3.1. Variations associated with large coefficients are more significant than those with small coefficients.

$$y = \alpha + \beta_1 x_1 + \beta_2 x_2 + ... + \beta_i x_i \tag{3.1}$$

To visualize the influence of the variations the multiple regression was plotted as a bar chart where each bar represents a variation. The magnitude and the sign of the bar is a measure of how big of an effect it has on the strain. In order to ensure a relevant representation of the effect of each variation, the inputs x_i were normalized within the range of -1 to 1. To be able to consider that a variant has a statistical effect on the strain, it requires that the p-value is below 0.05. The multiple regression model also has a 95% confidence bound output which was plotted for each variant.

3.4.4 Dynamic Response Index (DRI)

The DRI is an IC that was developed for ATDs and used to study the correlation of spinal injuries to acceleration in aircraft ejections [Lynch et al., 2012], and was an additional

potential IC that was examined. The DRI is a calculated value, see Eq. 3.2, equivalent to the maximum dynamic compression of the spinal column. The DRI is calculated based on a simplified single degree of freedom mass-spring-damper system representing the spine connected to the upper body, see Figure 3.7. The system can be described by the 2nd order Ordinary Differential Equation (ODE) presented in Eq. 3.3 [Lynch et al., 2012]. The purpose of examining the DRI as an injury criterion was because the ODE is described with the vertical acceleration-time profile as input from the ATD filtered according to Table 2.1, and the damping ratio $\xi = \frac{c}{2\sqrt{mk}}$, which would make it possible to tune the kinematics of the ATDs such that the measured peak values occur at the same time as the peak strain is measured in the SHBM. The relative displacement δ was calculated by explicitly solving the 2nd order ODE using the Euler forward method. The optimal damping ratio ξ was then determined by iteration until the highest R^2 value was reached between DRI and the SHBM peak lumbar strain.

$$DRI = \frac{\omega_n^2 \delta_{max}}{g} \tag{3.2}$$

$$\ddot{\delta} + 2\xi\omega_n\dot{\delta} + \omega^2\delta = a_z \tag{3.3}$$

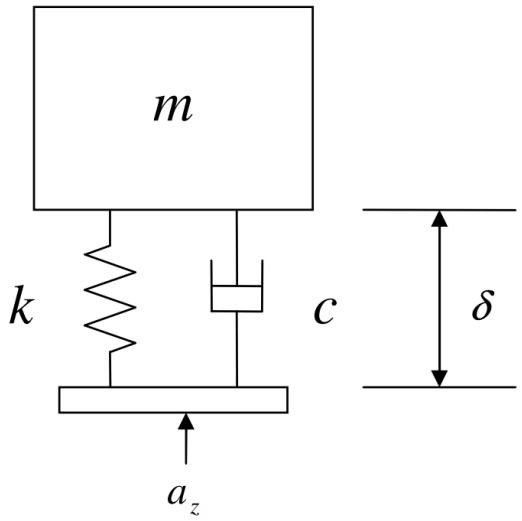

Figure 3.7: Visualization of simplified single degree of fredom mass-spring-damper system respresenting the dynamics in the spine column [Lynch et al., 2012].

3.5 Construction of IRFs

The construction of an IRF can be approached through various methods, yet the ultimate outcomes remain consistent. An IRF encapsulates data regarding how the risk of injury changes across a defined measure. Typically, an IRF follows a $Logit^{-1}$ pattern, with the intersection of the risk axis positioned at 0. The procedure for creating an IRF involved first establishing a transfer function between the maximum compressive strain from the SHBM and the lumbar spine injury criteria from the ATDs. This function was then applied to Equation 2.1. The transfer function, depicted in Equation 3.4, was linear, with C_2 representing the intersection on the strain axis and C_1 denoting the slope. These coefficients varied depending on the chosen injury criteria, loading case, and ATD used. Standard errors resulting from linear regressions using `fitlm` were accessible. They, along with the standard error from the SHBM IRF, were utilized using bootstrapping to determine the probability of fracture function in Equation 2.1, with substituted strain, and to establish a 95% confidence interval [Tibshirani, 2024]. It's important to note that this method relies heavily on a strong correlation between strain and the IC, otherwise, errors in both the transfer function and the IRF could lead to wide confidence bounds. The bootstrap method of calculating involved selecting coefficient values and their corresponding standard errors and then randomized distributed along the normal curve. A total of 50,000 bootstrap variations were generated, and the 95% confidence bounds were determined by selecting the $1,250^{th}$ and $48,750^{th}$ IRFs, thereby establishing a 95% confidence area.

$$\epsilon_{SHBM} = C_1 \times IC_{ATD} + C_2 \tag{3.4}$$

3.6 Verification of IRFs using rear seat simulations

As a final step in this thesis, simulations in an alternate seat environment, represented by the rear-seat mid-position of a medium-sized SUV, was conducted to verify the applicability of the constructed IRF. The rear seat mid-position is different from the from the seat environment in that the belt load limit is higher, there is not airbag for distributed loading to the head and chest, and the seat pan consists of an Expanded Polypropylen (EPP) foam material with an antisubmarining ramp geometry instead of an adjustable mechanism [Lundell et al., 1981]. This positioning procedure was more complex as the legs of the occupant models needs to be positioned on the sides of the tunnel. The lower legs therefore need to be placed with a higher slope to the sides to fit between the front-row seats. This setup of simulation uses the default values for the seating angle (25°) with the arms beside the upper thigh. This setup is an imitation of the front row 25° cases. The simulation setup of the vehicle enviroment and the positioning of the SHBM is visualized in Figure 3.8.

Figure 3.8: Visualization of the positioned SHBM in the mid rear seat in the verification vehicle enviroment.

The pulses utilized in this setup were frontal impacts at 50, 54, and 60 kph. All models, including SHBM, THOR, and HIII, are simulated. This generate an additional 9 data points, which should be compared to the front seat setup. This is accomplished by selecting the IC that has the highest correlation for the models and calculating the risk corresponding to the IRF created for the ATDs. Then, this risk is compared to the SHBM IRF. By subtracting the two probabilities from each other, the results will indicate whether the model is over- or under-predicting the risk of lumbar fracture.

4

Results

The peak pelvis Z-acceleration plotted with respect to SHBM peak lumbar strain from all the 180 simulations for each occupant model for the full-factorial method described in Section 3.3 is shown in Figure 4.1. The scatter plots demonstrate a wide range of values which made it hard to identify any noticeable trends without conducting additional data analysis. Subsequent sections present results obtained from various data analysis methods aimed at identifying correlated ICs in both Hybrid III and THOR, along with corresponding IRFs based on these findings.

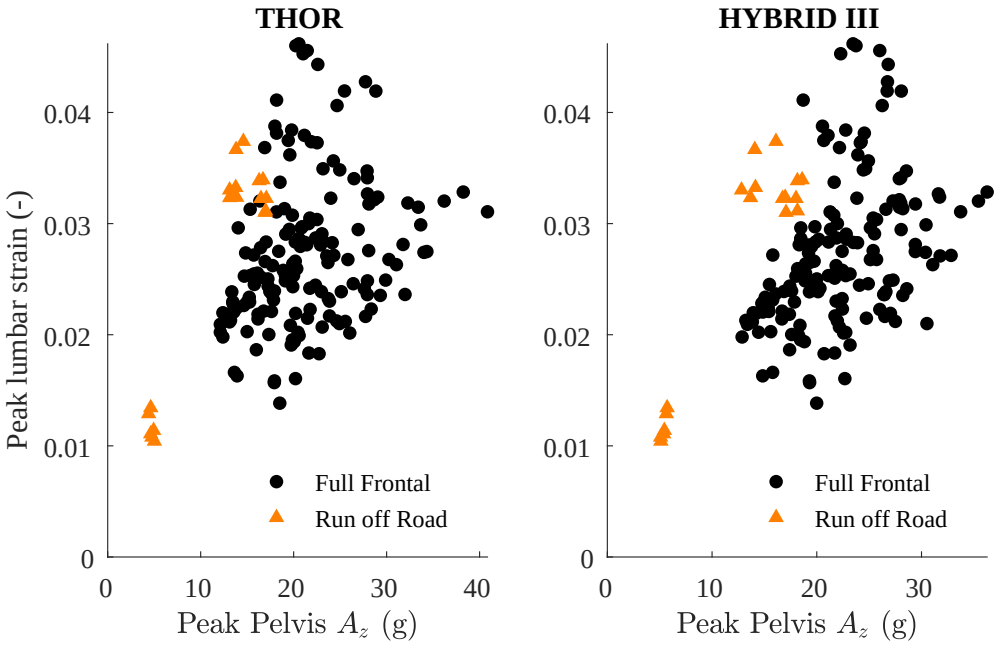

Figure 4.1: Scatter plot visualizing measured ATD pelvis z-acceleration responses against SHBM peak lumbar strain.

4.1 Distribution of predicted fracture risks

Based on the performed simulations, it was of interest to note the distribution of predicted fracture risks for vertebrae L1-L5 in the SHBM across a diversity of ages. The distributions for 25, 45, and 65-year-old occupants are shown in Figure 4.2, calculated using Eq. 2.1. The histograms illustrates a notable shift in risk density across different age categories. Specifically, for a 25-year-old occupant, the majority of risks reside in the low-risk region, whereas for a 65-year-old, risks tend to cluster more in the high-risk region. This observation reflects the influence of age as a covariate in the IRF, as described by Eq. 2.1.

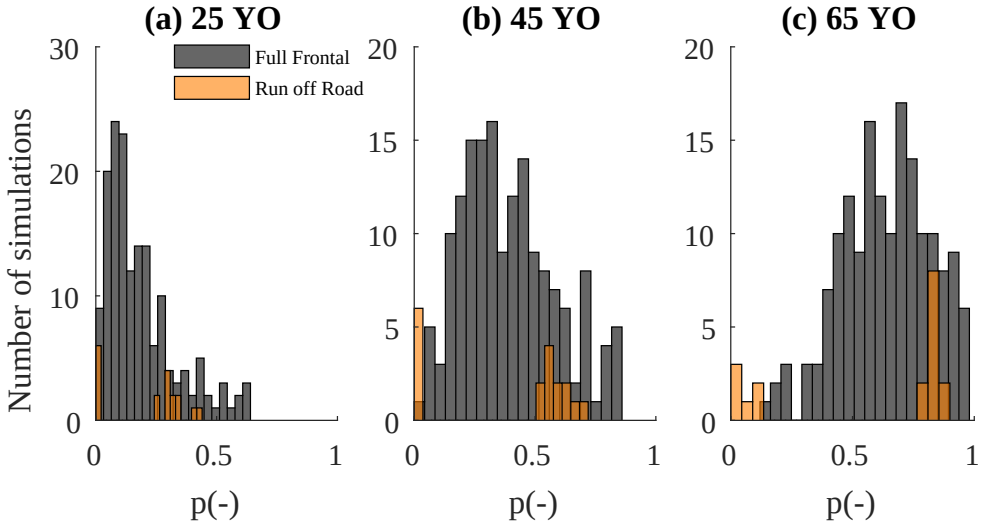

Figure 4.2: Bar charts presenting number of simulations with certain fracture risk for three occupant ages.

4.2 Correlation of ATD measures

Correlation results from linear regressions concerning the SHBM peak lumbar strain as described in Section 3.4.1 can be shown tabulated for all outputted sensor values in Appendix A.1 for Hybrid III and A.2 for THOR. A subset of measures that were considered as potential IC for the ATDs are presented in Table 4.1. Comparing the subset with the total set of output measures shows that the selected subset also represents the majority of measures with the highest correlation. Other measures with R^2 measures close to 0 were excluded from further analysis. Still linear regression on the full combined data sample results in relatively low correlation throughout the lists with the highest R^2 of 0.44 for Hybrid III Lower Lumbar spine peak F_Z and 0.23 for THOR T12 peak A_Z. Because of the low correlations for the full data set, linear regression was performed on subsamples divided into full frontal and run-off road crashes to see if loading cases follow different trends. The results of dividing the datasample info full frontal and run-off road showed an increase in R^2, especially for the run-off road cases. This means that for the current data, the more accurate correlation between ATD measures and SHBM lumbar strain can be found if run-off road scenarios are treated separately. Visualizations of the regressions of measures with the most potential (highest R^2) are shown in Figure 4.3 and Figure 4.4 for Hybrid III and THOR, respectively.

Table 4.1: Linear regression results for some selected ATD peak measures with respect to SHBM peak lumbar strain.

ATD measures vs. SHBM Lumbar strain									
Peak Measure	Combined			Full Frontal			Run-off Road		
Hybrid III	R^2	R^2_{adj}	p	R^2	R^2_{adj}	p	R^2	R^2_{adj}	p
Pelvis A_Z	0.21	0.21	0.00	0.18	0.18	0.00	0.87	0.86	0.00
Pelvis A_R	0.01	0.01	0.14	0.00	-0.01	0.72	0.81	0.80	0.00
Lower Lumbar F_Z	0.44	0.44	0.00	0.40	0.40	0.00	0.86	0.86	0.00
Upper Lumbar F_Z	0.23	0.23	0.00	0.30	0.30	0.00	0.66	0.64	0.00
THOR	R^2	R^2_{adj}	p	R^2	R^2_{adj}	p	R^2	R^2_{adj}	p
Pelvis A_Z	0.12	0.12	0.00	0.08	0.07	0.00	0.88	0.88	0.00
Pelvis A_R	0.08	0.07	0.00	0.12	0.11	0.00	0.91	0.90	0.00
T-Spine F_Z	0.07	0.07	0.00	0.04	0.03	0.02	0.73	0.72	0.00
T12 A_Z	0.23	0.23	0.00	0.22	0.21	0.00	0.90	0.89	0.00

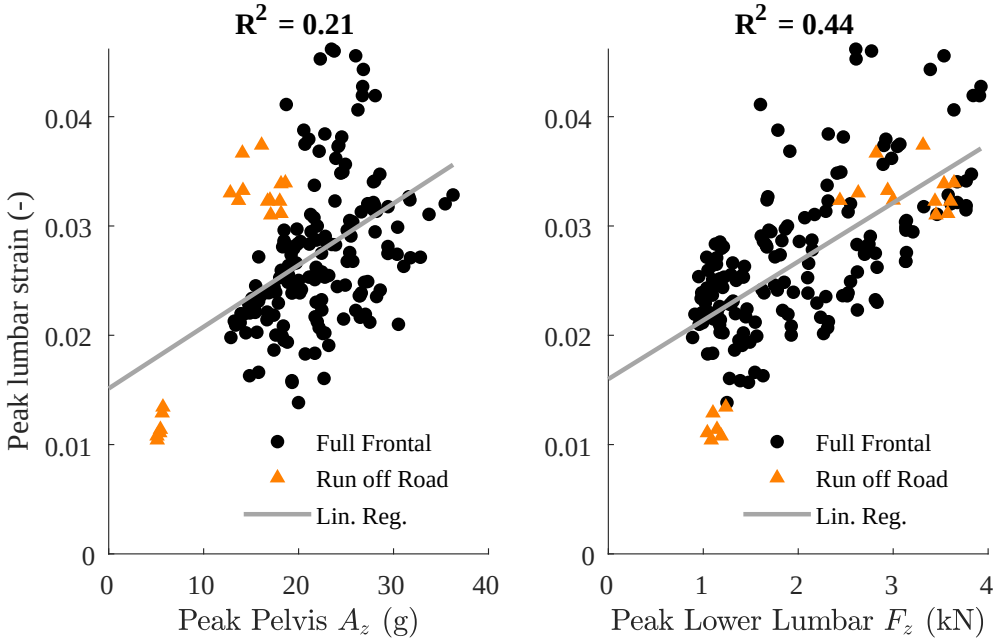

Figure 4.3: Linear regressions for measures in Hybrid III with highest R^2 in combined loading scenarios with respect to SHBM peak lumbar strain.

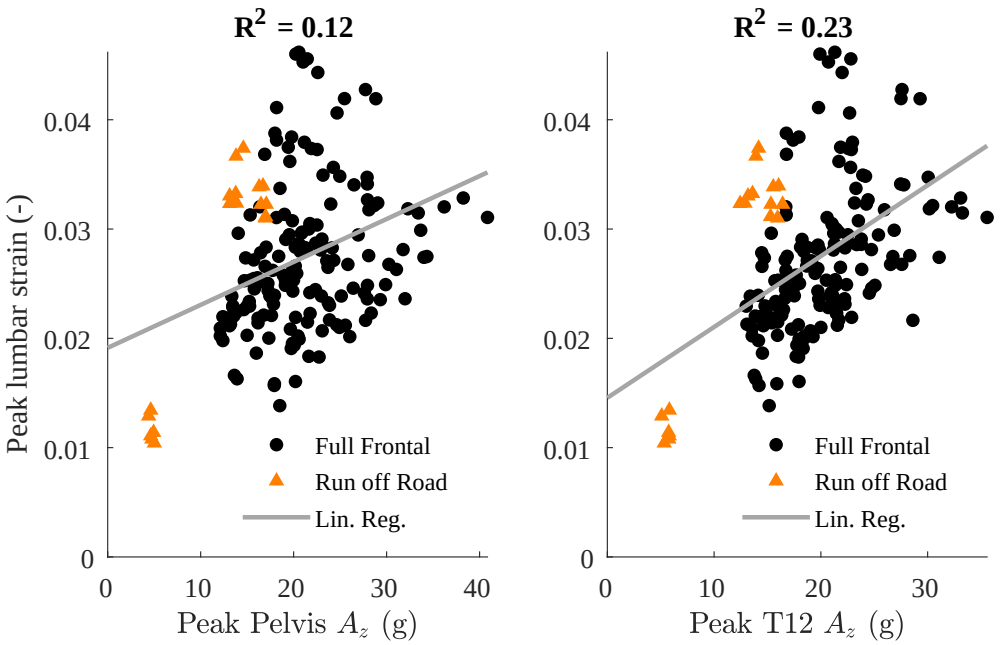

Figure 4.4: Linear regressions for measures in THOR with highest R^2 in combined loading scenarios with respect to SHBM peak lumbar strain.

4.3 SHBM internal correlation of measures with respect to peak lumbar strain

In the preceding section, a correlation analysis was conducted to examine the relationship between the evaluated ATD measures and SHBM peak lumbar strain. However, the analysis revealed a relatively weak correlation for the combined dataset. To delve deeper into the internal dynamics of the SHBM, an additional analysis was performed.This subsequent examination focused on exploring the internal correlations within the SHBM itself, employing a similar methodology as in the previous analysis. The results are detailed in Table 4.2, while visual representations of peak lumbar F_Z and Sacrum A_Z, comparable with pelvis A_Z, can be found in Figure 4.5. As for the ATDs, the correlation between observed measures and the peak lumbar strain shows a low correlation for the combined case but is better when dividing into full frontal and run-off road scenarios separately.

Table 4.2: Linear regressions results for SHBM measures with respect to lumbar compression strain.

SHBM measures vs. SHBM Lumbar strain									
Peak Measure	Combined			Full Frontal			Run-off Road		
SHBM	R^2	R^2_{adj}	p	R^2	R^2_{adj}	p	R^2	R^2_{adj}	p
Lumbar F_Z	0.33	0.32	0.00	0.41	0.40	0.00	0.98	0.98	0.00
Lumbar M_Y	0.06	0.06	0.00	0.19	0.18	0.00	0.01	-0.05	0.72
Sacrum A_X	0.00	0.00	0.58	0.00	-0.01	0.82	0.82	0.80	0.00
Sacrum A_Y	0.14	0.14	0.00	0.17	0.17	0.00	0.67	0.65	0.00
Sacrum A_Z	0.01	0.00	0.19	0.00	-0.01	0.82	0.65	0.63	0.00
Sacrum A_R	0.01	0.01	0.14	0.00	-0.01	0.70	0.65	0.62	0.00

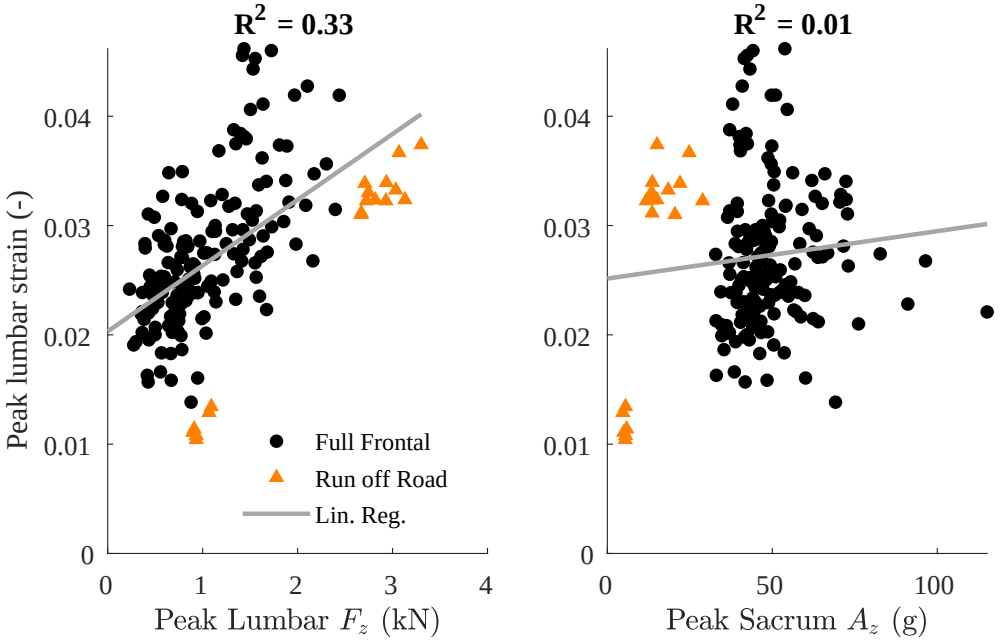

Figure 4.5: Linear regression plots for two selected internal SHBM measures with respect to corresponding SHBM peak lumbar strain.

In the subsequent Histogram 4.6, multiple linear regression is visualized with simulation variations on the X-axis and SHBM strain on the Y-axis. This figure illustrates the effect each variation has on the strain. Since the independent variables are normalized, each variation is weighted equally, and the magnitude of the bar represents its influence on the strain of the SHBM. Each variation demonstrates a positive impact on the SHBM strain, suggesting that a more reclined position of the seat results in higher strains. The same trend applies to increased seatpan stiffness, oblique impact angle, and belt force. The only excluded variation is pulse severity, due to its p-value above 0.05. No statistical measure confirms that this variation has an impact on the strain.

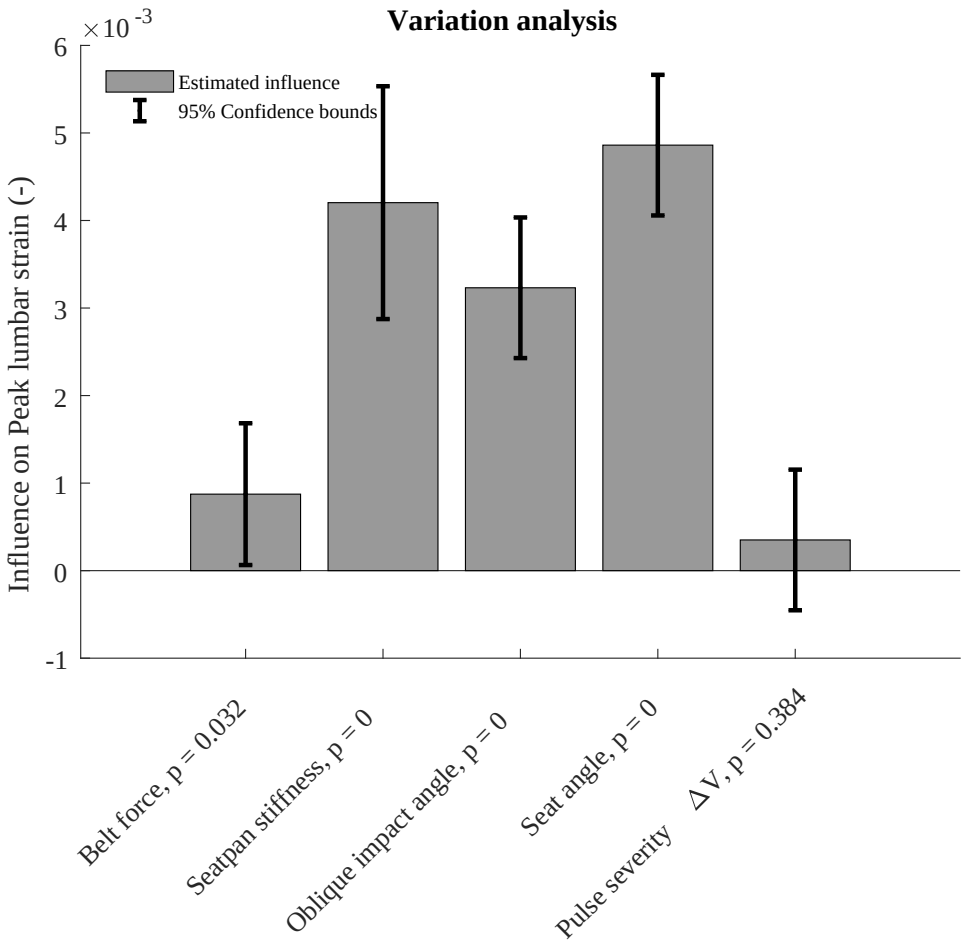

Figure 4.6: Multiple Regression analys of how the peak lumbar strain is influenced by simulation variations.

To find patterns in the cluster of points for the model, separated linear regressions with corresponding $R^2 - value$ was made for all types of variations and some selected IC and these are plotted in the Figures 4.7-4.9. The plots show that linear regression using strain as a dependent value and lumbar compression force as an independent can capture every variation similarly.

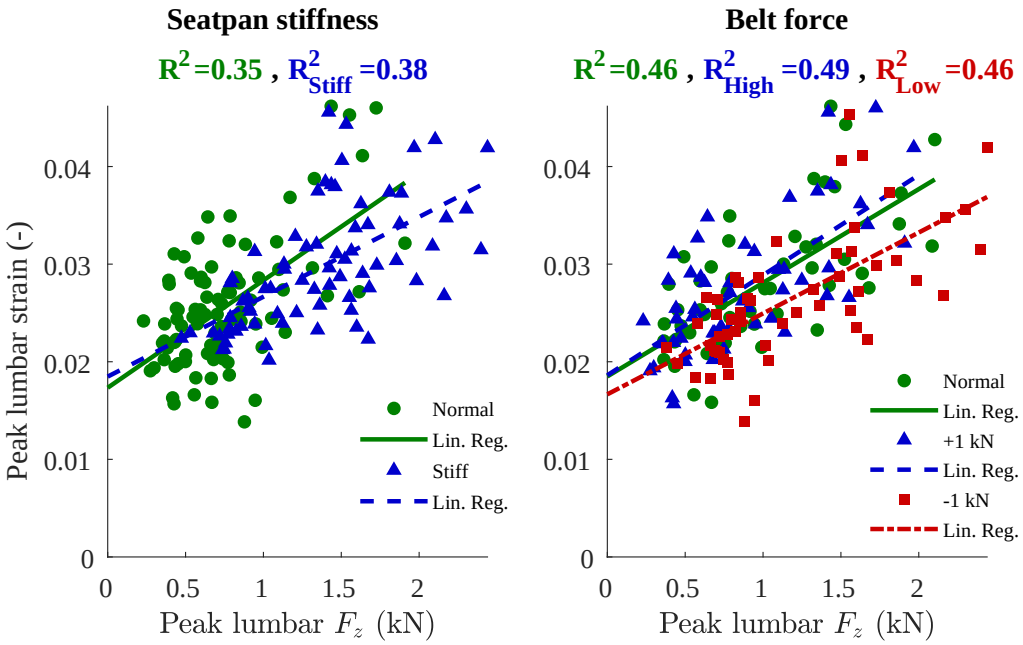

Figure 4.7: Linear regression and visualization of data sample for variation of seatpan stiffness and belt force using SHBM and Peak F_Z as IC.

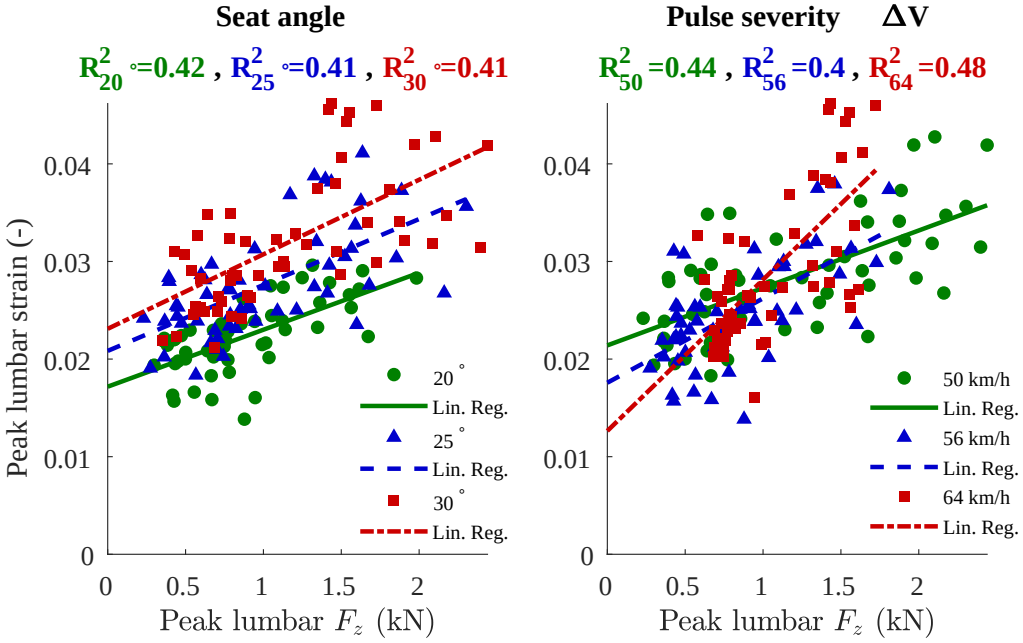

Figure 4.8: Linear regression and visualization of data sample for variation of seat back angle and pulse severity using SHBM and Peak F_Z as IC.

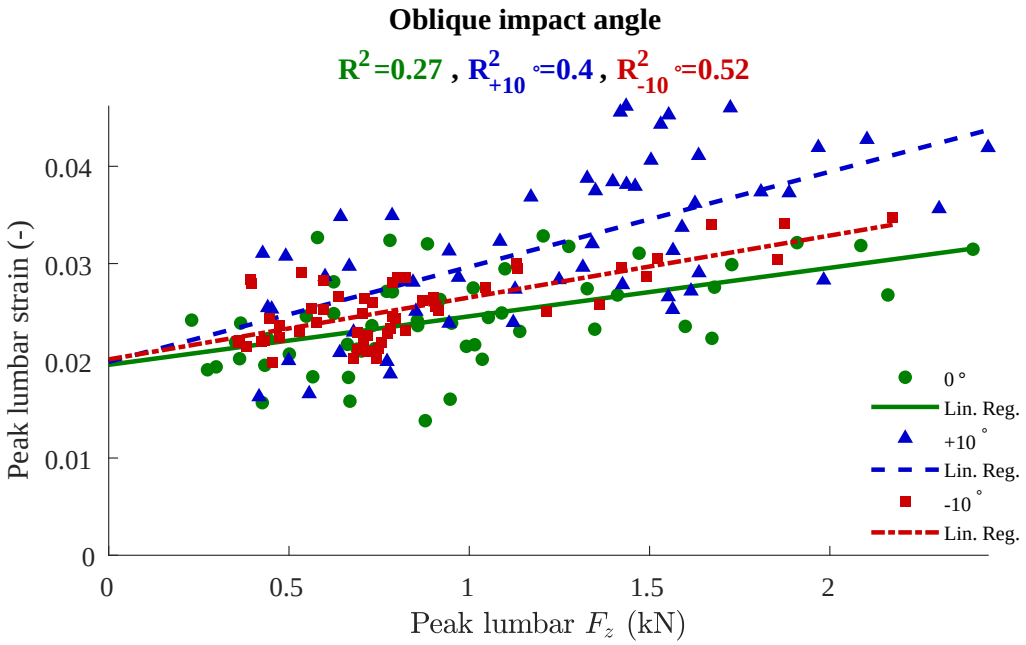

Figure 4.9: Linear regression and visualization of data sample for variation of oblique impact angle using SHBM and Peak F_Z as IC.

4.4 Correlational effects of variable changes using Hybrid III ICs

For the measures with highest R^2 which could be used as IC, presented in Table 4.1 the effect of simulation variations was analyzed as described in Section 3.4.3. The effect of each variation in the full frontal simulations is visualized for peak pelvis A_Z as ATD measure in Figure 4.10-4.12. From the figures, it is evident that the dataset could be distinctly divided into subsets showing different trends. Especially the oblique angle variation, Figure 4.12, shows that from the linear regression on the subsamples the R^2 values for the corresponding subsample significantly increased, meaning that the angled pulses gave rise to different loading scenarios onto the lumbar spine. For the other variations, the R^2 values were low meaning that the single variations were not changing the overall trend significantly. The analysis were made for all ICs presented in Table 4.1, except Peak Pelavis A_R which was excluded due to its low correlation, and can be found in Appendix A.4. From the analysis it was noted that the stratification of the data into the different oblique impact angles gave highest correlation for respectively impact angle using Peak Pelvis A_Z as injury criteria with $R^2_{0^\circ} = 0.62$, $R^2_{+10^\circ} = 0.49$ and $R^2_{-10^\circ} = 0.85$. From Table 4.1 it can also be noted that Peak Pelvis A_Z had the highest correlation for run-off road scenarios with $R^2 = 0.87$. As a result of this Peak Lower- and Upper Lumbar F_Z was excluded for further analysis as IC due to the presence of better options.

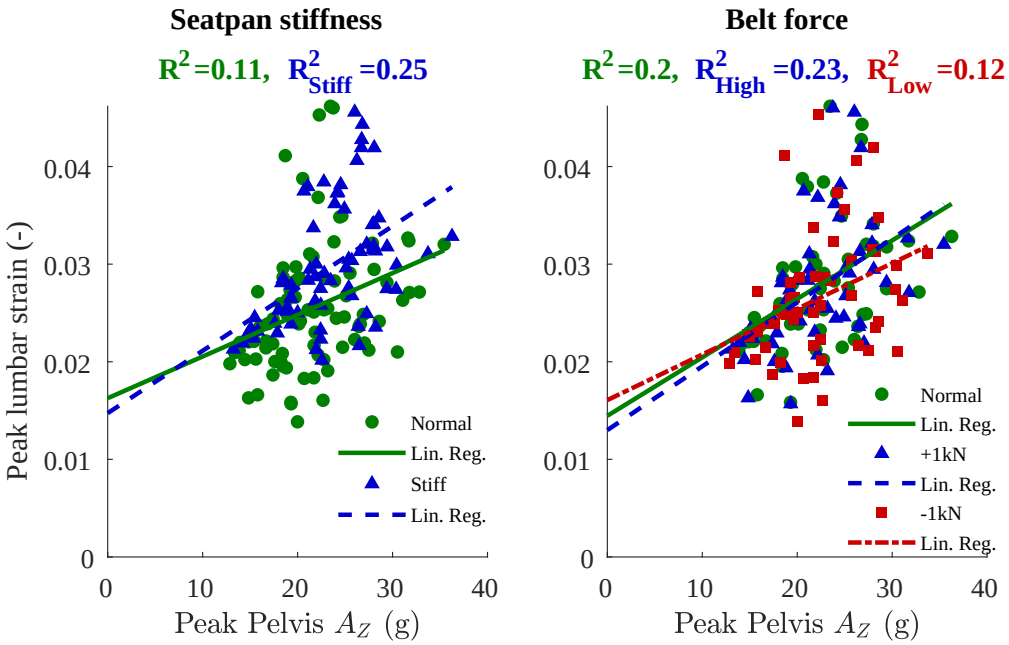

Figure 4.10: Linear regression and visualization of data sample for variation of seatpan stiffness and belt force using Hybrid III and Peak Pelvis A_Z as IC.

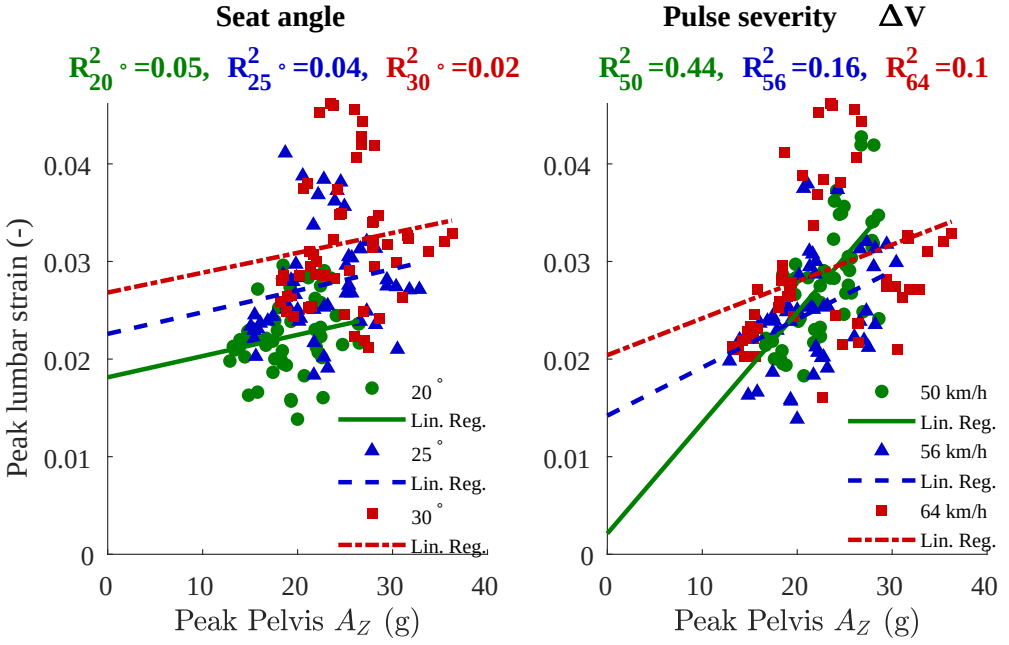

Figure 4.11: Linear regression and visualization of data sample for variation of seat back angle and pulse severity using Hybrid III and Peak Pelvis A_Z as IC.

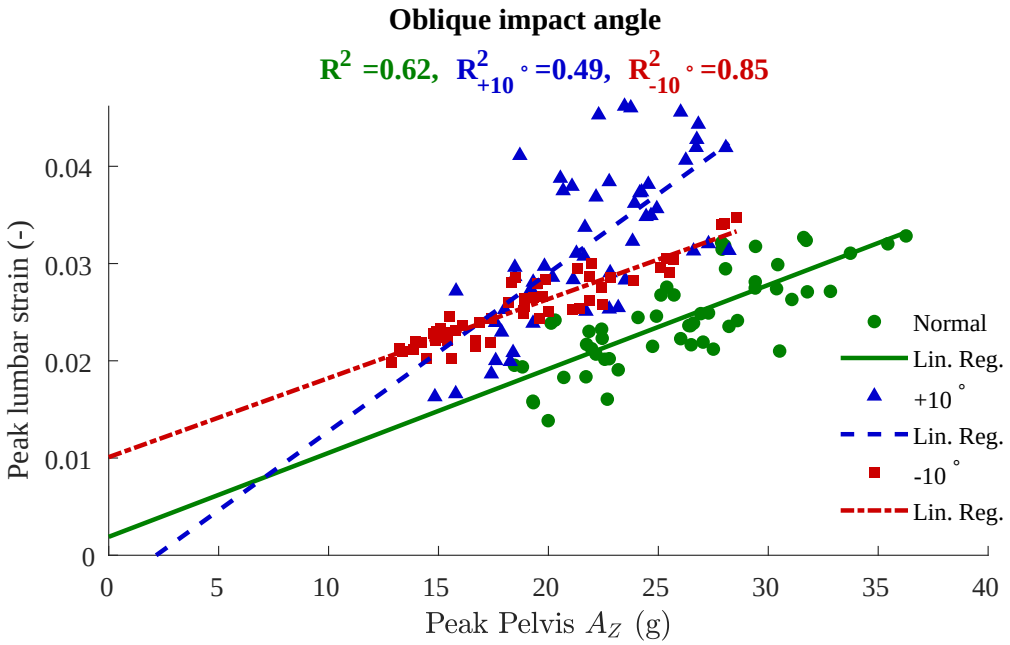

Figure 4.12: Linear regression and visualization of data sample for variation of oblique impact angle using Hybrid III and Peak Pelvis A_Z as IC.

4.5 Correlational effects of variable changes using THOR ICs

A similar analysis as for Hybrid III was conducted and the effect of each variation was scattered for the ICs presented in Table 4.1. The corresponding plots are displayed in Figures 4.13-4.15 for Peak Pelvis A_Z and the rest in Appendix A Figure A.15-A.23. Similar to the Hybrid III, the dataset for THOR exhibits diverse trends. Notably, an increase in seatpan stiffness influences the strain, also captured by the IC in THOR. Although multiple regression analysis suggests that belt force also affects strain, its impact is less discernible in the plots. Specifically, increasing belt force marginally elevates the SHBM strain. Seat angle caused an interesting pattern, the dataset divided into three angles implied that a more reclined seat angle caused higher strain. Additionally, it is important to note a distinct observation regarding the oblique variations, it results in a separation within the dataset. This divergence is attributed to the dispersion of data points resulting from different impact angles, possibly indicating diverse injury mechanisms experienced by the model causing a decrease in correlation for the full model. In a similar manner as for Hybrid III, increased correlation for the corresponding oblique impact angles could be seen for the ICs. Largest correlation was found using Peak Pelvis A_Z and Peak T12 A_Z. Other ICs such as Peak Pelvis A_R and Peak T-Spine F_Z was excluded for further analysis.

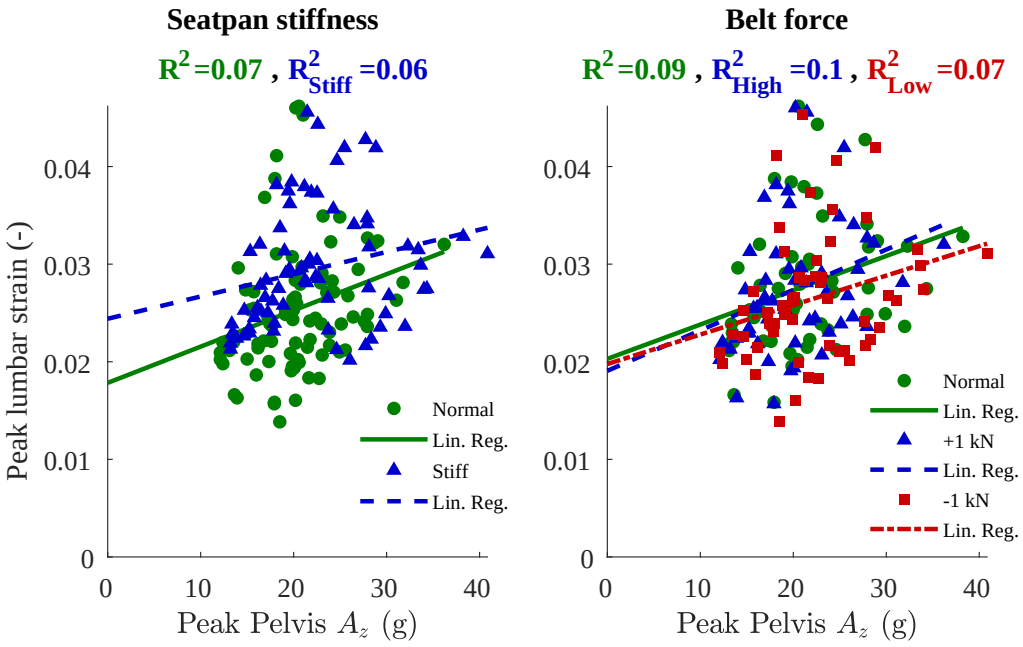

Figure 4.13: Linear regression and visualization of data sample for variation of seatpan stiffness and belt force using THOR and Peak Pelvis A_Z as IC.

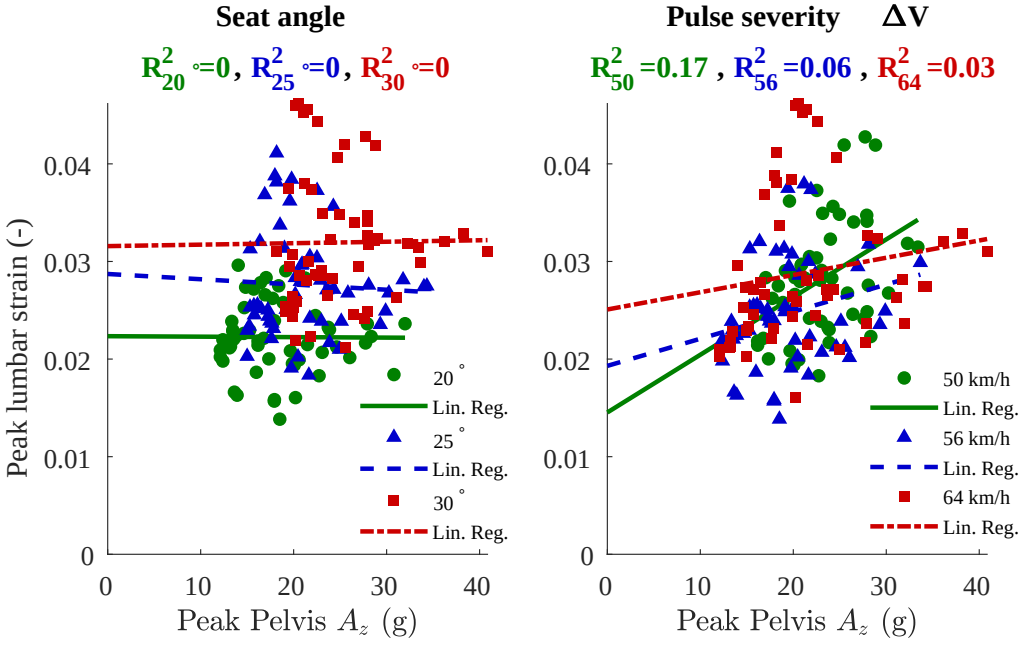

Figure 4.14: Linear regression and visualization of data sample for variation of seat back angle and pulse severity using THOR and Peak Pelvis A_Z as IC.

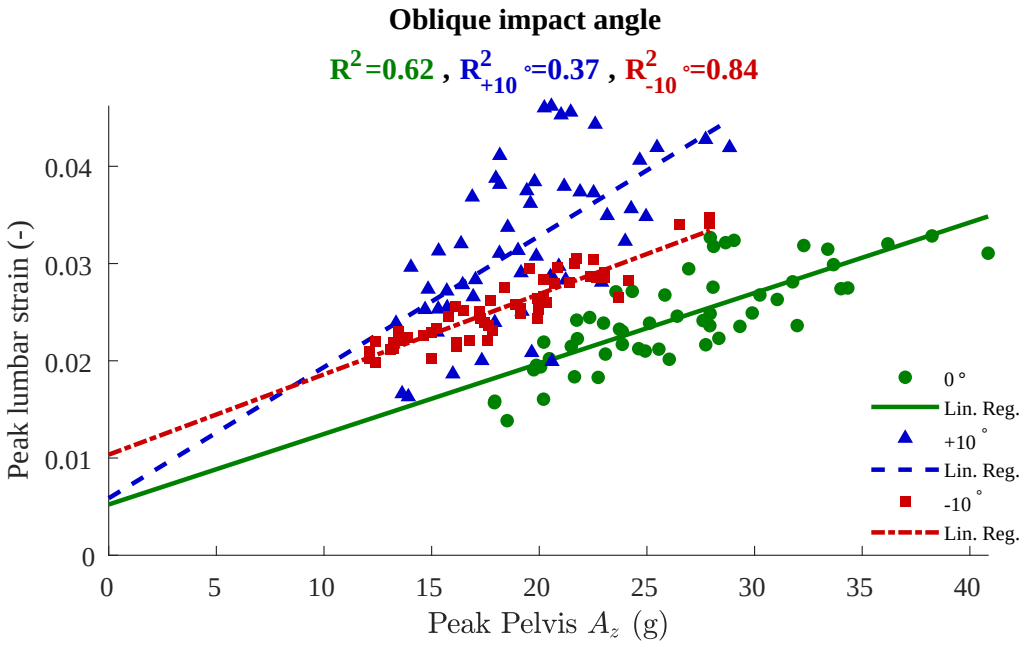

Figure 4.15: Linear regression and visualization of data sample for variation of oblique impact angle using THOR and Peak Pelvis A_Z as IC.

4.6 Dynamic Response Index (DRI)

As a consequence of the findings in the variation analysis, DRI was calculated for the stratification of data by impact angle. From this, a higher R^2 value was obtained for each impact pulse and to further optimize the output of the models DRI was calculated for the pelvis acceleration. The DRI calculation required an optimization for the natural frequency and the damping constant which was made to fit the acceleration of the model into the strain.

4.6.1 Hybrid III

Frontal scenarios using default values of the natural frequency and damping ratio can be viewed in Figure 4.17. DRI for the run-off road scenarios was not calculated since the correlation of those measures already showed high R^2-values. The optimized DRI regressions after conducting the parametric sweep can be shown in Figure 4.16. In the figure, the DRI-based linear regressions are visualized for the oblique pulse variations with corresponding R^2-values and optimized parameters ω and ξ. It can be noted that for the $+10°$ oblique case no extreme point was found in the parameter sweep interval but on the boundary. In this case, the default parameter values from Lynch *et al.* (2012) were used. Comparing the obtained R^2-values with the ones based on the correlation analysis using Peak Pelvis A_Z, Figure 4.12, it can be noted that all $R^2_{0°}$, $R^2_{+10°}$ and $R^2_{-10°}$ has increased from 0.62, 0.49 and 0.85 to 0.88, 0.56 and 0.87.

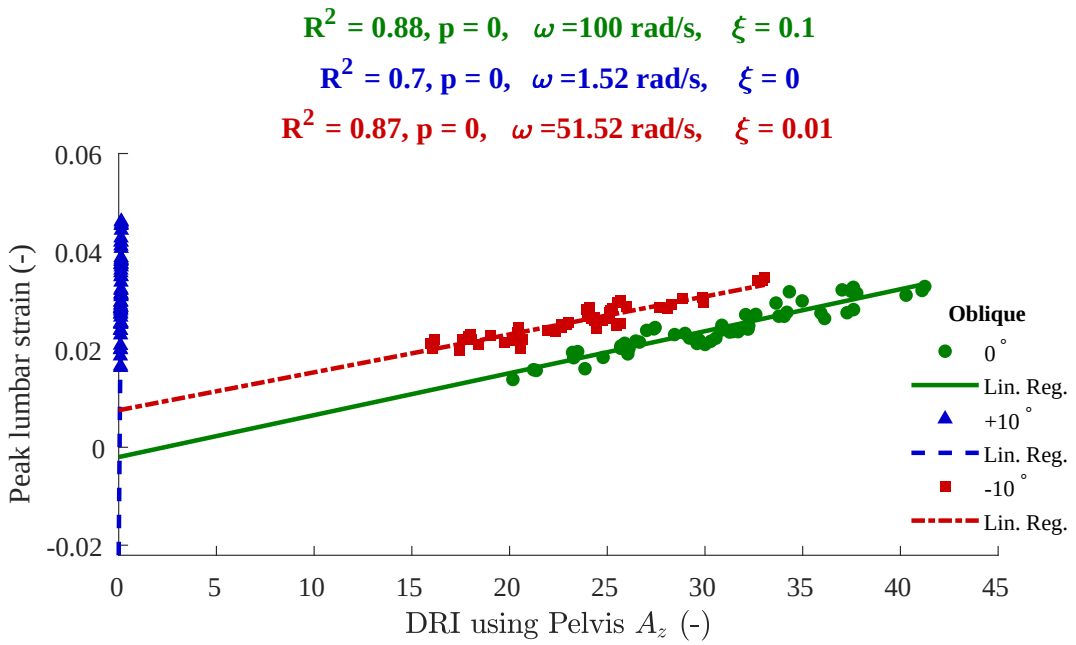

Figure 4.16: Correlation of DRI based on Hybrid III Pelvis A_Z with respect to SHBM peak lumbar strain for different oblique angles for full frontal loadcases using optimized values of ω and ξ.

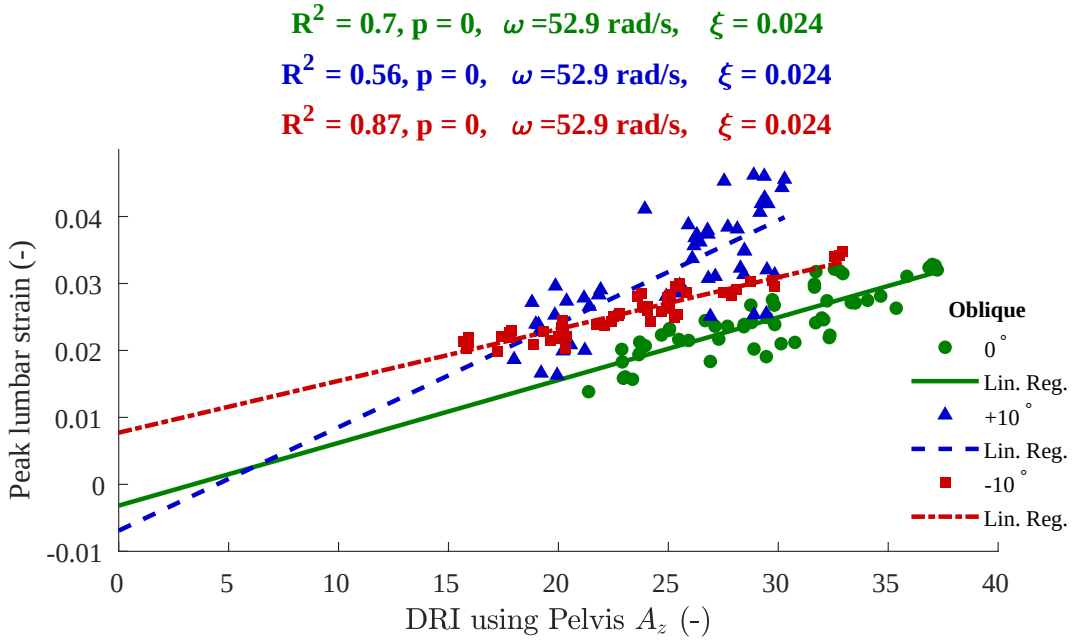

Figure 4.17: Correlation of DRI based on Hybrid III Pelvis A_Z with respect to SHBM peak lumbar strain for different oblique angles for full frontal loadcases using default values of $\omega = 52.9$ rad/s and $\xi = 0.024$ according to [Lynch et al., 2012].

4.6.2 THOR

As Figure A.20 showed, a high correlation was obtained for separation in the dataset. By calculating the DRI value for the pelvis acceleration and optimizing the free parameters, an increase in correlation was expected. This could be shown in Figure 4.18. The effect of calculating the DRI value is almost 0.2 in R^2 magnitude compared to the acceleration on its own in Figure 4.15. This increase in correlation enables a more reliable connection between the output from THOR and SHBM.

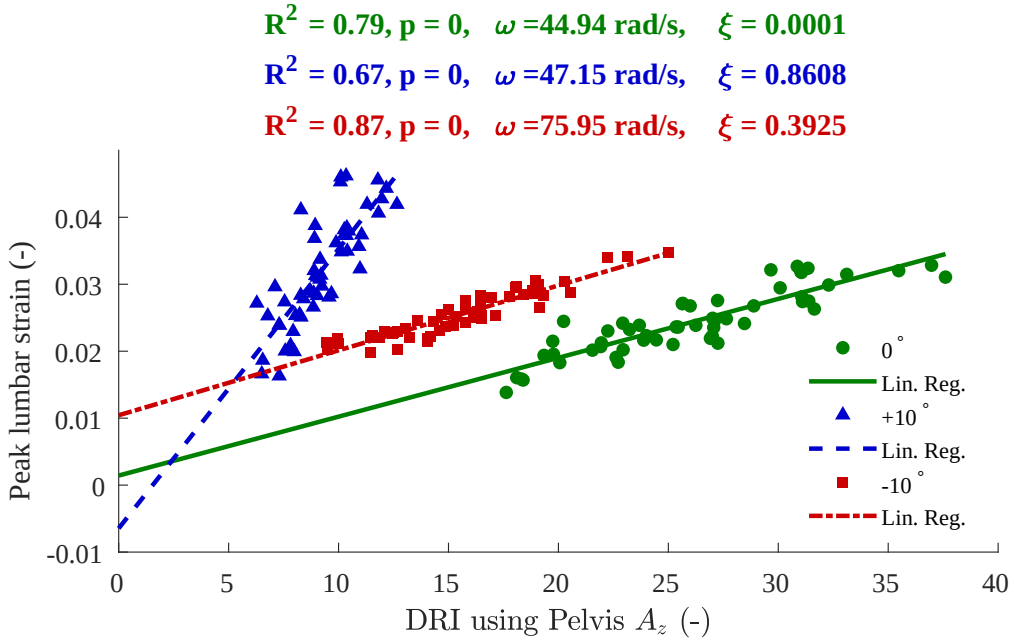

Figure 4.18: Correlation of DRI based on THOR Pelvis A_Z with respect to SHBM peak lumbar strain for different oblique angles for full frontal loadcases using optimized values of ω and ξ.

By reusing parameters of ω and ξ according to Lynch*et al.*,(2012), high correlation was obtained but according to the previous figure does further tuning of parameters increase correlation. By using the same parameters, comparison of the DRI value and the corresponding risk of lumbar fracture could be analysed in the IRF chapter 4.8 and 4.9.

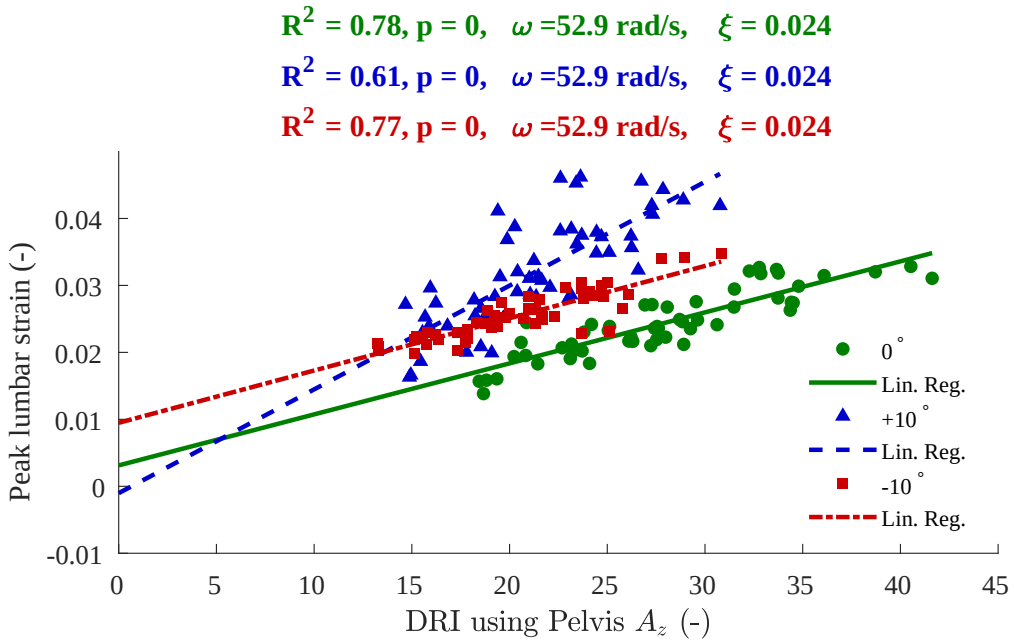

Figure 4.19: Correlation of DRI based on THOR Pelvis A_Z with respect to SHBM peak lumbar strain for different oblique angles for full frontal loadcases using default values of $\omega = 52.9$ rad/s and $\xi = 0.024$ according to [Lynch et al., 2012].

4.7 Selected Injury Criteria

Based on the correlation analysis and the analysis of variational effects performed in previous sections the selected ICs for creation of IRFs are summarized in Table 4.3. The selected ICs show an increase in correlation when the loading cases were separated within the full frontal oblique pulse variations and run-off road scenarios, which also the new IRFs will be generated for. The DRI IC is a more complex measure to be used and needs to be solved explicitly for every simulation, but was kept with the motivation that it showed such good optimizations for more accurate risk predictions.

Table 4.3: Summary of selected ICs for the ATDs.

Hybrid III	THOR
Peak Pelvis A_Z	Peak Pelvis A_Z
DRI based on Pelvis A_Z	DRI based on Pelvis A_Z
	Peak T12 A_Z

4.8 Hybrid III Injury Risk Functions

In the following subsections generated IRFs are presented for the separated load scenarios full frontal and run-off road based on the method described in Section 3.5, where the linear regressions with selected ICs were integrated into the SHBM IRF.

4.8.1 Full Frontal with separated impact angle

The injury risk curves for a 45-year-old occupant are shown in Figure 4.20 and Figure 4.21. Injury risk curves for occupants aged 25 and 65 are provided in Appendix B. Since the ATD measures are in the range between approximately 12 to 35 g for the pelvis peak acceleration and 15 to 40 for DRI, the risk prediction curves are generated by extrapolation of the linearly regressed strain to obtain risks from 0 to 1. Due to the uncertainty of the SHBM IRF Eq.2.1, and the linear regressions, there is a combined uncertainty that is also visualized with a 95% confidence interval. Due to the improved correlation using DRI, the confidence bounds using DRI are narrower than those using peak pelvis A_Z as the IC.

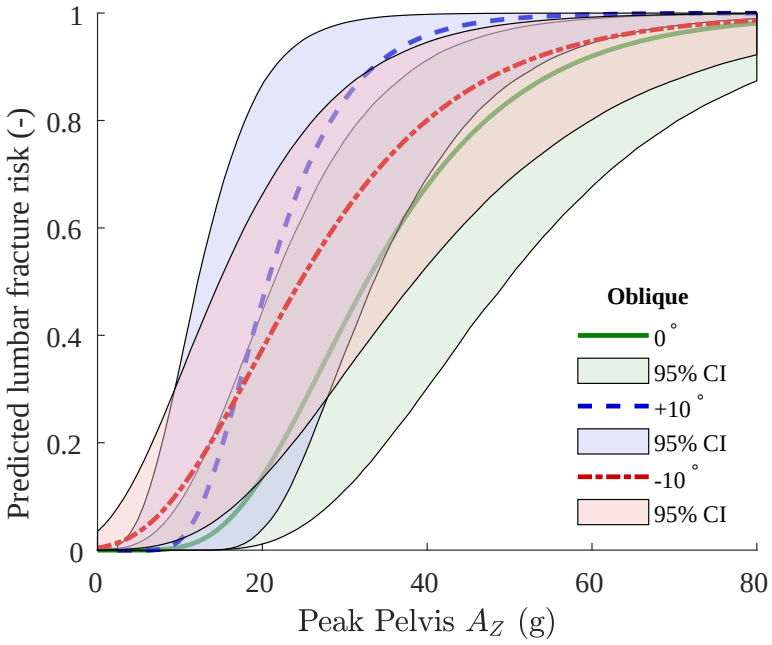

Figure 4.20: Injury risk curves genererated by inserting a transfer function of the strain using Hybrid III Peak Pelvis A_Z as IC into the SHBM IRF [Iraeus et al., 2023] for a 45 year old occupant.

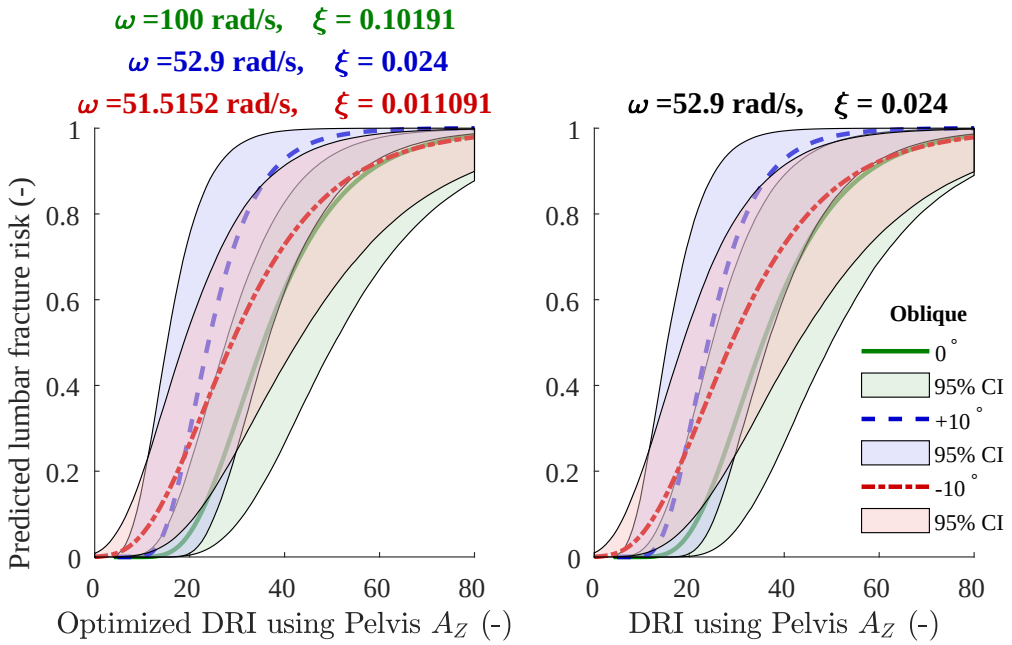

Figure 4.21: Injury risk curves genererated by inserting a transfer function of the strain using Hybrid III DRI Peak Pelvis A_z as IC into the SHBM IRF [Iraeus et al., 2023] for a 45 year old occupant.

4.8.2 Run off road loadcase

In Figure 4.22 the risk curve using Hybrid III for run of road scenarios can be shown. In the simulations ATD peak pelvis accelerations were registered in the range between 5 to 20 g, meaning that this risk curve also is generated by extrapolation of the linearly regressed strain in order to get risks from 0 to 1.

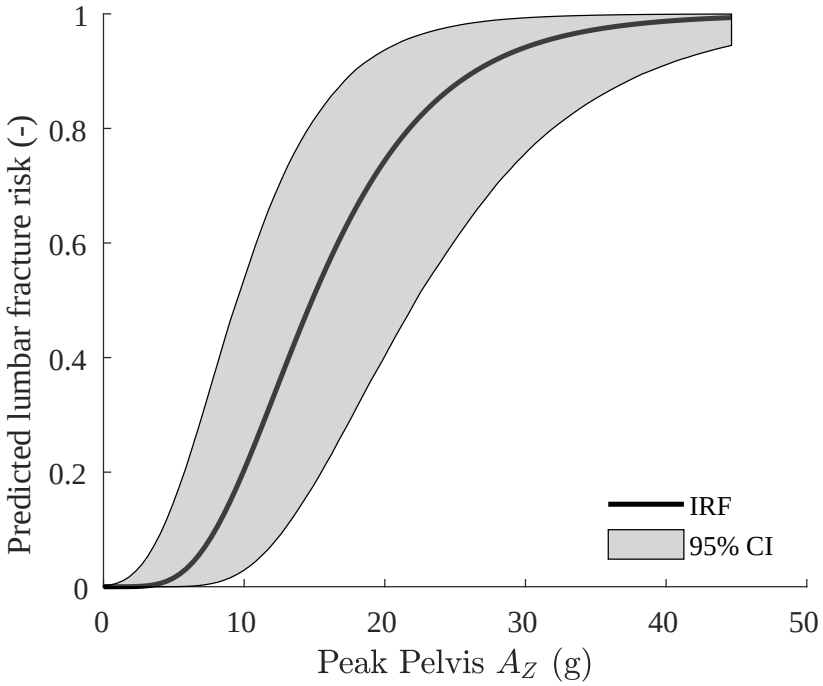

Figure 4.22: Injury risk curves genererated by inserting a transfer function of the strain using Hybrid III Peak Pelvis A_z as IC into the SHBM IRF [Iraeus et al., 2023] for a 45 year old occupant for run off road loadcases.

4.9 THOR Injury Risk Functions

In the subsequent section, IRF of different injury criterias with separated datasample is presented for THOR ATD.

4.9.1 Full Frontal with separated impact angle

For the full frontal dataset, four injury criteria are presented as IRF. These are the pelvis acceleration with DRI using optimized values, DRI using values from [Lynch et al., 2012] followed by the peak values of the pelvis and T12 acceleration. Unfortunately, there weren't any maxima within the range of the optimized values for DRI using $0°$ impact angle. The IRF shows a variety in precision that could be observed by the confidence bounds. This is a result of the insecurities of the coefficient in the IRF.

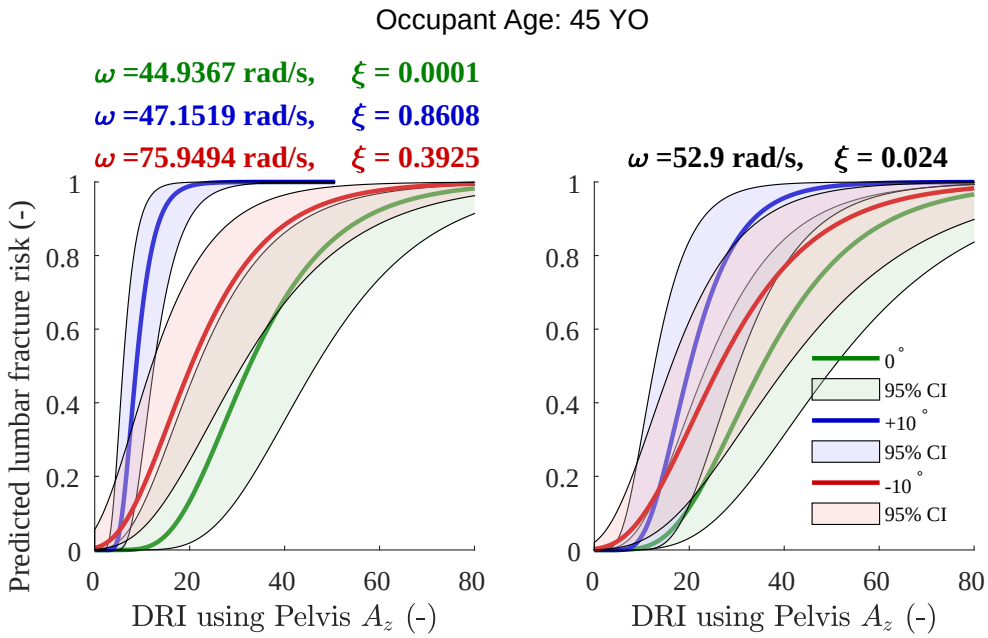

Figure 4.23: Injury risk curves genererated by inserting a transfer function of the strain using THOR DRI Pelvis A_Z as IC into the SHBM IRF [Iraeus et al., 2023] for a 45 year old occupant.

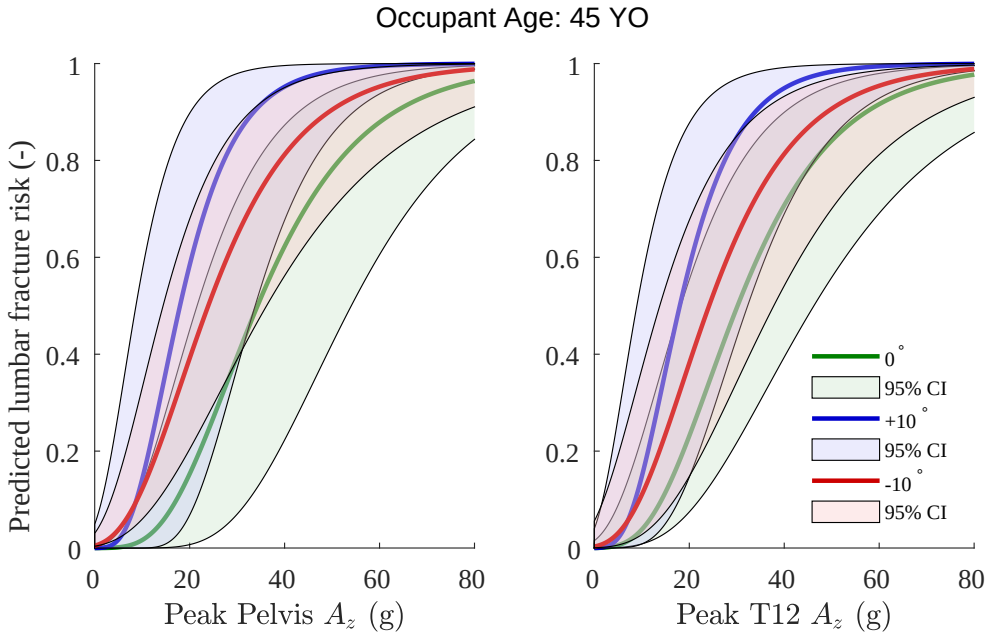

Figure 4.24: Injury risk curves genererated by inserting a transfer function of the strain using THOR Peak Pelvis and T12 A_z as IC into the SHBM IRF [Iraeus et al., 2023] for a 45 year old occupant.

4.9.2 Run off road loadcase

The run-off-road IRFs is created using Peak Pelvis and T12 A_z as IC and is shown in figure 4.25. The high linear correlation for this dataset is observed to cause more narrow confidence bounds.

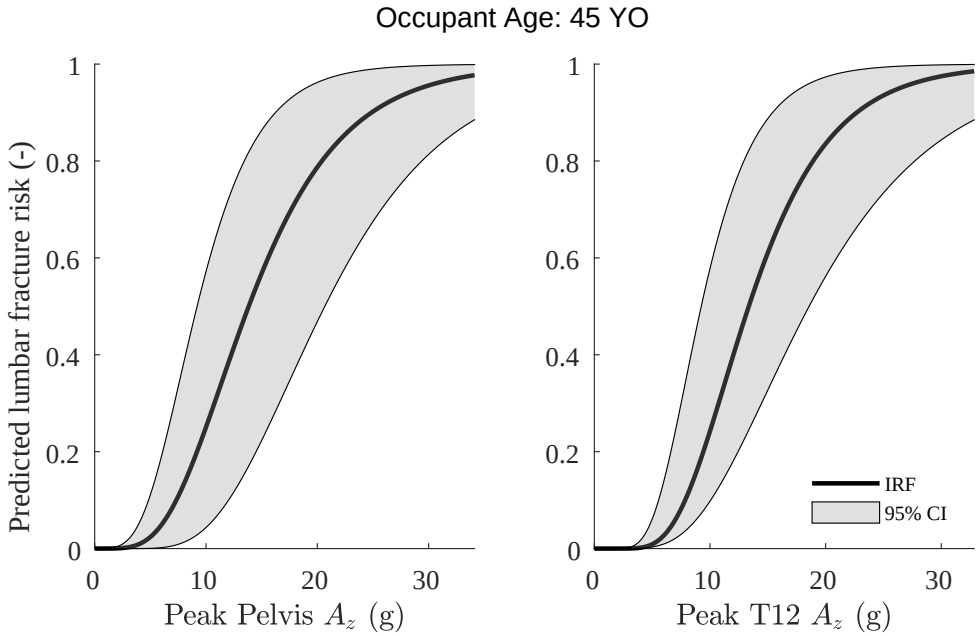

Figure 4.25: Injury risk curves genererated by inserting a transfer function of the strain using THOR Peak Pelvis and T12 A_z as IC into the SHBM IRF [Iraeus et al., 2023] for a 45 year old occupant.

4.10 IRF for ATDs

The coefficients used to create the IRF in the previous chapter are all listed in table 4.4 with their corresponding standard error. Similar to the fracture risk curve in [Iraeus et al., 2023] but with the exception of a linear interpolator of the strain.

$$Risk = \frac{1}{2} + \frac{1}{2} erf\left(\frac{ln(C_1 * IC_{ATD} + C_2) - (\beta_1 + age * coef_{age})}{\sqrt{2 * (\beta_2)^2}}\right) \tag{4.1}$$

Table 4.4: Coefficients for the IRF for both Hybrid III and THOR using the best correlating lumbar spine ICs

IRF coefficients [Iraeus et al., 2023]							
β_1	β_2	$coef_{age}$	$\beta_{1,SE}$	$\beta_{2,SE}$	$coef_{age,SE}$		
-2.833	0.41254	-0.0149	0.10983	0.02924	0.00218		
Full Frontal							
ATD	**IC**	**Impact angle**	C_1	C_2	$C_{1,SE}$	$C_{2,SE}$	Ref
Hybrid III	Peak Pelvis A_Z	Oblique $0°$	0.000863435	0.001893915	0.000094639	0.002498527	4.20
Hybrid III	Peak Pelvis A_Z	Oblique $+10°$	0.001626725	-0.00351536	0.000231939	0.005117668	4.20
Hybrid III	Peak Pelvis A_Z	Oblique $-10°$	0.000813200	0.010091716	0.000047221	0.000913212	4.20
Hybrid III	DRI Peak Pelvis A_Z opt	Oblique $0°$	0.000857010	-0.00200186	0.000044330	0.001384164	4.21
Hybrid III	DRI Peak Pelvis A_Z opt	Oblique $+10°$	0.001545502	-0.00691279	0.000190211	0.004838276	4.21
Hybrid III	DRI Peak Pelvis A_Z opt	Oblique $-10°$	0.000774564	0.007565842	0.000040949	0.000962751	4.21
Hybrid III	DRI Peak Pelvis A_Z std	Oblique $0°$	0.000937290	-0.00317138	0.000085474	0.002538568	4.21
Hybrid III	DRI Peak Pelvis A_Z std	Oblique $+10°$	0.001545502	-0.006912796	0.000190211	0.004838276	4.21
Hybrid III	DRI Peak Pelvis A_Z std	Oblique $-10°$	0.000773751	0.007722373	0.000041077	0.000958594	4.21
THOR	Peak Pelvis A_Z	Oblique $0°$	0.000725183	0.005221352	0.000079195	0.002132036	4.24
THOR	Peak Pelvis A_Z	Oblique $+10°$	0.001348814	0.005862466	0.000243154	0.004782827	4.24
THOR	Peak Pelvis A_Z	Oblique $-10°$	0.000825575	0.010346121	0.000050075	0.000938515	4.24
THOR	Peak T12 A_Z	Oblique $0°$	0.000773424	0.006756491	0.000078884	0.001839980	4.24
THOR	Peak T12 A_Z	Oblique $+10°$	0.001319315	0.006347106	0.000211213	0.004181980	4.24
THOR	Peak T12 A_Z	Oblique $-10°$	0.000843872	0.009696337	0.000066185	0.001260779	4.24
THOR	DRI Peak Pelvis A_Z opt	Oblique $0°$	0.000879618	0.001427268	0.000063818	0.001693398	4.23
THOR	DRI Peak Pelvis A_Z opt	Oblique $+10°$	0.004173332	-0.00645508	0.000405540	0.003784753	4.23
THOR	DRI Peak Pelvis A_Z opt	Oblique $-10°$	0.000969155	0.010435689	0.000051289	0.000814992	4.23
THOR	DRI Peak Pelvis A_Z std	Oblique $0°$	0.000761809	0.003122050	0.000056695	0.001612855	4.23
THOR	DRI Peak Pelvis A_Z std	Oblique $+10°$	0.001549731	-0.00102159	0.000171235	0.003706737	4.23
THOR	DRI Peak Pelvis A_Z std	Oblique $-10°$	0.000780846	0.009483855	0.000059920	0.001249800	4.23
ATD Combined	Peak Pelvis A_Z	Oblique $0°$	0.000794309	0.003557634	0.000086917	0.002315281	5.5
ATD Combined	Peak Pelvis A_Z	Oblique $+10°$	0.001487769	0.001173552	0.000237547	0.004950247	5.5
ATD Combined	Peak Pelvis A_Z	Oblique $-10°$	0.000819388	0.010218919	0.000048648	0.000925863	5.5
Run off Road							
Hybrid III	Peak Lumbar A_Z	-	0.001805034	0.003333107	0.000174169	0.002384068	4.22
THOR	Peak Lumbar A_Z	-	0.001899949	0.003804653	0.000171416	0.002192907	4.25
THOR	Peak T12 A_Z	-	0.002246251	0.000093147	0.000186201	0.002302685	4.25

4.11 Verification of IRFs using rear seat simulations

The verification of the IRF is shown in figure 4.26 and the ICs used is the peak pelvis A_Z and Peak T12 A_Z. For Hybrid III does the difference in fracture risk remain under 0.3 while THOR reaches up to 0.4. By overviewing the full figure one could conclude that the ATDs IRF underpredicts the risk of fractures exept from the full frontal 64 kph loadcase for Hybrid III.

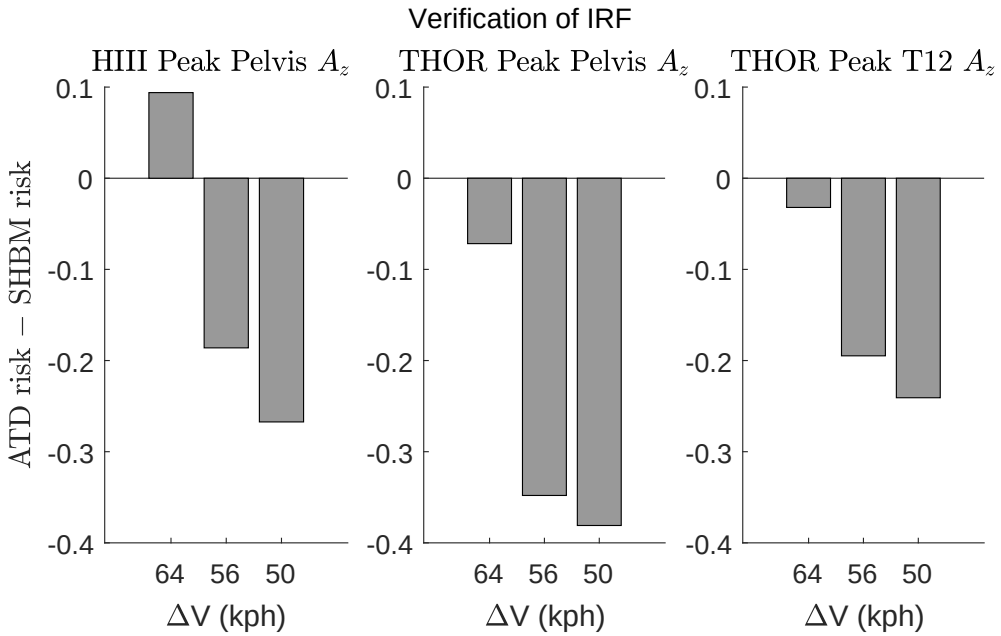

Figure 4.26: Difference between the predicted ATD and SHBM fracture risk for crash simulations in rear seat occupant in mid position.

5
Discussion

In this thesis, 180 paired simulations with the SAFER HBM, THOR and Hybrid III frontal impact ATDs were conducted to generate IC and IRFs for the ATD based on a correlation analysis of recorded measures in the ATDs and the peak lumbar strain in the SHBM. This was followed by a parameter substitution of the original SHBM IRF to generate new ATD IRFs. The method for the project yielded results valuable for fracture risk prediction using the ATDs. However, the kinematics between the ATDs and the SHBM were not fully linear, and some uncertainty and trends when transferring the SHBM IRF to the ATDs must be accounted for under different conditions, which is discussed in this chapter.

5.1 Correlation of measures with respect to SHBM peak lumbar strain

It became apparent relatively early in the analysis process that the correlation between many of the output measures from the ATDs and the SHBM peak lumbar strain for all combined loading cases was surprisingly low and no clear trend could be seen. A range of ATD measures was analyzed in order to find the most promising ones, and the ones with most potential was noted to be different spine loadcells and accelerometers which seemed logical in a kinematical perspective. In order to see what correlation that could be expected an internal correlation analysis of the SHBM was made where lumbar forces and moments and sacrum accelerations were analyzed against the peak lumbar strain. The internal correlation within the SHBM showed similar trends with relatively low correlation observed in the analysis of the ATDs, which verified that it was not possible to find any better correlation with the specific measures without any further treatment of the data sample. This suggests that the kinematics between the ATDs and SHBM may not be poor. Rather, it implies that distinct loading scenarios and variations may influence the recorded measures and the SHBM lumbar strain with different proportions contributing to the spread of data.

5.2 Correlation optimization of ATD measures

As a consequence of the low correlations found between ATD measures and the peak lumbar spine, alternative ICs was examined. One of them was the DRI which was an attempt trying to capture the kinematics in the ATD during the whole time history of the crash by explicitly solving the for the relative lumbar spine displacement, which was used to calculate a DRI value to be used as IC for each simulation. The idea with the DRI

was that the natural eigenfrequency and the damping ratio of the simplified mass-spring-damper upper body model could be tuned to archive a better proportion of the peak DRI value relative to the SHBM peak lumbar strain for a certain loading scenario. This was made by a parametric sweep in an interval around a reference solution where R^2 values was calculated for each change of the eigenfrequency and damping ratio and the parameters resulting in highest R^2 value was considered as optimized. DRI as IC is beneficial in terms of increased correlation leading to more confident fracture risk prediction. On the other hand it is an abstract measure depending on both the natural frequency and the relative spine displacement making it hard to compare different loading cases that has been tuned with different natural frequencies. It can also be noted that in the analysis of DRI for THOR, the optimized DRI for +10° oblique pulse, Figure 4.18, showed lower correlation than when calculating DRI with the standard settings, Figure 4.19. The result is probably due to a to coarse parametric sweep which is not capturing all extreme points in the interval. This means that in order to gain from the benefits of DRI the natural frequency and damping ratio are two additional parameters that has to be considered and treated with a certaint precision in order to increase the correlation.

5.3 Data sample method

In our project, a full factorial have been utilized as sampling method to analyze the effects of various parameters on our outcomes. However, it is pertinent to consider the implications of employing alternative sampling methods, such as Latin Hypercube Sampling (LHS), and how they might influence our findings and conclusions. Full factorial sampling offers a systematic approach by considering all possible combinations of the chosen variables. This comprehensive exploration of the parameter space allows us to assess the individual and interactive effects of each parameter. By examining every combination, detailed insights into the relationships between variables and their impact on the outcome is of interest. However, full factorial sampling has limitations, particularly in studies with a large number of variables or when the parameter space is extensive. The exponential growth in the number of combinations can lead to a substantial increase in computational burden and resource requirements. This could also be considered as an advantage for the project where there is a fixed number of variations. This results in fewer time-consuming adjustments such as repositioning the dummies or stiffening up the elements around the seatpan. The results will still end up in an arbitrary dataset to analyze how the strain is affected by the change of parameters.

In contrast, LHS offers a more efficient approach to sampling the parameter space. By stratifying each variable into equally probable intervals and sampling from each interval, LHS provides a representative subset of the parameter space with fewer samples. This stratified sampling helps capture the variability and interactions among variables while reducing the computational cost associated with exploring all possible combinations. Moreover, LHS uses the Cumulative Distribution Function (CDF), which can better represent real-world scenarios. By sampling according to these distributions, LHS can generate a more realistic representation of the parameter space and the underlying relationships between variables. However, it's essential to recognize that LHS is a

stochastic method and may not capture every possible combination of variables. While it provides a more efficient exploration of the parameter space, there is a risk of missing certain configurations or interactions that could be significant [Huang et al., 2016].

5.4 Trends for the oblique impact angles

During the analysis, it was found that the simulations with different oblique impact angles needed to be divided into separate cases to increase the correlation for each respective case. From the results, it can be noted that a normal full frontal impact with a 0° oblique angle gives the least peak lumbar strain as a function of peak pelvis A_Z, see Figures 4.12 and A.20. For the -10° oblique angle, the strain was slightly offset upwards, and for the +10° oblique angle, the strain was offset with a steeper slope. Looking at the range of the measurements, the ATDs seem to capture the oblique pulses with relatively equal magnitudes in a range slightly below the pure full frontal crashes. The decrease in recorded peak accelerations could be due to that the oblique pulses are forcing the ATD to the side in the seat, which could result in a softer seat response in the case of sliding a bit over the seat pan.

It can also be noted that the peak lumbar strain was increasing more considerable in the SHBM for the oblique cases. To understand the load sequences better the time history of the strains was visualized in Figure 5.1. Around 60 ms or slightly after, the peak strain appears in the pure full frontal crashes. A similar trend can be noted for the -10° oblique impacts except for some amplification of the peak strains which was relatively well illustrated in Figures 4.12 and A.20. For the +10° oblique impacts, a different behavior was observed, where the peak strain in high-severity crashes was amplified more and the peak strains tended to be shifted a bit.

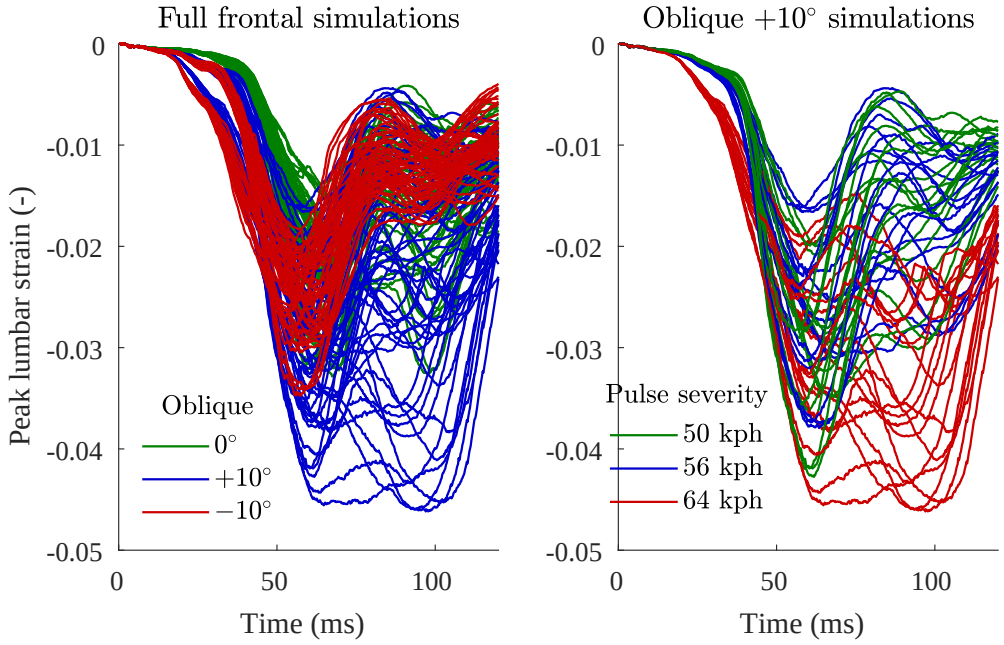

Figure 5.1: (Left) Time history of peak lumbar strain for all full frontal crashes. (Right) Time history of peak lumbar strain for all oblique $+10°$ crashes.

By visual observations in Figure 5.2, where a pure full frontal 64 kph was compared with one of the most severe oblique +10° crashes with the stiff seat pan, 30° seatback angle and increased belt force, it was noted that the SHBM, as it leans to the side relieves the seat a bit and does not seem to hit the seat pan equally hard, explaining the lack of early strain peaks. The motion is then stopped later by a combination of seatbelt, airbag and door panel interaction causing some sideward bending and twisting of the upper body. Strain distributions from the lumbar spine vertebrae were extracted and the peak was found to be in vertebrae L5. Visualization of vertebrae L5 fringe top can be viewed in Figure 5.3. The figure shows that the peak vertebrae strain was achieved on the side edge of the vertebrae for this oblique case in contrast to the pure full frontal cases where the peak strain used to be more symmetric distributed along the anterior part of the vertebrae. Based on the observations a conclusion was drawn that oblique pulses might give higher peak strains in the SHBM due to the differences in how the spine column is bent.

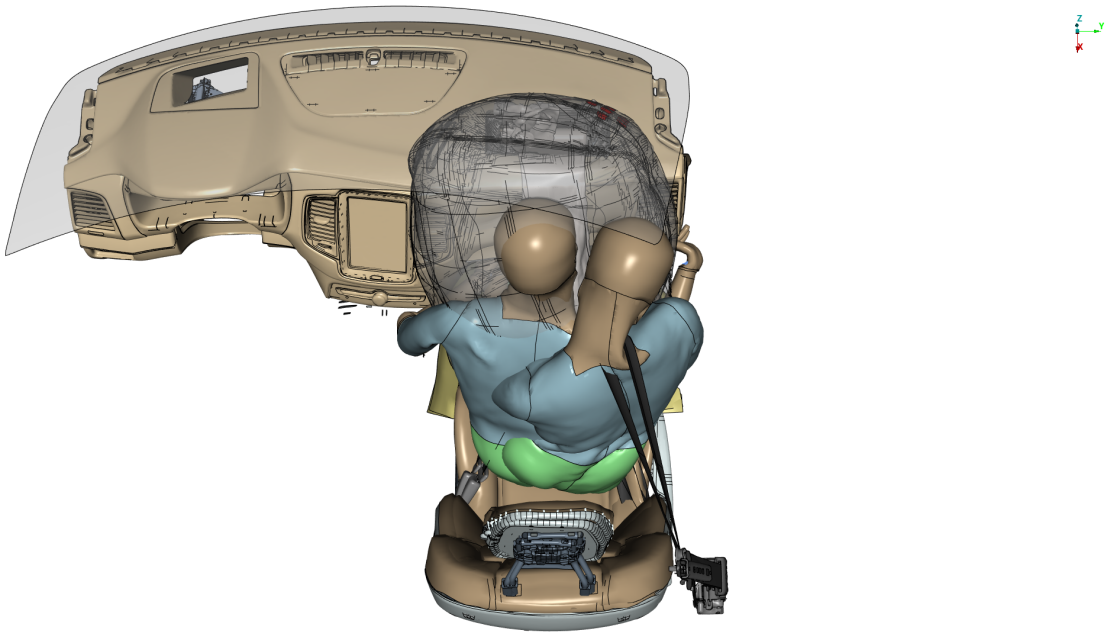

Figure 5.2: Visualization of SHBM postures in simulations with a pure full frontal 64 kph pulse (occupant with straight upper body), and a 64 kph pulse with with +10° oblique impact angle, stiff seat pan, 30° seat back angle and increased belt force (occupant leaned against door panel).

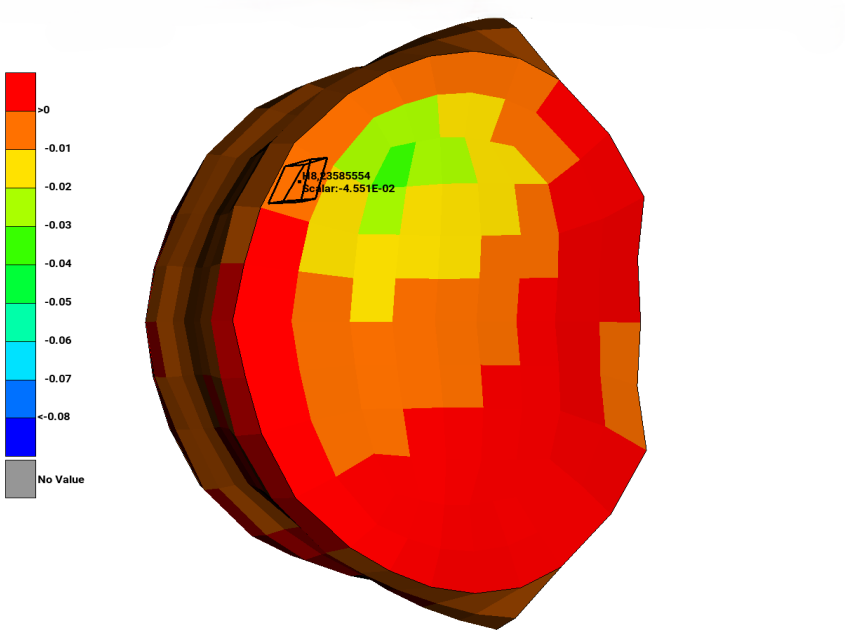

Figure 5.3: Peak strain distribution at L5 top fringe for full frontal 64 kph pulse with +10° oblique impact angle, stiff seat pan, 30° seat back angle and increased belt force. Peak strain at the side edge of top fringe with peak value of -0.045.

5.5 Insecurities of the ATD IRF

The presented IRF in section 4.8 and 4.9 can be used as an indication of the fracture risk resulting from the IC measure. This function is based on the validated IRF generated in [Iraeus et al., 2023], which includes an inherent uncertainty. To recreate the confidence bounds of the function, bootstrapping was performed using the standard error of the coefficients. The results did not match the confidence bounds from the article, possibly due to differences in software. The confidence bounds appear to vary depending on the software used. The original curve and confidence bounds were created using R, whereas Matlab was used in this project. This discrepancy raises the question of which software provides more accurate results, though further investigation was not conducted. Consequently, the confidence bounds presented in this project are wider than they would have been if R had been used.

The IRF were created using linear interpolation of the strain from the paired simulations. As the results showed, the highest attainable R^2 value was achieved with the DRI method, reaching $R^2 = 0.8$ for $-10°$. Compared to linear regression models in biomechanical studies, where R^2 values are often close to 0.8, these results are slightly poorer resulting in larger errors. Without DRI, the maximum R^2 value reached only 0.65, resulting in even greater uncertainties in validation. This discrepancy could result from a change in the injury mechanism of the models. There is no definitive threshold for how high the correlation must be for a good model, but the results of this project suggest it is on the lower boundary of a moderate model. To improve the correlation, further data is needed at the design position, and combining different ICs could better capture the behavior of the changed injury mechanism.

The IRF is created using the estimated coefficient values and their confidence bounds by assuming a normal distribution of the coefficients and their standard error. Bootstrapping was the method used, which, while simple and computationally efficient, has limitations such as requiring a high number of iterations. Another drawback is the difficulty in extracting exact values for the coefficients used for the bounds because the bounding lines are selected from the IRF. Nonetheless, bootstrapping allows for a large number of iterations, which aids in finding convergence. Through trial and error, it was determined that 50,000 iterations were necessary to achieve convergence of the coefficient values distributed over the normal curve.

Another interesting consideration is that by separating the loading scenarios based on the impact pulse angle, the confidence bounds intersect with one another. There may be a way to combine the cases and use the outer boundaries of the confidence interval, allowing all simulations to be analyzed uniformly, even if they have varying impact pulses. This could potentially be done, but it would result in significant uncertainty in the function, making it less useful. It's important to note that this approach would likely be similar to generating a linear regression with the full sample, which resulted in a very low correlation of $R^2 = 0.18$ for Hybrid III and $R^2 = 0.08$ for THOR using Peak Pelvis A_Z as the IC. This would not meet the criteria for a usable model.

5.6 Combined IRF for ATDs

As the coefficients for the linear regressions were presented, similar numbers between THOR and Hybrid III were observed. This led to the conclusion that the ATDs IRFs could be combined into one instead of being separated. The linear regression between Hybrid III and THOR for a determined IC showed a correlation of $R^2 = 0.7$. It appeard that Hybrid III has slightly higher acceleration in each of the simulations, which can be seen by the intersection of the Y-axis. This might have posed a potential issue for merging the IRFs because it would underpredict the risk of fracture when performing a mean of the linear coefficients.

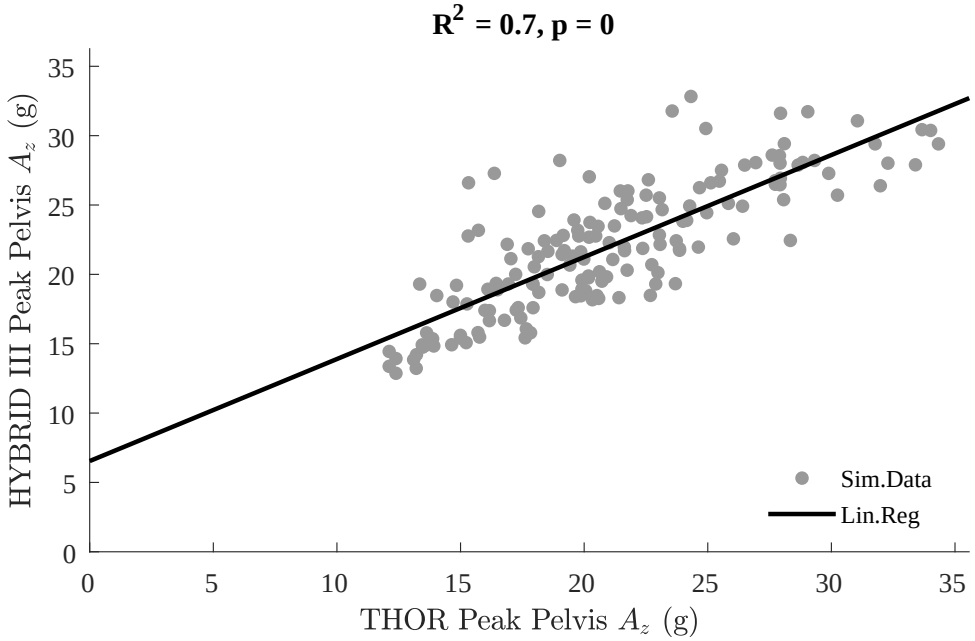

Figure 5.4: Linear Regression between Hybrid III and THOR using the same IC.

In Figure 5.5, IRFs for each ATD using Peak Pelvis A_Z as IC, are presented. The trend is very similar, which indicates that a merged IRF could be made, as visualized in the right figure. By generalizing the ATDs in this way, it should be noted that the uncertainties are increasing, but it could be a straightforward way of analyzing the results independent of the ATDs used.

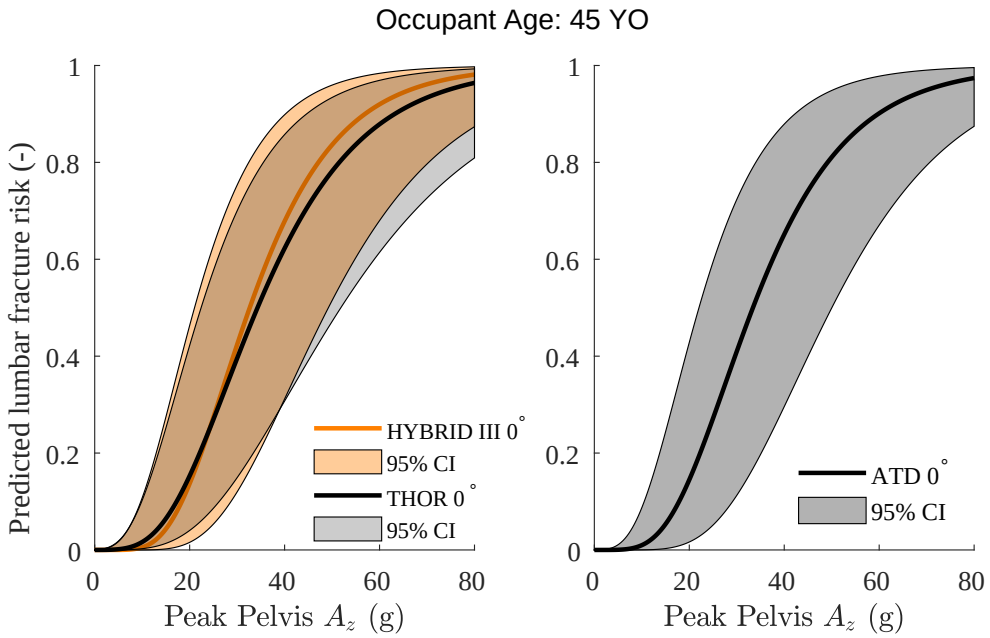

Figure 5.5: IRFs with $0°$ oblique impact angle for both THOR and Hybrid III (left) and a combinated IRF for both ATDs (right) using Peak Pelvis A_Z as IC.

5.7 Verification using rear seat simulation

The results from the verification were mixed. Hybrid III seemed to capture a similar injury mechanism as the SHBM, with the results falling within the confidence bounds. The peak pelvis A_z IRF overpredicted the risk for the 64 kph load case and underpredicted it for the others. The magnitude of the difference in predicted risk did not exceed 0.3, which could be considered acceptable given the wide confidence bounds of the IRF. THOR performed similarly, but for the pelvis measure, the differences were higher in magnitude, with the highest difference being 0.38 for Full frontal 50 kph. Peak T12 A_z was closer to the SHBM risk prediction, and it's possible that the T12 accelerometer is capturing the injury mechanism. It is important to note that the results were not expected to be exact due to the different seating postures of the models and the variations in seat belt routing. Another interesting result was that the risk of fracture increased as the simulation ΔV decreased. This behavior was not expected and could probably be due to the twisting of the upper body at higher speeds. It was of interest to see if the generated IRF could be applicable to the rear seat, despite its significant differences.

5.8 Recommendations for future work

A central part during the project was to find measures in the ATDs that correlated well with the peak lumbar strain in the SHBM, and gained results that indicated that different pulse variations tend to cluster data along different trends. In order to understand the effect of oblique impacts more future work could be to run simulations to generate an even larger data sample with oblique pulses ranging between -10° to 10° in order to see if the correlation between ATD ICs and SHBM peak lumbar strain can be improved even more. Another sampling method than the full factorial that was used for this project could be interesting to evaluate.

Optimization of the correlation using DRI was an approach that showed good potential and could be used in upcoming projects using a similar approach. In this project the DRI was optimized using a parametric sweep of the natural eigenfrequency and damping ratio, but other potential optimization methods for the DRI and the actual physical meaning of the optimization would be of interest to dig deeper into.

6
Conclusion

During this project, paired simulations of ATDs and the SHBM were conducted using both full frontal and run-off-road load cases. Variations such as stiffness of the seat pan, seat back angle, and belt force were considered. Several IC were evaluated to find correlation between SHBM strain and ATD measurements. Due to the inability of ATDs to capture certain injury mechanisms, the data sample was divided based on oblique impact angles to identify correlations. The final IC recommended for use is the Peak Pelvis A_Z for both models or Peak T12 A_Z for THOR. While DRI using pelvis acceleration could also be used, it requires more post-simulation work. The final attainable correlation between strain and acceleration for full frontal was $R^2 = 0.62$ for both THOR and Hybrid III. Higher correlations were obtained for the run-off-road load case, resulting in $R^2 = 0.86$ for Hybrid III and $R^2 = 0.88$ for THOR.

By using the existing IRF by [Iraeus et al., 2023] combined with a transfer function of the strain, it was possible to create lumbar spine fracture IRF based on ATD measurements. The transfer functions were based on results from linear regressions. The IC used was Peak Pelvis A_Z, allowing for post-processing analysis to easily indicate the risk of lumbar fracture in simulations for both full frontal and run-off-road load cases. The new IRFs provide a basis for fracure risk prediction using Hybrid III and THOR in frontal and run-off road crashes.

References

[Belytschko et al., 2014] Belytschko, T., Liu, W. K., Moran, B., and Elkhodary, K. I. (2014). *Nonlinear Finite Elements for Continua and Structures, Second Edition*. John Wiley & Sons.

[Hines, 2018] Hines, T. (2018). Spine anatomy, anatomy of the human spine.

[Huang et al., 2016] Huang, C., Hami, A. E., and Radi, B. (2016). Overview of structural reliability analysis methods — part ii: Sampling methods. Accessed: 2024-05-23.

[Humanetics, 2020] Humanetics (2020). *THOR 50M U.S. NCAP Dummy Model LS DYNA Release Version 1.7*. Humanetics CAE Department.

[Humanetics, 2023] Humanetics (2023). H-point manikin.

[Hurlston, 2021] Hurlston, R. (2021). Implicit and explicit methods in fea – which one should you choose?

[Iraeus et al., 2023] Iraeus, J., Niranjan, Y. P., Jaber, L., John, J., and Davidsson, J. (2023). A new open-source finite element lumbar spine model, its tuning and validation, and development of a tissue-based injury risk function for compression fractures. *IRCOBI Conference 2023*, pages 1048–1072.

[Isaksson Hellman and Norin, 2005] Isaksson Hellman, I. and Norin, H. (2005). How thirty years of focused safety development has influenced injury outcome in volvo cars. *Annual Proceedings. Association for the Advancement of Automotive Medicine*, 49:63–77.

[Izumiyama et al., 2018] Izumiyama, T., Nishida, N., Iwanaga, H., Chen, X., Ohgi, J., and Mori, K. (2018). The analysis of an individual difference in human skeletal alignment in seated posture and occupant behavior using hbms. *IRCOBI Conference 2018*, pages 549–560.

[Jakobsson et al., 2006] Jakobsson, L., Bergman, T., and Johansson, L. (2006). Identifying thoracic and lumbar spinal injuries in car accidents. *IRCOBI Conference 2016*, pages 61–71.

[Jakobsson et al., 2016] Jakobsson, L., Björklund, M., and Westerlund, A. (2016). Thoracolumbar spine injuries in car crashes. *IRCOBI Conference 2016*, pages 101–112.

[Jakobsson et al., 2014] Jakobsson, L., Lindman, M., Axelson, A., Lokensgard, B., Petersson, M., Svanberg, B., and Kovaceva, J. (2014). Adressing run off road safety. *2014 SAE International*, pages 132–144.

[Lundell et al., 1981] Lundell, B., Mellander, H., and Carlsson, I. (1981). Safety performance of a rear seat belt system with optimized seat cushion design. *SAE Technical Paper*, 810796. Downloaded from SAE International by Chalmers University of Technology, Thursday, May 04, 2023.

[Lynch et al., 2012] Lynch, R., McDonough, D., and Keon, T. (2012). An update to the dynamic response index (dri) model for use in assessing seat performance in military

ground vehicles.

[Ortiz-Paparoni et al., 2021] Ortiz-Paparoni, M., Op 't Eynde, J., Kait, J., Bigler, B., Shridharani, J., Schmidt, A., Cox, C., Morino, C., Pintar, F., Yoganandan, N., Moore, J., Zhang, J., and Bass, C. R. (2021). The human lumbar spine during high-rate under seat loading: A combined metric injury criteria. *Traffic Inj Prev*.

[Pintar et al., 2012] Pintar, F., Yoganandan, N., Maiman, D., Scarboro, M., and Rudd, R. (2012). Thoracolumbar spine fractures in frontal impact crashes. *Annals of advances in automotive medicine / Annual Scientific Conference ... Association for the Advancement of Automotive Medicine. Association for the Advancement of Automotive Medicine. Scientific Conference*, 56:277–83.

[Pipkorn et al., 2023] Pipkorn, B., Jakobsson, L., Iraeus, J., and Östh, J. (2023). The safer hbm – a human body model for seamless integrated occupant analysis for all road users.

[Schmitt et al., 2019] Schmitt, K.-U., Niederer, P. F., Cronin, D. S., III, B. M., Muser, M. H., and Walz, F. (2019). *Trauma biomechanics: An introduction to injury biomechanics*. Springer International Publishing, 5 edition.

[Schneider et al., 2010] Schneider, A., Hommel, G., and Blettner, M. (2010). Linear regression analysis: part 14 of a series on evaluation of scientific publications. *Deutsches Arzteblatt international*, page 776–782.

[Society of Automotive Engineers, 2007] Society of Automotive Engineers (2007). Sae j211-1 instrumentation for impact test, surface vehicle recommended practice. Accessed: 2024-05-24.

[Taylor, 2024] Taylor, S. (2024). Multiple linear regression. *Corporate Finance Institute*.

[Tibshirani, 2024] Tibshirani, R. (2024). Bootstrap methods. Accessed: 2024-05-23.

[Tushak et al., 2022] Tushak, S. K., Paul Donlon, J., Gepner, B. D., Chebbi, A., Pipkorn, B., Hallman, J. J., Forman, J. L., and Kerrigan, J. R. (2022). Failure tolerance of the human lumbar spine in dynamic combined compression and flexion loading. *Journal of Biomechanics*, 135:111051.

[Vijay, 2023] Vijay, K. (2023). What is linear regression? types, equation, examples, and best practices for 2022. *Artificial Intelligence*.

[Wang et al., 2009] Wang, M., Pintar, F., Yoganandan, N., and Maiman, D. (2009). The continued burden of spine fractures after motor vehicle crashes. *Neurosurg Spine*, 10:86–92.

[Östling and Larsson, 2019] Östling, M. and Larsson, A. (2019). Occupant activities and sitting positions in automated vehicles in china and sweden.

A

Appendix

A.1 Correlation results Hybrid III

Measure		Combined			Full Frontal			Run-off road		
Hybrid III	SHBM	R^2	R^2_{adj}	p	R^2	R^2_{adj}	p	R^2	R^2_{adj}	p
Peak Pelvis A_R	Peak Lumbar strain	0.01	0.01	0.14	0.00	-0.01	0.72	0.81	0.80	3.4E-07
Peak Pelvis A_X	Peak Lumbar strain	0.8E-04	-0.01	0.90	0.01	0.00	0.23	0.20	0.15	6.1E-02
Peak Pelvis A_Y	Peak Lumbar strain	0.17	0.16	1.3E-08	0.19	0.18	9.0E-09	0.36	0.32	8.1E-03
Peak Pelvis A_Z	Peak Lumbar strain	0.21	0.21	1.0E-10	0.18	0.18	1.6E-08	0.87	0.86	1.7E-08
Peak Lower Lumbar F_Z	Peak Lumbar strain	0.44	0.44	3.7E-24	0.40	0.40	1.6E-19	0.86	0.86	2.3E-08
Min Lower Lumbar M_Y	Peak Lumbar strain	0.02	0.02	0.04	0.47	0.46	1.1E-23	0.02	-0.04	5.5E-01
Max Lower Lumbar M_Y	Peak Lumbar strain	0.5E-03	-0.5e-3	0.77	0.01	0.01	0.15	0.00	-0.06	9.1E-01
Peak Upper Lumbar F_Z	Peak Lumbar strain	0.23	0.23	8.4E-12	0.30	0.30	3.3E-14	0.66	0.64	4.5E-05
Min Upper Lumbar M_Y	Peak Lumbar strain	0.03	0.03	0.01	0.08	0.07	0.4E-3	0.24	0.19	4.0E-02
Max Upper Lumbar M_Y	Peak Lumbar strain	2.8E-03	-0.3e-2	0.48	0.14	0.04	0.01	0.83	0.82	1.5E-07

Figure A.1: Hybrid III linear regression analysis for all loadcases with R^2, R^2_{adj} and $p - value$ as measures.

A.2 Correlation results THOR

Measures		Combined			Full Frontal			Run off Road		
THOR measure	SHBM measure	R^2	R^2_{adj}	p	R^2	R^2_{adj}	p	R^2	R^2_{adj}	p
Peak Pelvis A_x	Peak Lumbar strain	0.02	0.01	0.10	0.05	0.04	0.00	0.28	0.23	0.02
Peak Pelvis A_y	Peak Lumbar strain	0.07	0.06	0.00	0.09	0.09	0.00	0.26	0.22	0.03
Peak Pelvis A_z	Peak Lumbar strain	0.12	0.12	0.00	0.08	0.07	0.00	0.88	0.88	0.00
Peak Pelvis A_R	Peak Lumbar strain	0.08	0.07	0.00	0.12	0.11	0.00	0.91	0.90	0.00
Peak T-Spine F_X	Peak Lumbar strain	0.04	0.04	0.00	0.04	0.03	0.01	0.09	0.04	0.22
Peak T-Spine F_y	Peak Lumbar strain	0.01	0.00	0.19	0.01	0.00	0.35	0.32	0.28	0.01
Min T-Spine F_z	Peak Lumbar strain	0.07	0.07	0.00	0.04	0.03	0.02	0.73	0.72	0.00
Peak T-Spine M_y	Peak Lumbar strain	0.02	0.01	0.07	0.00	0.00	0.55	0.79	0.78	0.00
Peak T-Spine F_R	Peak Lumbar strain	0.03	0.03	0.01	0.00	0.00	0.42	0.68	0.66	0.00
Peak T4 A_x	Peak Lumbar strain	0.00	-0.01	0.75	0.00	0.00	0.37	0.42	0.39	0.00
Peak T4 A_y	Peak Lumbar strain	0.13	0.13	0.00	0.16	0.16	0.00	0.35	0.31	0.01
Peak T4 A_z	Peak Lumbar strain	0.02	0.01	0.06	0.00	-0.01	0.73	0.82	0.81	0.00
Peak T4 A_R	Peak Lumbar strain	0.03	0.03	0.01	0.00	0.00	0.41	0.89	0.88	0.00
Peak T12 A_x	Peak Lumbar strain	0.01	0.01	0.14	0.01	0.00	0.27	0.42	0.38	0.00
Peak T12 A_y	Peak Lumbar strain	0.13	0.12	0.00	0.16	0.15	0.00	0.44	0.40	0.00
Peak T12 A_z	Peak Lumbar strain	0.23	0.23	0.00	0.22	0.21	0.00	0.90	0.89	0.00
Peak T12 A_R	Peak Lumbar strain	0.14	0.14	0.00	0.24	0.24	0.00	0.91	0.91	0.00

Figure A.2: THOR linear regression analysis for all loadcases with R^2, R^2_{adj} and $p-value$ as measures.

A.3 Correlational effects of variable changes using SHBM ICs

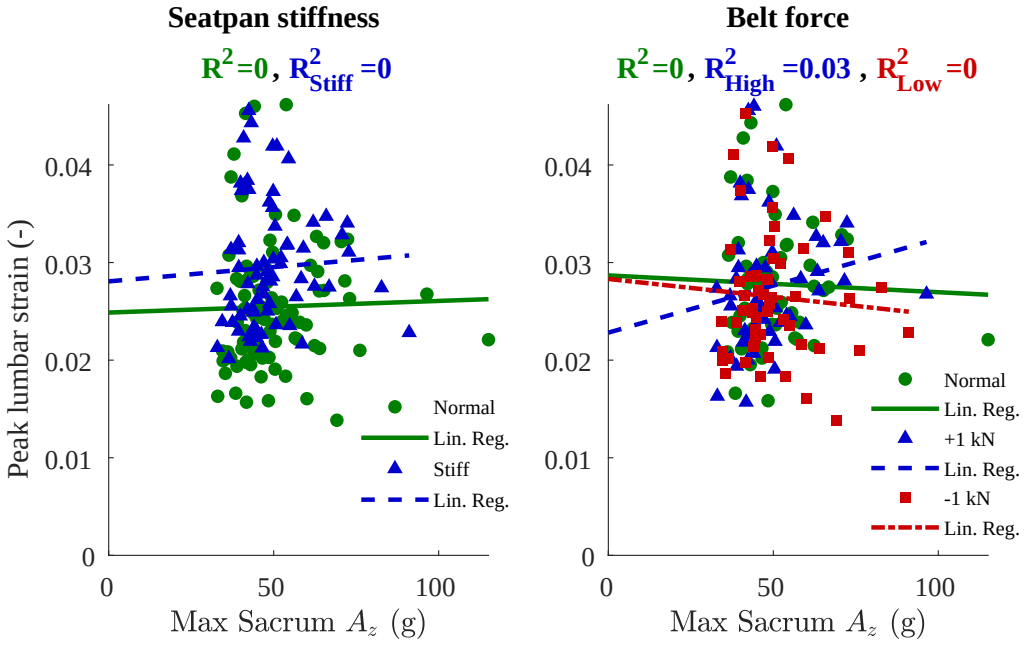

Figure A.3: Linear regression and visualization of data sample for variation of seatpan stiffness and belt force using SHBM and Peak Sacrum A_Z as IC.

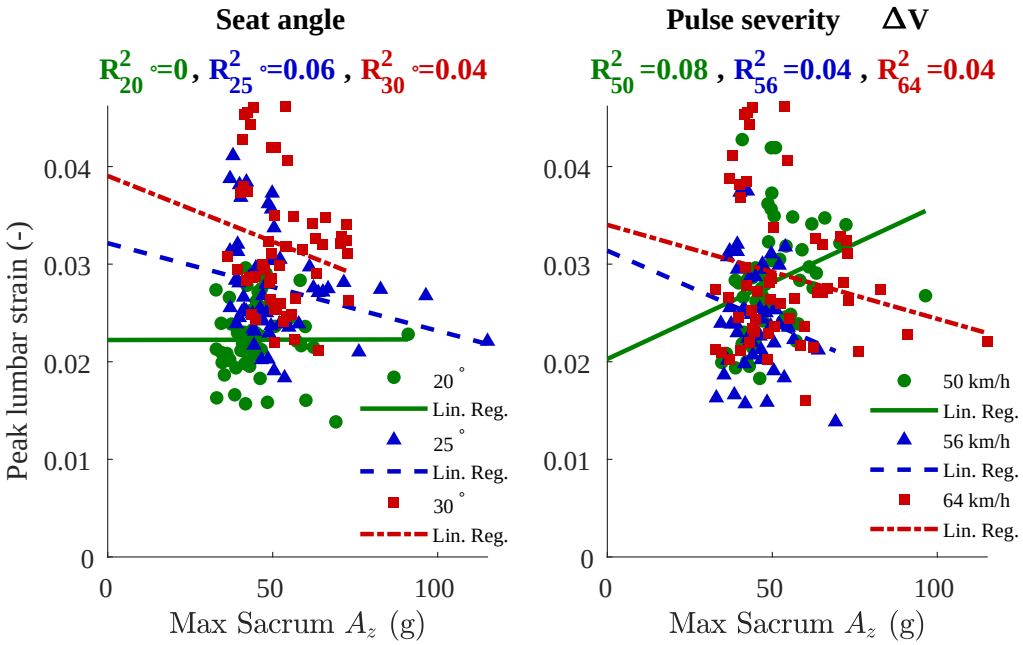

Figure A.4: Linear regression and visualization of data sample for variation of seat back angle and pulse severity using SHBM and Peak Sacrum A_Z as IC.

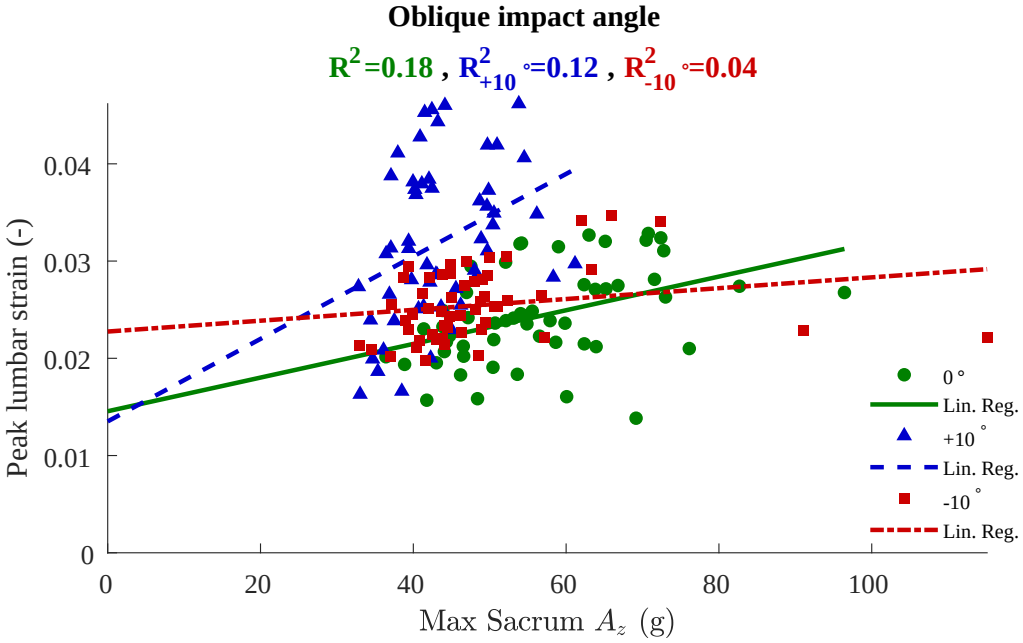

Figure A.5: Linear regression and visualization of data sample for variation of oblique impact angle using SHBM and Peak Sacrum A_Z as IC.

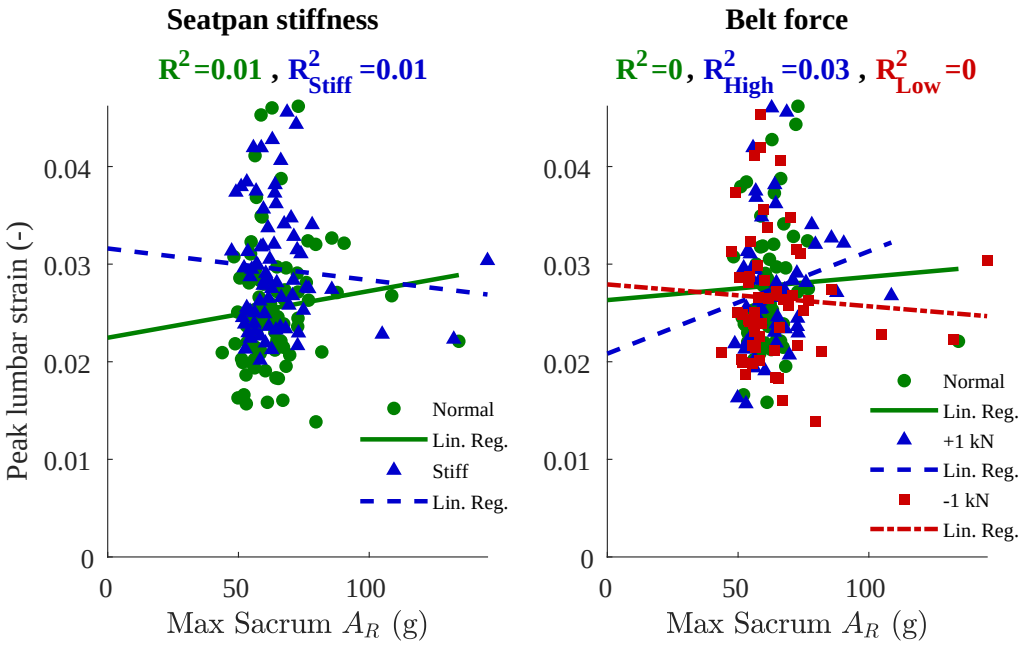

Figure A.6: Linear regression and visualization of data sample for variation of seatpan stiffness and belt force using SHBM and Peak Sacrum A_R as IC.

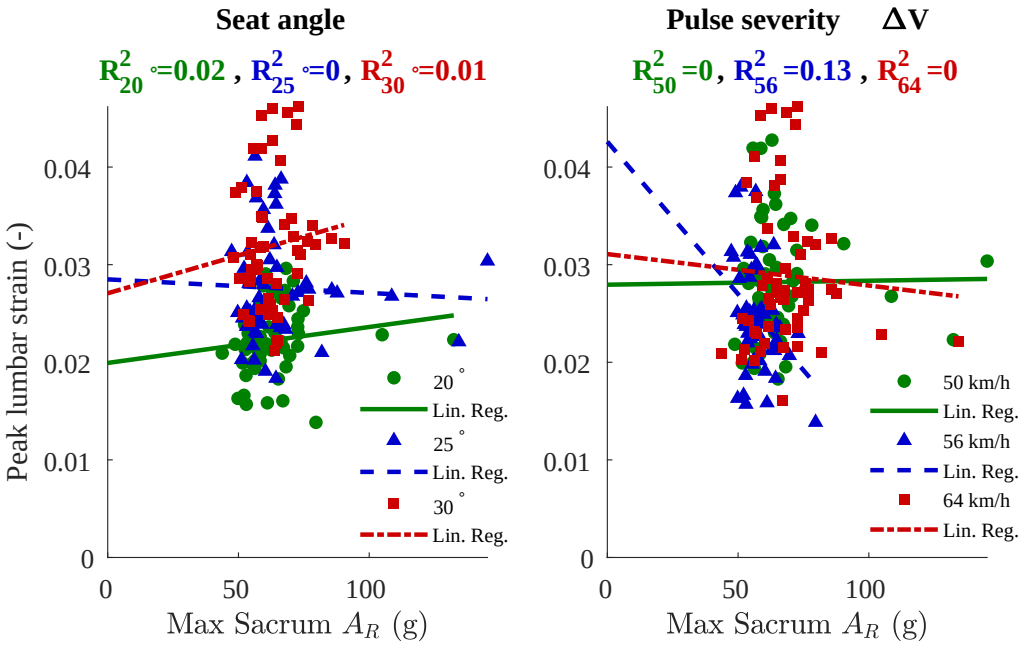

Figure A.7: Linear regression and visualization of data sample for variation of seat back angle and pulse severity using SHBM and Peak Sacrum A_R as IC.

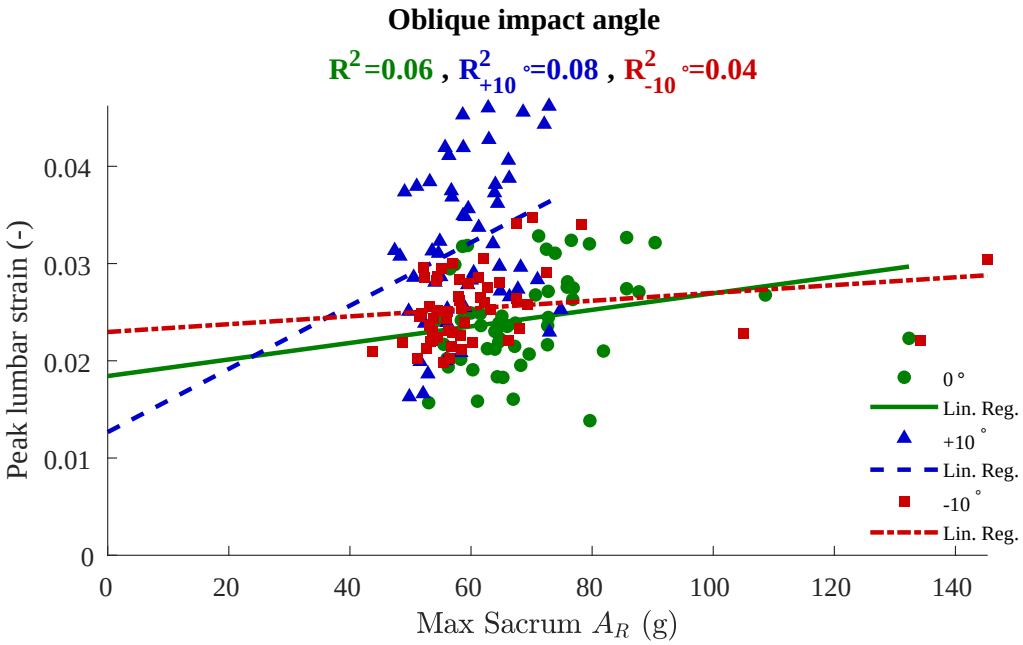

Figure A.8: Linear regression and visualization of data sample for variation of oblique impact angle using SHBM and Peak Sacrum A_R as IC.

A.4 Correlational effects of variable changes using Hybrid III ICs

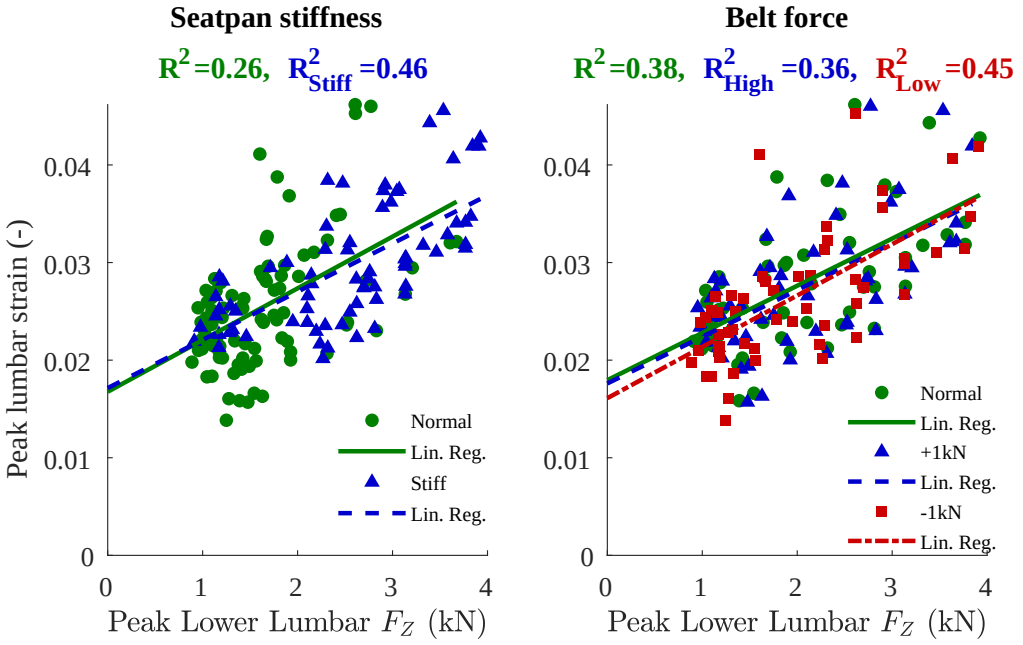

Figure A.9: Linear regression and visualization of data sample for variation of seatpan stiffness and belt force using Hybrid III and Peak Lower Lumbar F_Z as IC.

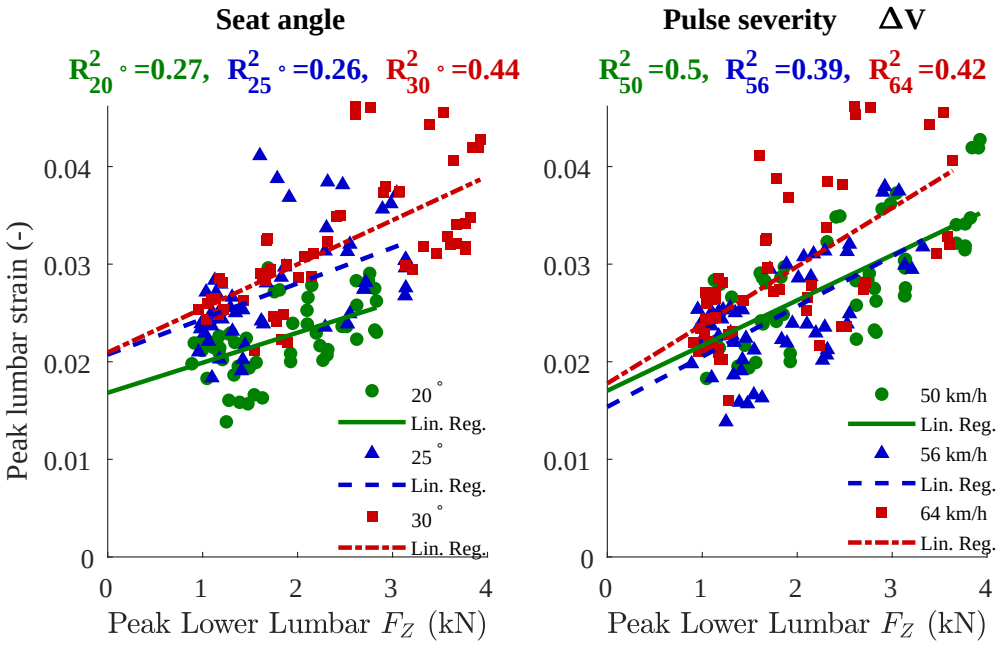

Figure A.10: Linear regression and visualization of data sample for variation of seat back angle and pulse severity using Hybrid III and Peak Lower Lumbar F_Z as IC.

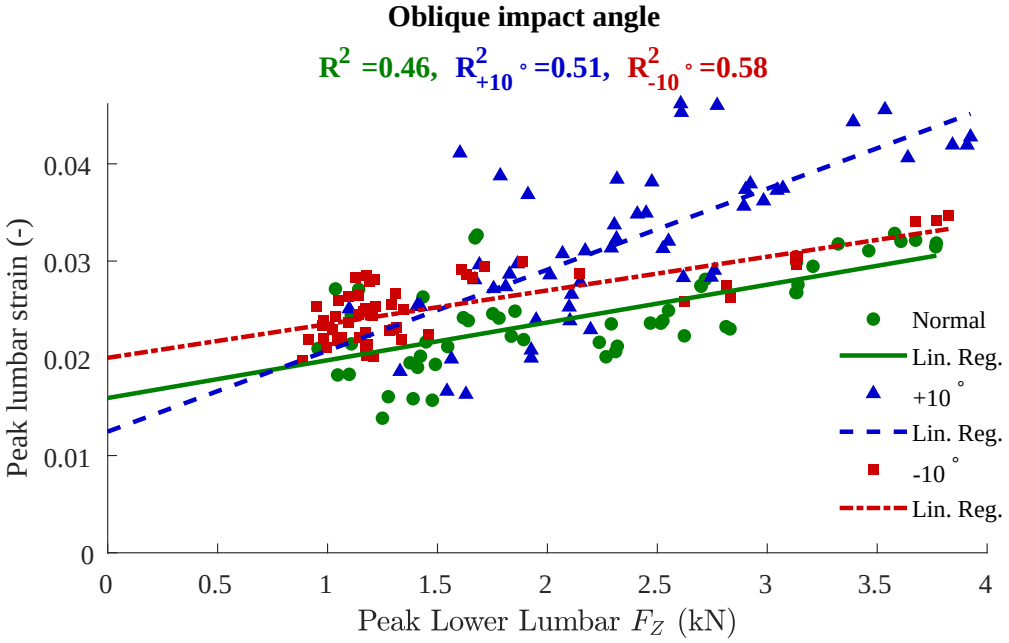

Figure A.11: Linear regression and visualization of data sample for variation of oblique impact angle using Hybrid III and Peak Lower Lumbar F_Z as IC.

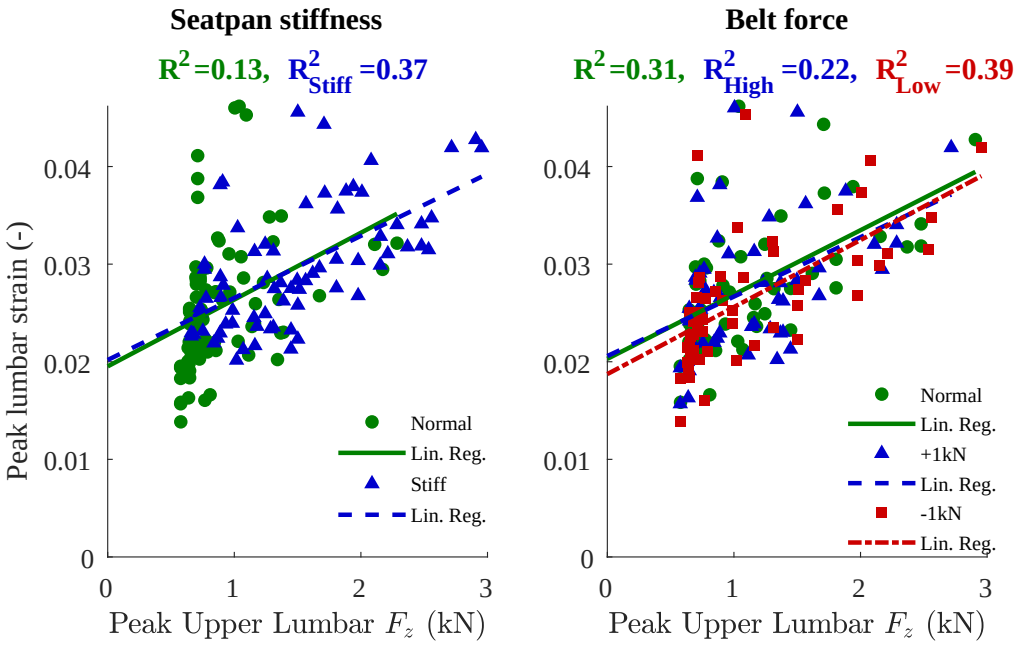

Figure A.12: Linear regression and visualization of data sample for variation of seatpan stiffness and belt force using Hybrid III and Peak Upper Lumbar F_Z as IC.

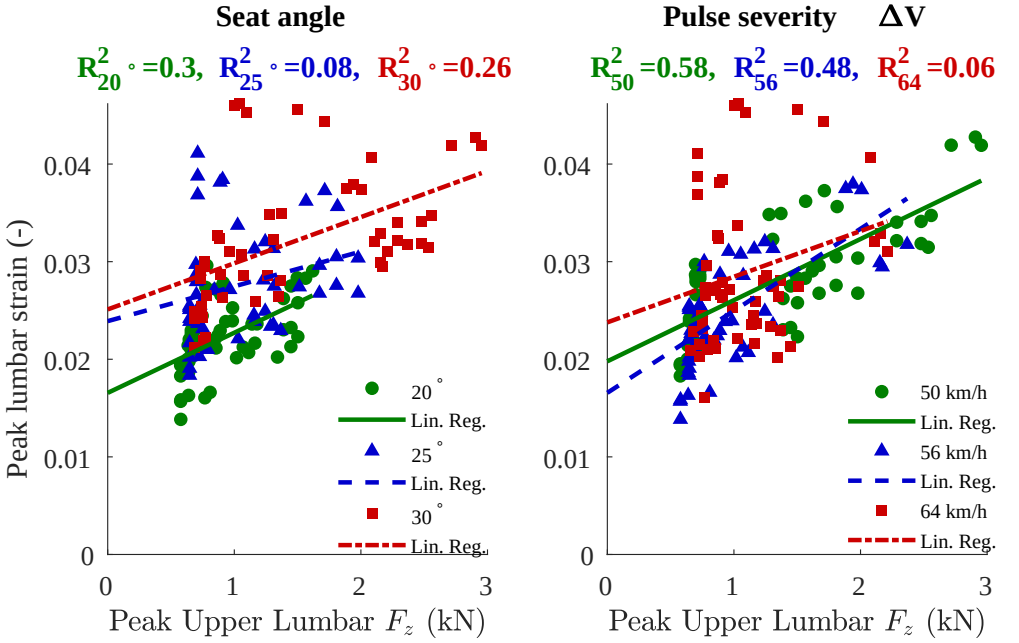

Figure A.13: Linear regression and visualization of data sample for variation of seat back angle and pulse severity using Hybrid III and Peak Upper Lumbar F_Z as IC.

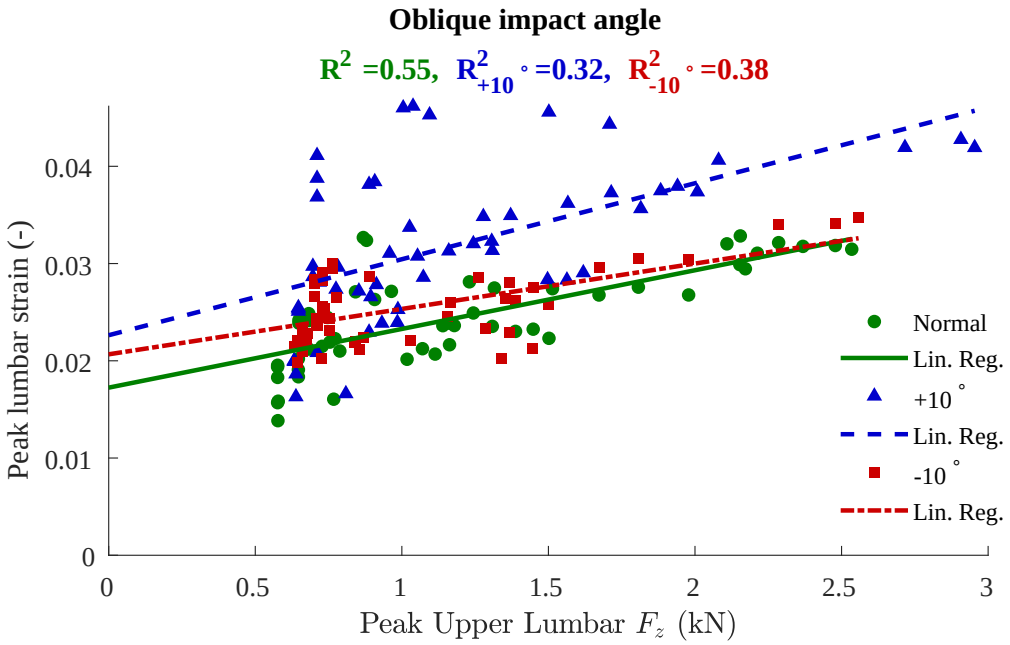

Figure A.14: Linear regression and visualization of data sample for variation of oblique impact angle using Hybrid III and Peak Upper Lumbar F_Z as IC.

A.5 Correlational effects of variable changes using THOR ICs

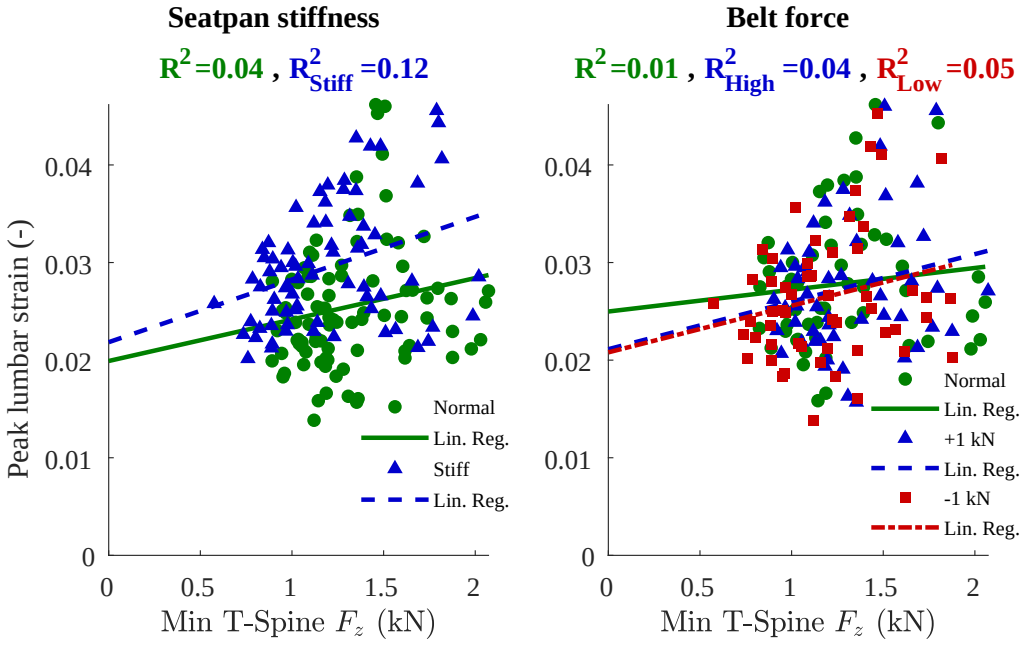

Figure A.15: Linear regression and visualization of data sample for variation of seatpan stiffness and belt force using THOR and Min T-spine F_Z as IC.

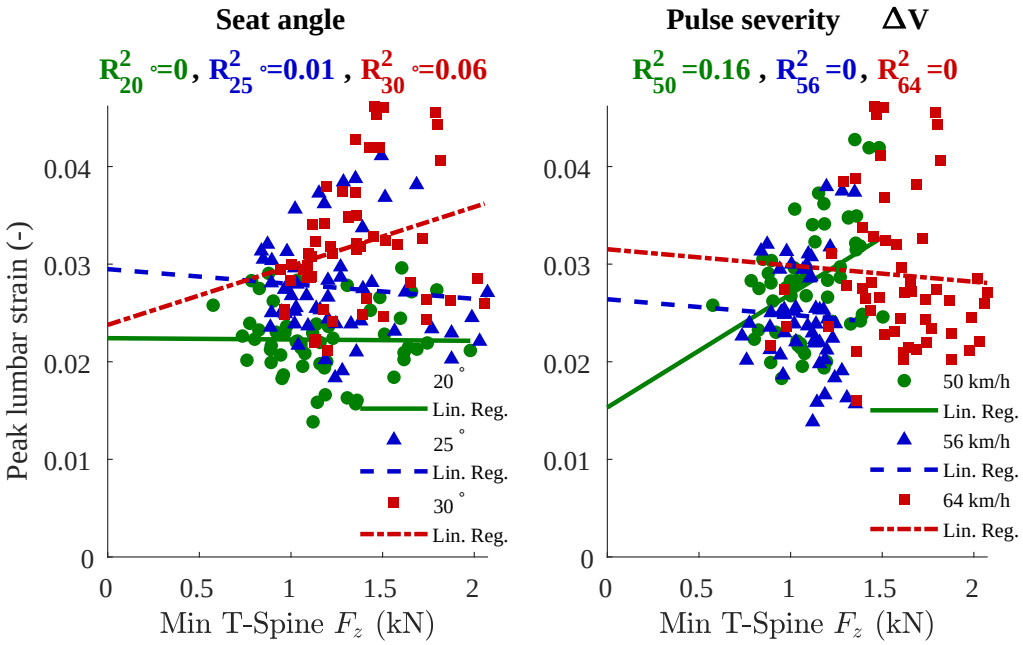

Figure A.16: Linear regression and visualization of data sample for variation of seat back angle and pulse severity using THOR and Min T-spine F_Z as IC.

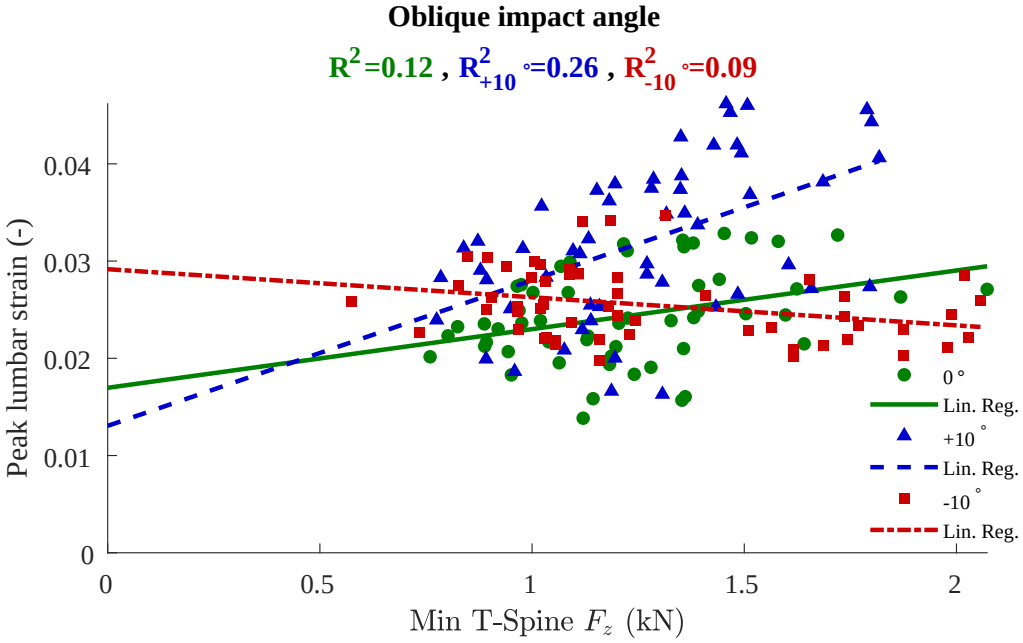

Figure A.17: Linear regression and visualization of data sample for variation of oblique impact angle using THOR and Min T-spine F_Z as IC.

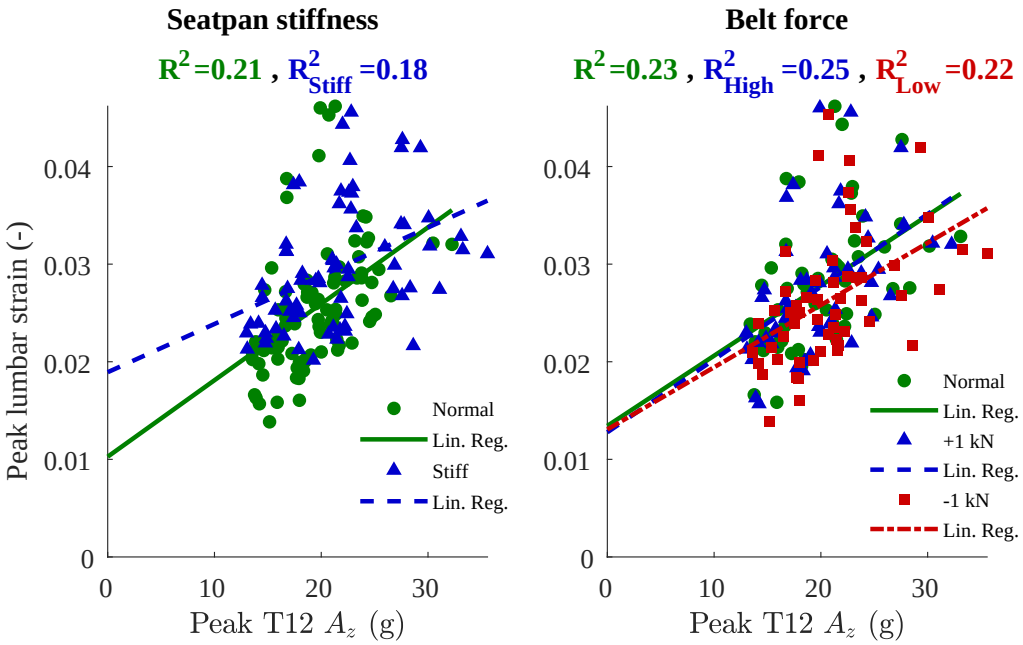

Figure A.18: Linear regression and visualization of data sample for variation of seatpan stiffness and belt force using THOR and Peak T12 A_Z as IC.

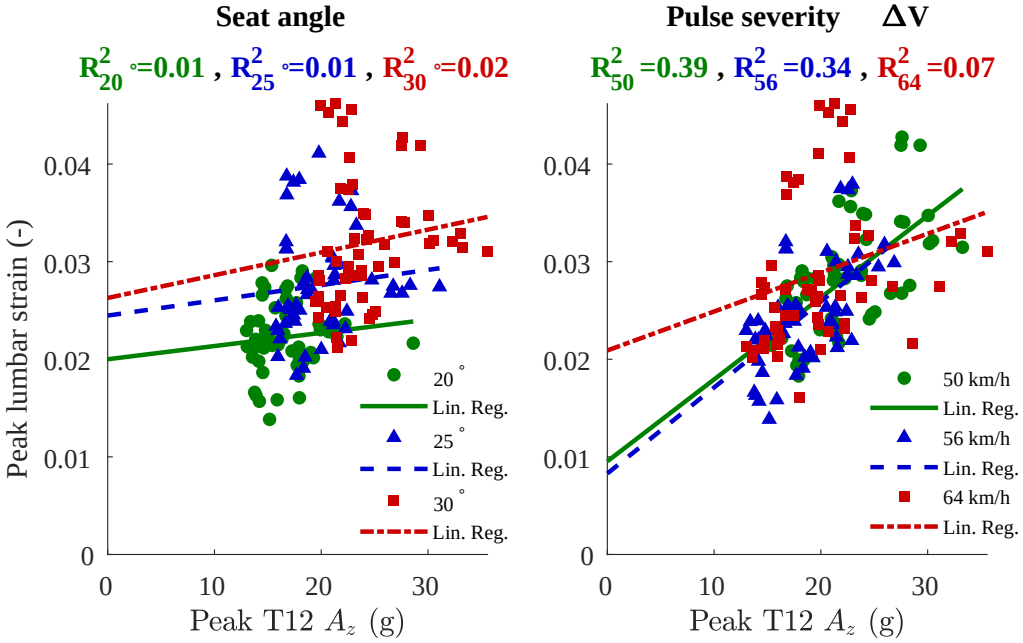

Figure A.19: Linear regression and visualization of data sample for variation of seat back angle and pulse severity using THOR and Peak T12 A_Z as IC.

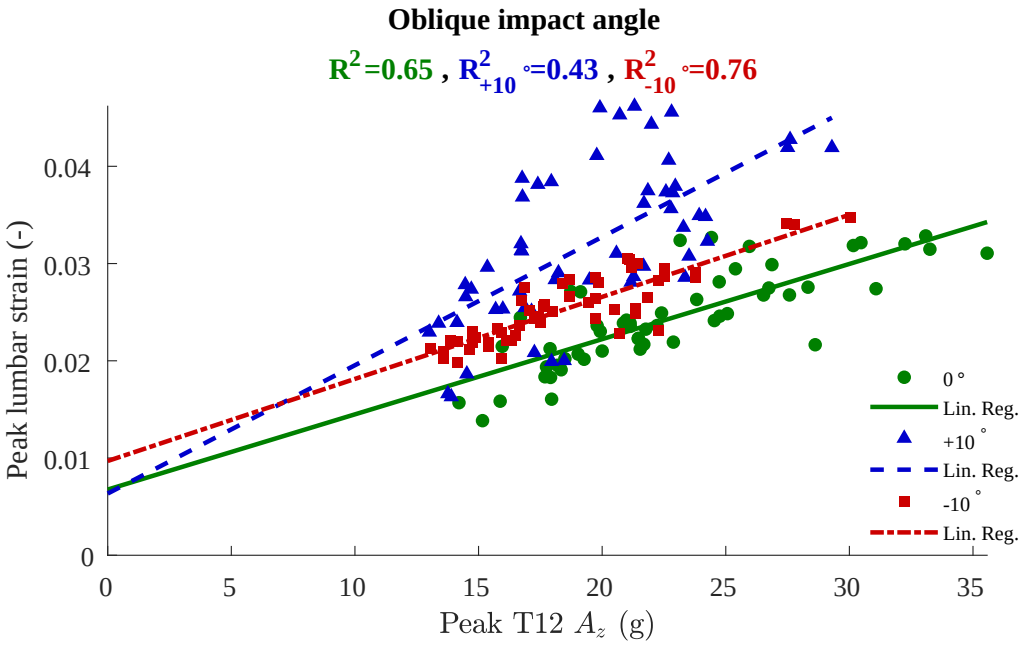

Figure A.20: Linear regression and visualization of data sample for variation of oblique impact angle using THOR and Peak T12 A_Z as IC.

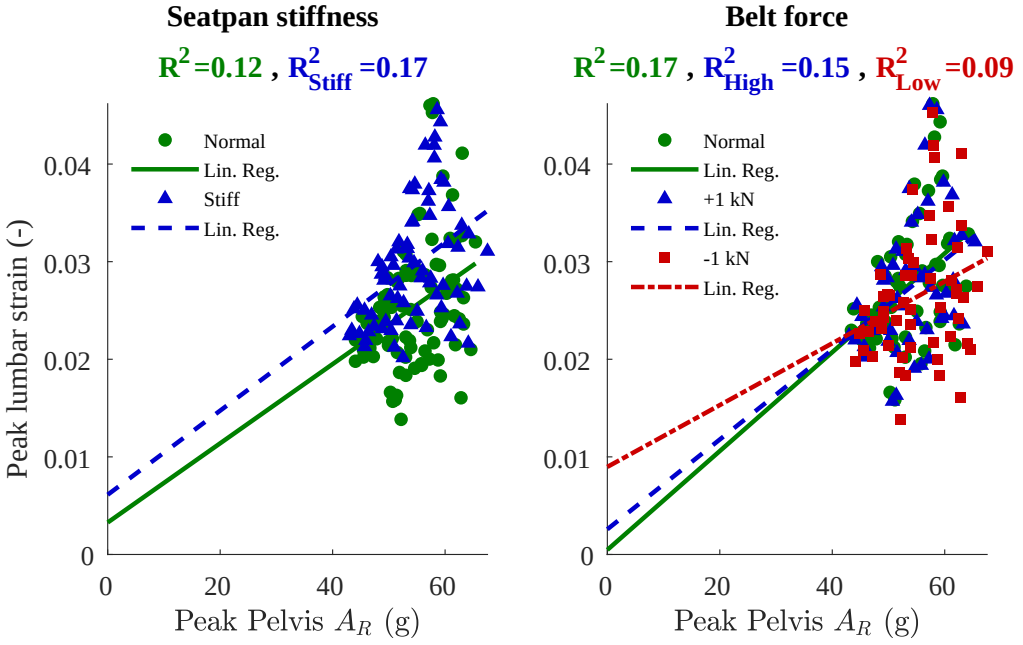

Figure A.21: Linear regression and visualization of data sample for variation of seatpan stiffness and belt force using THOR and Peak Pelvis A_R as IC.

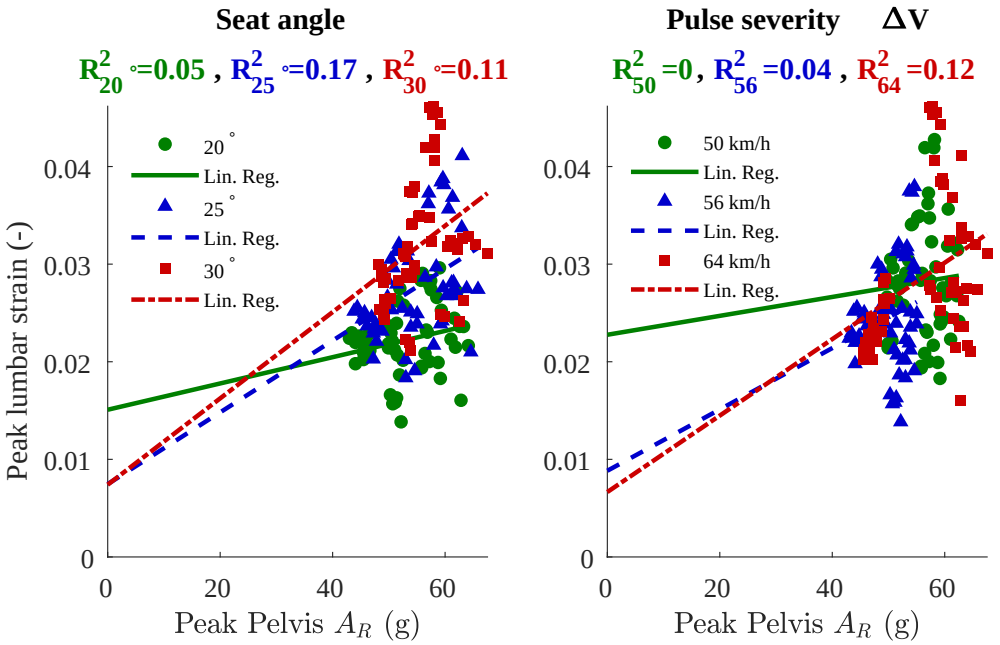

Figure A.22: Linear regression and visualization of data sample for variation of seat back angle and pulse severity using THOR and Peak Pelvis A_R as IC.

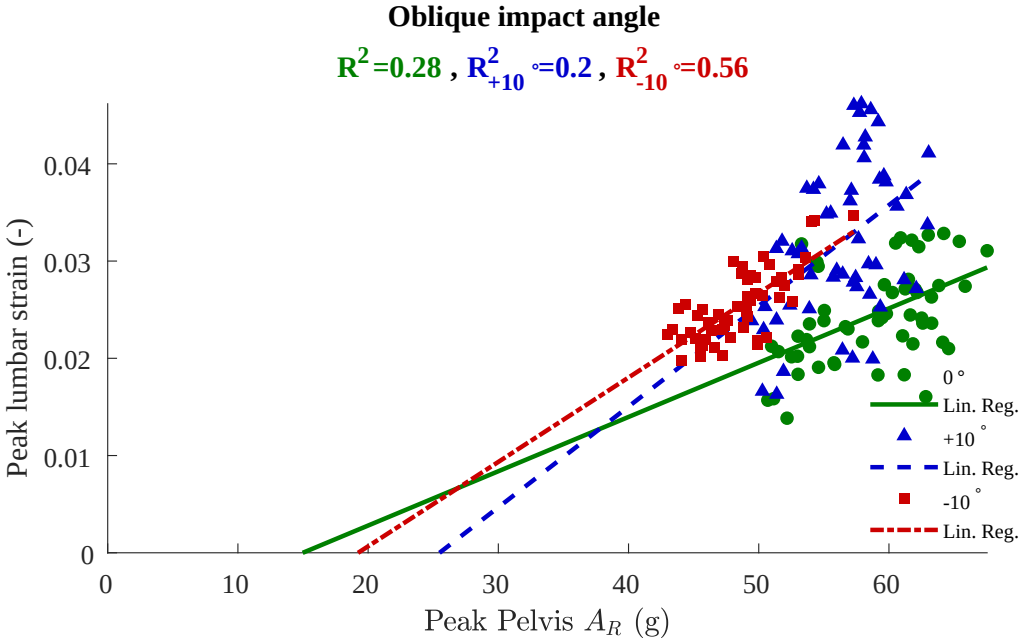

Figure A.23: Linear regression and visualization of data sample for variation of oblique impact angle using THOR and Peak Pelvis A_R as IC.

B

Appendix

B.1 Hybrid III risk prediction curves

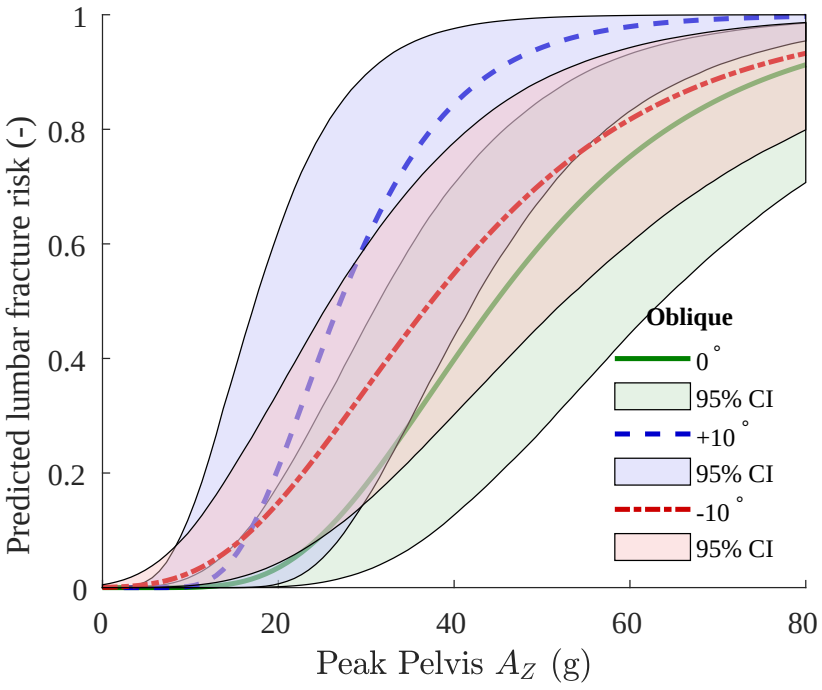

Figure B.1: Injury risk curves genererated by inserting a transfer function of the strain using Hybrid III Peak Pelvis A_Z as IC into the SHBM IRF [Iraeus et al., 2023] for a 25 year old occupant.

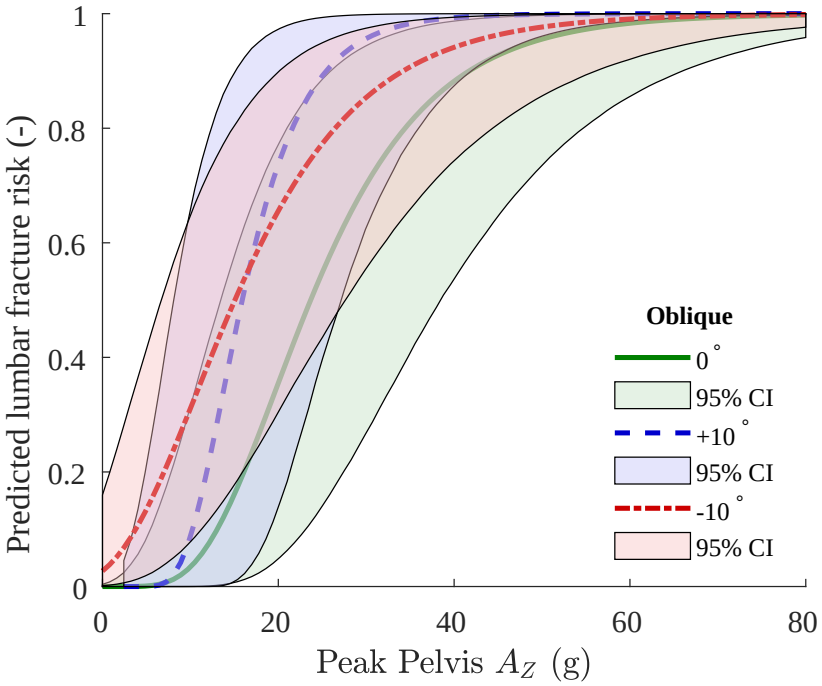

Figure B.2: Injury risk curves genererated by inserting a transfer function of the strain using Hybrid III Peak Pelvis A_Z as IC into the SHBM IRF [Iraeus et al., 2023] for a 65 year old occupant.

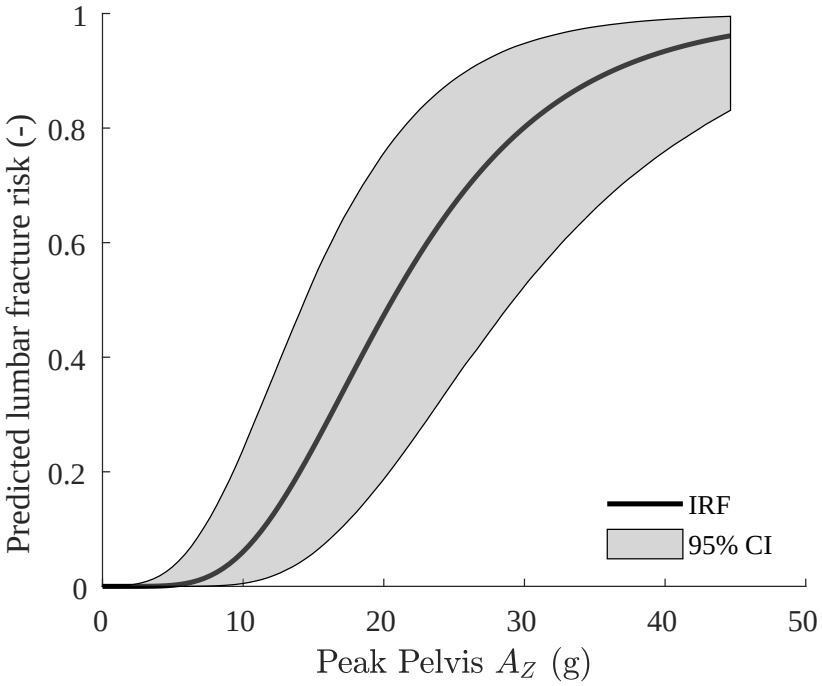

Figure B.3: Injury risk curves genererated by inserting a transfer function of the strain using Hybrid III Peak Pelvis A_Z as IC into the SHBM IRF [Iraeus et al., 2023] for a 25 year old occupant for run off road loadcases.

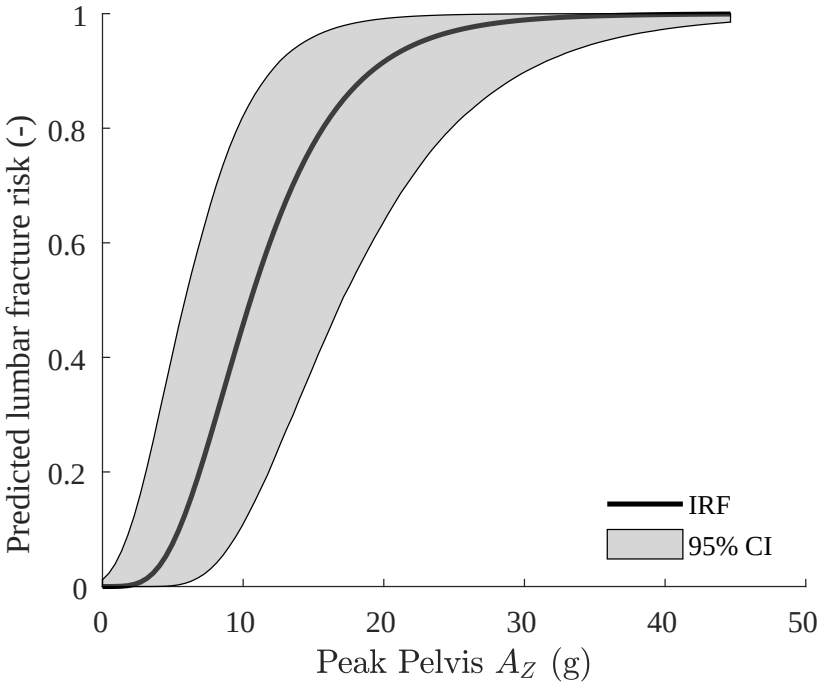

Figure B.4: Injury risk curves genererated by inserting a transfer function of the strain using Hybrid III Peak Pelvis A_Z as IC into the SHBM IRF [Iraeus et al., 2023] for a 65 year old occupant for run off road loadcases.

B.2 THOR risk prediction curves

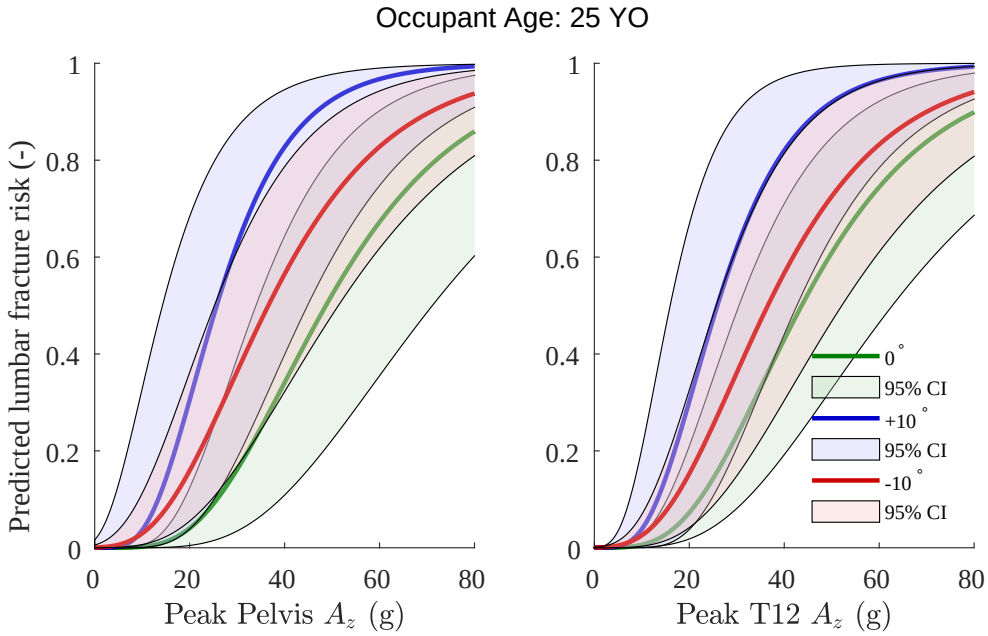

Figure B.5: Injury risk curves genererated by inserting a transfer function of the strain using THOR Peak Pelvis and T12 A_Z as IC into the SHBM IRF [Iraeus et al., 2023] for a 25 year old occupant.

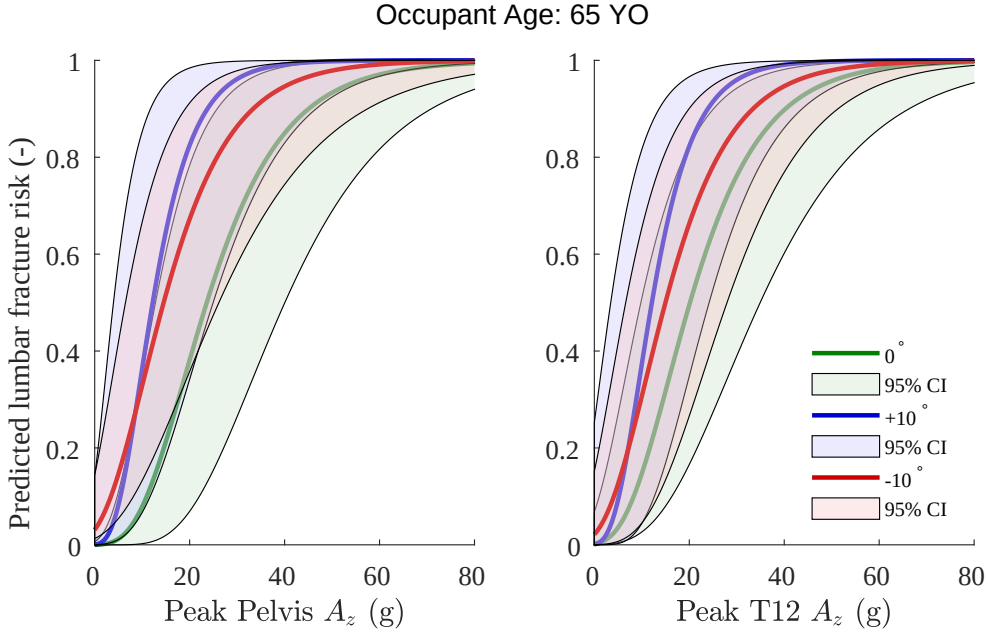

Figure B.6: Injury risk curves genererated by inserting a transfer function of the strain using THOR Peak Pelvis and T12 A_Z as IC into the SHBM IRF [Iraeus et al., 2023] for a 65 year old occupant.

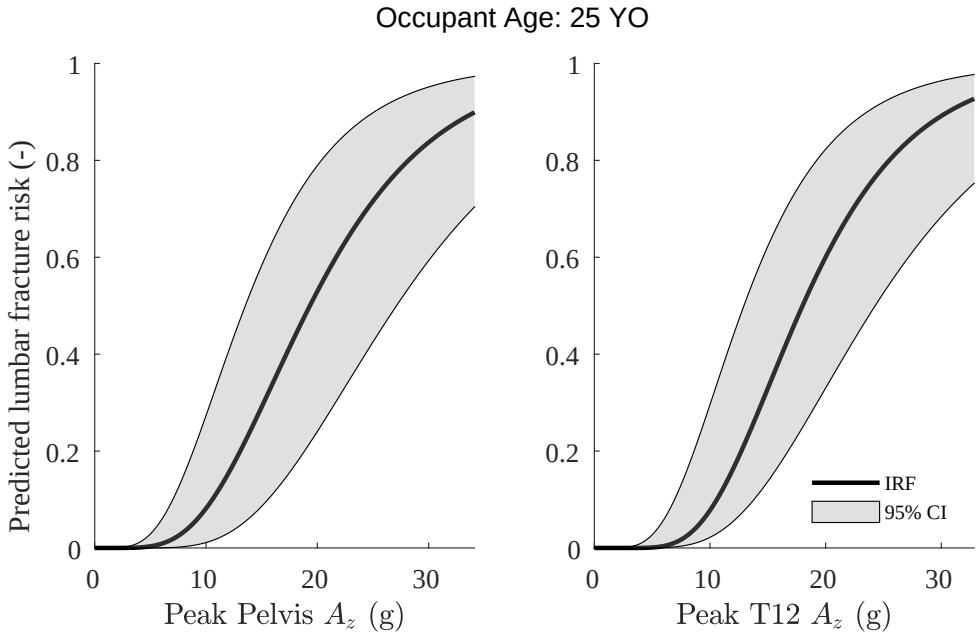

Figure B.7: Injury risk curves genererated by inserting a transfer function of the strain using THOR Peak Pelvis and T12 A_Z as IC into the SHBM IRF [Iraeus et al., 2023] for a 25 year old occupant.

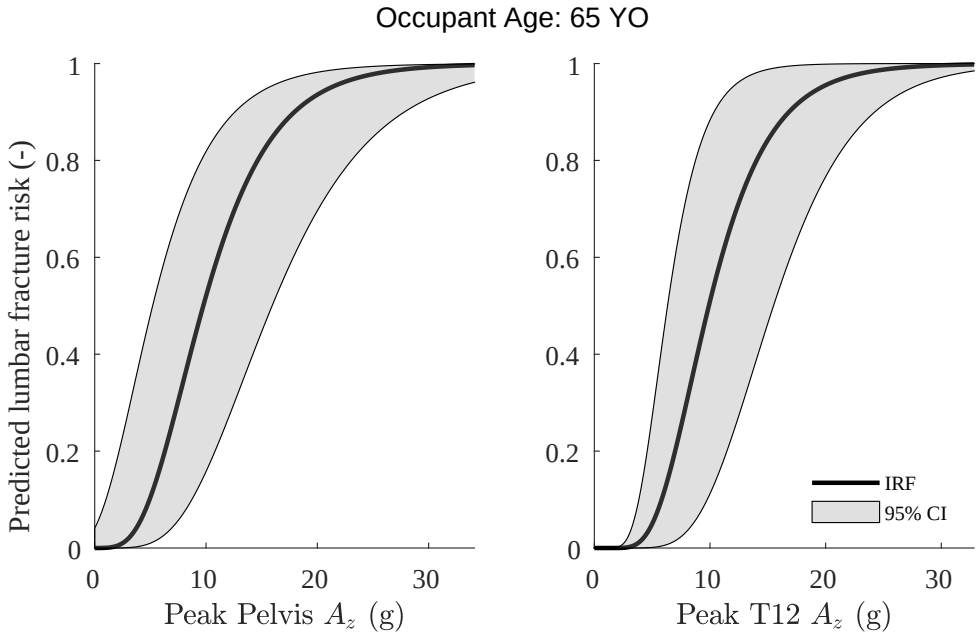

Figure B.8: Injury risk curves genererated by inserting a transfer function of the strain using THOR Peak Pelvis and T12 A_Z as IC into the SHBM IRF [Iraeus et al., 2023] for a 65 year old occupant.

DEPARTMENT OF MECHANICS AND MARITIME SCIENCES
CHALMERS UNIVERSITY OF TECHNOLOGY
Gothenburg, Sweden
www.chalmers.se

CHALMERS
UNIVERSITY OF TECHNOLOGY